

Review

# Recent Advancements in Surface Modification, Characterization and Functionalization for Enhancing the Biocompatibility and Corrosion Resistance of Biomedical Implants

Abhinay Thakur <sup>1</sup>, Ashish Kumar <sup>2,\*</sup>, Savaş Kaya <sup>3</sup>, Riadh Marzouki <sup>4,5</sup>, Fan Zhang <sup>6</sup> and Lei Guo <sup>7</sup>

<sup>1</sup> Department of Chemistry, School of Chemical Engineering and Physical Sciences, Lovely Professional University, Phagwara 144411, India

<sup>2</sup> NCE, Department of Science and Technology, Government of Bihar, Bihar 803108, India

<sup>3</sup> Department of Pharmacy, Health Services Vocational School, Sivas Cumhuriyet University, Sivas 58140, Turkey

<sup>4</sup> Chemistry Department, College of Science, King Khalid University, Abha 61413, Saudi Arabia

<sup>5</sup> Chemistry Department, Faculty of Sciences, University of Sfax, Sfax 3038, Tunisia

<sup>6</sup> Department of Engineering and Design, School of Engineering and Information, University of Sussex, Brighton BN1 9RH, UK

<sup>7</sup> School of Materials and Chemical Engineering, Tongren University, Tongren 554300, China

\* Correspondence: drashishchemlpu@gmail.com



**Citation:** Thakur, A.; Kumar, A.; Kaya, S.; Marzouki, R.; Zhang, F.; Guo, L. Recent Advancements in Surface Modification, Characterization and Functionalization for Enhancing the Biocompatibility and Corrosion Resistance of Biomedical Implants. *Coatings* **2022**, *12*, 1459. <https://doi.org/10.3390/coatings12101459>

Academic Editor: Devis Bellucci

Received: 16 September 2022

Accepted: 29 September 2022

Published: 3 October 2022

**Publisher's Note:** MDPI stays neutral with regard to jurisdictional claims in published maps and institutional affiliations.



**Copyright:** © 2022 by the authors. Licensee MDPI, Basel, Switzerland. This article is an open access article distributed under the terms and conditions of the Creative Commons Attribution (CC BY) license (<https://creativecommons.org/licenses/by/4.0/>).

**Abstract:** Metallic materials are among the most crucial engineering materials widely utilized as biomaterials owing to their significant thermal conductivity, mechanical characteristics, and biocompatibility. Although these metallic biomedical implants, such as stainless steel, gold, silver, dental amalgams, Co-Cr, and Ti alloys, are generally used for bone tissue regeneration and repairing bodily tissue, the need for innovative technologies is required owing to the sensitivity of medical applications and to avoid any potential harmful reactions, thereby improving the implant to bone integration and prohibiting infection lea by corrosion and excessive stress. Taking this into consideration, several research and developments in biomaterial surface modification are geared toward resolving these issues in bone-related medical therapies/implants offering a substantial influence on cell adherence, increasing the longevity of the implant and rejuvenation along with the expansion in cell and molecular biology expertise. The primary objective of this review is to reaffirm the significance of surface modification of biomedical implants by enlightening numerous significant physical surface modifications, including ultrasonic nanocrystal surface modification, thermal spraying, ion implantation, glow discharge plasma, electrophoretic deposition, and physical vapor deposition. Furthermore, we also focused on the characteristics of some commonly used biomedical alloys, such as stainless steel, Co-Cr, and Ti alloys.

**Keywords:** biomedical implants; corrosion; Ti alloys; surface modification; thermal spraying; PVD; SEM

## 1. Introduction

Owing to their superior thermal and mechanical conductance, metals are often utilized as biomaterials. Biomaterials are synthetic or organic materials that are utilized to construct implants or other devices that restore damaged or diseased biological matter and recover shape and functionality. Therefore, biomaterials contribute to increasing individual lifespan and standard of living, and the area of biomaterials has experienced significant expansion to meet the expectations of an elderly society [1–4]. Undoubtedly, the use of biomaterials in a multitude of medical procedures such as skin operations, synthetic vasculature, ophthalmic implantation, dentistry, and knee and prosthetic transplants improves people's comfort in life. While an estimate from the 1990s stated that approximately 250,000 knee implants and 1 million hip transplants are executed each year, and those numbers are expected to climb

enormously in the future [5]. As a result of the rise in pro-inflammatory and deteriorating (corrosion) conditions, there is an urgent need for advanced bio-implants, particularly in the physical realm [6–8]. However, the discovery of materials that fits therapeutic needs was as a result of the biological advancement of biomaterials throughout antiquity, and this led to the development of suitable preliminary biomedical implants accompanied by the stability of the attachment or assimilation over a lengthy period. Obligations aside, bioactivity is a crucial criterion for the capability of tissues to attach inside the body devoid of creating unfavorable discomfort [9–13]. By spreading nascent cells all over the restored marrow and implantation interface, the subsequent osseointegration procedure aids in the formation of fresh marrow. Consequently, within several weeks following treatment, the required characteristics for effective osseointegration include tribological properties, surface tension, and contour. Additionally, the fundamental criteria for choosing a substance include physiological characteristics such as micro-hardness, maximum strain or compression toughness, crack resilience, and wear rigidity [14–21]. The levels of bone stiffness, which are substantially smaller than the yield strength of transplanted substances, range between 4 and 30 GPa based on the kind of bone fragment or ligaments. As a result, different tension concentrations at different interacting surfaces could be caused by the lower flexibility of bone fragments and an inescapable disparity in implanted stiffness. Titanium (Ti) and their alloys, cobalt (Co)-based alloys, stainless steels, magnesium (Mg)-based alloys, and other metals with similar compositions are by far the most frequently utilized biocompatible metals for biomedical devices and implants. Implantable implants for various uses regularly utilize biocompatible metal elements, as shown in Figure 1.

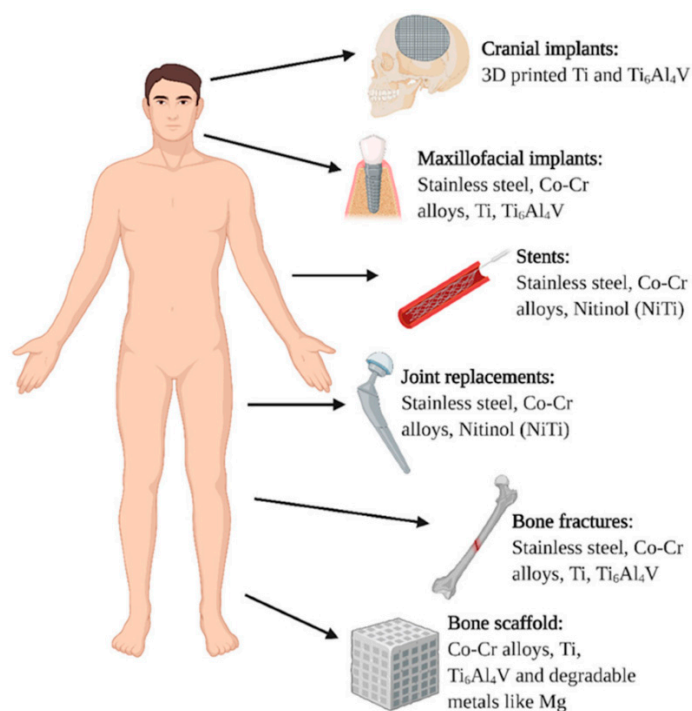


**Figure 1.** Kinds of metallic implants utilized in the human body. Reprinted with permission from [22]. Copyright 2021 MDPI. Distributed under Creative Commons Attribution-based license (CCBY 4.0.).

Additionally, the proper surface attributes of biomaterials are centered on an excellent wear-resistant substrate that reduces the development of abrasive wear in the body. Similar to this, the creation of fatigue remnants at interface areas caused by implants with significant coefficients of wear or lower fatigue capacity can damage healthy bones. Similar to this, the ability of the implant to prevent corrosion is a crucial feature of the choice of biomaterials. Due to the body's extremely sensitive chemical equilibrium, implanted substances must possess bio-inert characteristics to prevent corrosion and the unintentional discharge of

metallic ions. Furthermore, these damaging substances can accumulate in the tissues and combine with the invasive material, or they can go into different body systems [23,24]. As a result, the quantity of metallic ions in plasma and various bodily biological fluids rises. Because of this, it is a great challenge to identify a substance that fits every need of a perfect biomaterial and biomedical implant. For instance, metals have excellent tensile qualities but, on the other hand, have a low capacity for corrosion resistance. As a result, the subject of surface modification is crucial for attaining the integrated qualities of these metals and other substances. Consequently, any change in the material's interface or mass features, such as tribo-mechanical behavior, corrosion resistance, and morphological incorporation into host cells, offers excellent potential to enhance the general efficiency of the implant. In an experiment, Ti alloys, stainless steel, Co-Cr alloys, as well as other popular biomedical alloys, were all evaluated for their qualities by Yan et al. [25]. Generally, biomedical alloys constitute approximately 80% of all elements utilized for bioimplants. Stainless steel, Co-Cr, and Ti alloys are perhaps the most widely used biomedical alloys. Figure 2 compares the characteristics of these three groups. The usage of other biomedical alloys centered on Mg, iron (Fe), tantalum (Ta), and niobium (Nb) alloys is less common. In summary, to meet the expanding range of medical purposes, the bio functionality and mechanical and biological biocompatibility of the presently employed biomedical metals and alloys must be increased. Several articles contain numerous discussions and attempt to enhance the structural biocompatibility of these alloys, particularly their stiffness, flexibility, fatigue strength, hardness, and corrosion resistance [26–31].

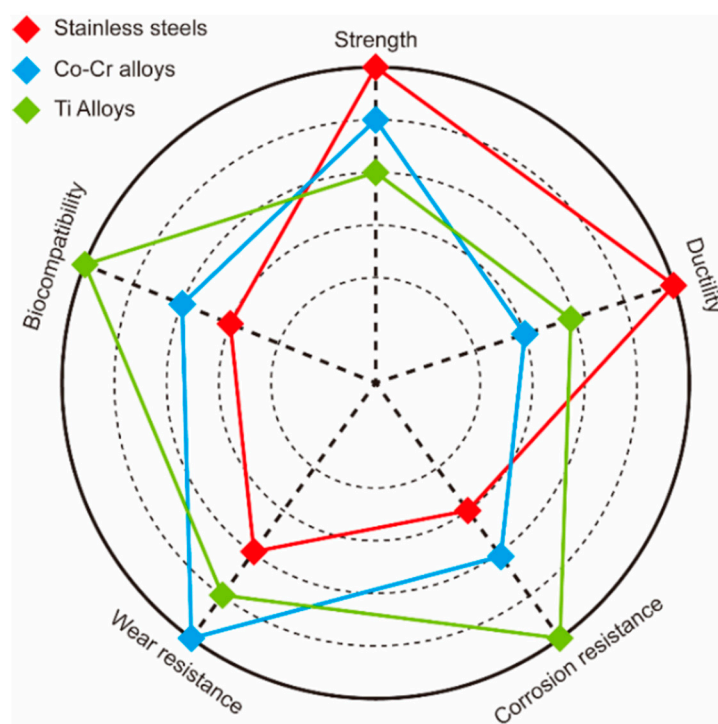


**Figure 2.** Evaluation of ductility, strength, corrosion, wear resistance, and biocompatibility of stainless steel (red), Co-Cr (blue), and Ti (green) alloys. Reprinted with permission from [25]. Copyright 2022 MDPI. Distributed under Creative Commons Attribution-based license (CCBY 4.0.).

The production of an equivalent structural regulation from a distinct biomaterial might not be feasible or even conceivable. This could provide several issues when the substrate topography is intricate. To alter the form or composition of the biomedical implant, surface modification techniques employ mechanical stimuli, coatings, or a combination of these. In order to acquire the necessary features, such as biocompatibility and anti-corrosion characteristics, several devised processes such as cleansing, surface coating,

sealant, and thin layer stacking techniques are used for the physiological modifications of a biomedical implant [32]. The most common thin coating generation method for producing the incredibly thin coverings utilized in implants is Physical Vapor Deposition (PVD). In an experiment, Schafer et al. [33] investigated potential improvements in the ability of nickel–Ti K-files with PVD coating to carve. In this experiment, various procedure variables were used to fabricate films composed of Ti nitride. Seven sets of twelve devices were created out of an aggregate of 84 nickel–Ti K-files (size 35). The devices were covered using Ti nitride in Groups A through F (empirical) utilizing various processing variables for the substrate's temperature, applying current, covering depth, and ion irradiation. Components in Group K (controlled) did not have Ti nitride coatings. A computer-driven measuring apparatus was used to measure the slashing effectiveness of each tool while it was being rotated. The criteria for cutting involved using special plastic specimens having a circular loop and the maximal probe immersion level further into the lumen. Tools from categories A, F, and C considerably outperformed uncoated devices from the reference category in terms of depth of penetration ( $p < 0.05$ ). As a result, PVD-coated Ni-Ti sheet cutting effectiveness improved by up to 26.2% when compared to untreated tools. In another experiment, to increase the bonding intensity across substrate and coating and to achieve an appropriate dissolving rate for rapid preliminary bone fixation, Zhou et al. [34] devised a unique fluoride hydroxyapatite/calcium silicate (FHA/CS) composite coating that was coated using suspension plasma spraying. By altering the suspension's formulation, composite coatings on Ti substrates were created with various FHA to CS proportions. The composite coatings had porosities between 7.4% and 8.3% and varied in thickness from 75 to 92  $\mu\text{m}$ . The composite coating exhibits the optimum bonding intensity and dissolving rate when the proportion of FHA to CS was 3:7. The capability of the coatings to generate apatite while being exposed to simulated body fluid (SBF) allowed researchers to quantify their in vitro bioactivity. The outcomes demonstrate that upon being dipped in SBF, the composite coatings exhibit a high level of reactivity. By counting the number of alive bacteria following incubation with the composite coatings, the antibacterial behavior of the coatings was also investigated. The results demonstrate that *Staphylococcus aureus* propagation could be reduced. The FHA/CS composite coating might be a very intriguing coating substance for implants considering the integration of strong bonding intensity, superior chemical resistance, outstanding apatite-forming capability, and antibacterial potential.

Similarly, Hacking et al. [35] described a method for successfully concealing surface chemistry without changing the contour of the substrate. In this experiment, PVD was used to create a thin coating of Ti upon several biomaterial substrates. In order to achieve a mirror-like quality, the discs were variously refined, grit-blasted using alumina granules, or plasma-sprayed using conventional hydroxyapatite (HA). A subset of each of these therapeutic modalities was subsequently processed by PVD-depositing a thin coating of conventional pristine Ti over the whole platter region. Among the platter in each intervention batch, an analysis of surface morphology and chemical concentration was performed. To evaluate the resilience of the PVD Ti mask during culture parameters, canine marrow cells were implanted on each target plate. The thin Ti coating entirely hid the fundamental biochemistry of the plasma-sprayed HA substrate and the chemistry of the plasma vapor-formed Ti coating did not distinguish it from that of the economically pristine Ti platters. Aliquots taken from the medium throughout the culture did not demonstrate any substantial variations in Ti content across the Ti and Ti-masked substrates. Ti integrated with PVD was applied to HA films to provide a robust, long-lasting, uniform coating that successfully concealed the surface chemistry of the substrate without changing the surface morphology [36–40].

Demirci et al. [41] produced Ti-6Al-4V alloys using admixture manufacturing and varied the laser output. They explored the impact of various surface alterations affecting the capacity to generate apatite. In this research, on the Ti-6Al-4V specimens, four different chemical modifications, sand blasting (S), acid etching (AE), anodic oxidation (AO), and

anodic spark oxidation (ASO), were accomplished. By using the direct metal laser sintering (DMLS) process and three distinct laser powers—150, 280, and 360 W, alloys of Ti-6Al-4V were produced. To study the impact of the composition and various interface modifications on the capacity to generate apatite, extensive surface modifications were applied to the Ti-6Al-4V alloy. The formation of equiaxed or needle-like manganites within the earlier crystalline grains was visible in fluorescence microscopy and SEM photographs. The growth patterns of the short and long lamellae-type manganites were different. According to X-ray powder diffraction (XRD) data, hematite, and phases were found in the ASO specimen, whereas phases were found in the S, AE, and AO specimens. Following surface treatment, the Ti-6Al-4V alloys' surface roughness was  $S > ASO > AE > AO$ , in that order. S specimens' surface roughness ranged from 3.20 to 2.11  $\mu\text{m}$ . With an increase in laser power, the contact angles of group S, E, and AO specimens exhibited an increased development, while the contact angles of group ASO specimens exhibited a steady decline. For two weeks, the bioactivity assessment was carried out in simulated bodily fluid (SBF). The outcomes showed that apatite production was impacted by morphology, surface roughness, stiffness, and water sorption. For the Ti-6Al-4V alloys, the calcium (Ca) and phosphorous (P) ion proportion ratios increased as the laser intensity increased. Due to the proportion of component quantity and the existence of bioactive stages on the interfaces, the AE specimens often displayed a larger Ca and P ion proportion value than the other specimens. The widely used theoretical apatite establishment was seen in the AE specimens. The apatite development on the alloy specimens was shown by the Fourier-transform infrared spectroscopy (FTIR) spectrum. The suggested technique enhances the capability of Ti-6Al-4V alloys to generate apatites.

In a study, Ti6-Al-4V specimens (AECT surfaces) created by targeted laser melting were subjected to sequential procedures of chemical etching, advanced oxidation processes, and thermochemical processing. The results of this research were assessed by González et al. [42]. It was discovered that when compared to the AE surface, AECT coatings displayed appreciable variations in both topology and constituent content. The specimens' surface characteristics were more significantly impacted by the temperature utilized in the AE procedure. Based on the acid etching temperatures, two topographies were produced on the AECT substrates. The specimens treated to acid etching at 40 °C (AECT-1 and AECT-2 specimens) following the thermal processing at 400 °C for 1 h displayed large patterns mixed with submicron and nanoscale scale surface features, distinguished by the paucity of small pores. The AECT-3 and AECT-4 specimens, which experienced acid peeling at a temperature of 80 °C, likewise displayed a multiresolution structure, wherein nanopores were visible. All interfaces, including their protuberances and the holes they had earlier produced during the acid etching, were found to have a network-shaped architecture. Additionally, the Ti6-Al-4V interface underwent thermo-chemical processing to boost its oxygen concentration, generated a highly crystalline thin coating, and reduced the diameter of its nanopores. The interface of the SLM specimens' XRD signals following the initial various coating procedures considered in this study is shown in Figure 3. It was evident that the hexagonal close-packed (hcp) crystal structure-containing stage was present. It is impossible to dismiss the possibility of a trace quantity of the cubic structure. Nanocrystalline titanium oxide ( $\text{TiO}_2$ ) ( $2\theta = 25.28$  and  $75.03$ ) was identified as the lower intensity XRD features, as shown in Figure 3. These spikes had a modest amplitude because the oxide film was just thinly covering them. Following being heated to around 400 and 500 °C, the titania gel created from the processing of Ti in hydrogen peroxide ( $\text{H}_2\text{O}_2$ ) solution changed into an anatase crystal lattice. The proportion of bone-implant contact (BIC) among the anatase layering and regulated implants was significantly different throughout the initial phases of bone tissue regeneration because anatase has great biocompatibility. On either side, the development of a  $\text{TiO}_2$  coating improves the Ti alloy's corrosion resistance and inhibits ions from penetrating bodily fluids.

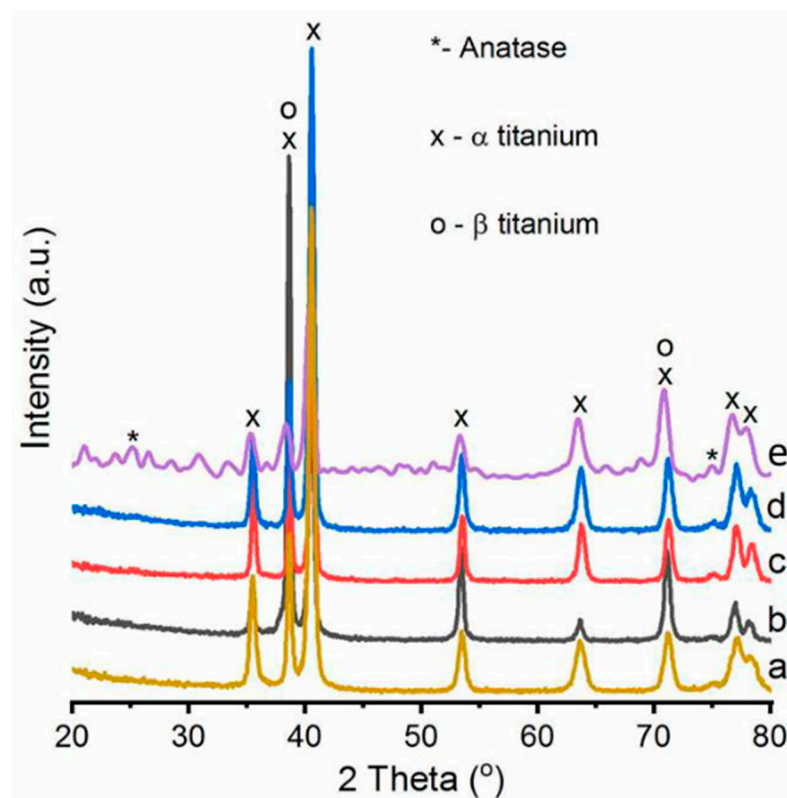


**Figure 3.** XRD spectra of AECT and SLM interfaces: (a) SLM, (b) AECT-1, (c) AECT-2, (d) AECT-3, and (e) AECT-4. Reprinted with permission from [42]. Copyright 2021 MDPI. Distributed under Creative Commons Attribution-based license (CCBY 4.0.).

With an emphasis on (i) the most popular techniques for Ti surface hydroxylation, (ii) self-assembled monolayers (SAMs)-mediated active adhesives progression, and (iii) the most recent developments in active agent immobilization and polymeric surface coating for sustained discharge on Ti substrates, Bodon et al. [43] evaluated the most recent methodologies in the biomedical field to acquire bioactive adhesives onto Ti substrates. They explained the adsorption behavior of hydrogels' hydrophilic, three-dimensional (3D), and elastic permeable architecture to absorb huge amounts of water or biological fluids that were laden with active ingredients. This makes it simple to regulate the precise moderate to maximal concentration of the active substance, which is injected and gradually distributed through a resilient hydrogel matrix. Additionally, hydrogel films may often have significant adhesion sites and a better aptitude for biomolecules exhibiting large molecule mass as compared to multilayer films. Figure 4 shows macro- and scanning electron microscopy (SEM) images of an active covering on a Ti6-Al-4V surface produced by the i+Med S. Coop. research team. It is predicated on a hydrogel comprised of hyaluronic acid.

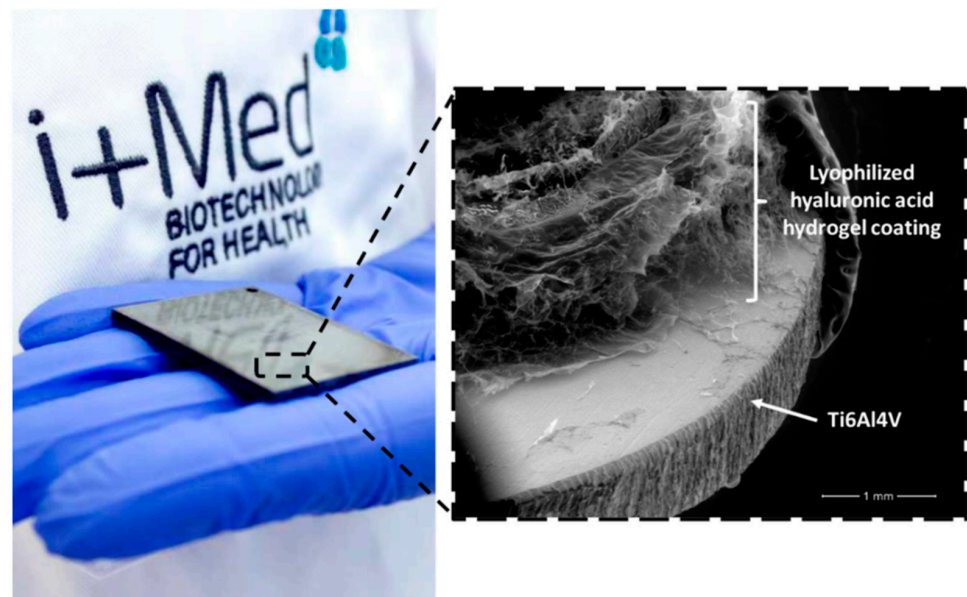


**Figure 4.** An illustration of a hyaluronic acid hydrogel film for putative active reagent distribution on a Ti6Al4V substrate. Reprinted with permission from [43]. Copyright 2021 MDPI. Distributed under Creative Commons Attribution-based license (CCBY 4.0.).

Taking this all into account, this review article presents a critical examination of the crucial role of several surface modification techniques such as thermal spraying, ion implantation, glow discharge plasma, electrophoretic deposition, and physical vapor deposition in the treatment of biomedical implants for the enhancement of their corrosion resistance, stress resistance, osteogenesis, and antimicrobial capabilities. An emphasis on the utilization and protection of several metals and alloys such as stainless steel, Co-Cr, Mg, Ti, etc., used as biomedical implants in numerous operations, is discussed deeply in this review article.

## 2. Commonly Utilized Biomedical Alloys and Their Corrosion Mitigation

### 2.1. Stainless Steel

Amongst metallic biomaterials, stainless steel possesses the oldest tradition of use in biomedical applications. Stainless steel (SS) is effectively produced by advanced contemporary metallurgy and has outstanding characteristics. The reason stainless steel is an attractive substance is that it can be produced using established, simple, and affordable methods. Excellent tensile hardness and corrosion protection are other qualities of stainless steel [44–48]. Compared to Co-Cr and Ti alloys, stainless steels have greater flexibility and cyclical twisting resistance. Additionally, the most generally utilized stainless steel for interim and persistent implants is 316 L (Cr-Ni-Mo, “L” stands for low carbon), which also reduces the development of Co-Cr and improves corrosion resistance. Austenitic 316 L stainless steels are utilized often because they satisfy this criterion. Specifications for austenitic stainless steels include ASTM F138, ASTM F1586, and ASTM F2581. Steels made as ASTM F1586 and F2581 have superior corrosion resistance. These steels, however, included hazardous and non-biocompatible Ni. In an experiment, Singh et al. [49] addressed the impact of laser surface treatment on the surface morphology and corrosion activity of stainless steel 316 L (SS316 L) and Ti-6Al-4V, wherein metal ions were produced throughout the corrosion phase when conducted at a spectrum of laser intensities of 500 to 1500 W in an ambient environment. In the resolidified area of SS316 L, column dendrites and tiny crystalline grains compensate for uniform surface morphology. It was discovered that the particle diameter gradually increased from the substrate to the treated interface. Ti-6Al-4V was laser processed to form a surface covered in dendrites, accompanied by acicular martensite at the junction. The laser surface modification of both SS316 L and

Ti-6Al-4V increased the open circuit potential (OCP), according to the corrosion investigations in Ringer's physiological fluid. In comparison to their corresponding unprocessed predecessors, the corrosion characteristics of Ti-6Al-4V were found to increase, and those of SS316L to degrade, following laser treatment. SS316L's corrosion behavior was affected by variations in laser power; however, Ti-6Al-4V's was not substantially affected. The leaking of particular metallic ions from SS316L and Ti-6Al-4V after dissolution in Ringer's physiological solution was minimized by laser surface modifications at increased powers (1000 W). Similarly, as 316L stainless steel is frequently utilized in healthcare, meal preparation, mechanical, and maritime sectors, Bagherifard et al. [38] assessed the impact of extreme shot drilling on its mechanical and microstructural characteristics. The structural and morphological characteristics, dislocation density, size distribution, phase separation, surface characteristics, surface water sorption, fatigue strength, and micro-hardness of 316 L specimens shot peened using various peening variables were examined. The findings showed that intense shot peening caused changes in the surface grain growth to nanoscale and sub-micron ranges as well as the transformation of the austenite phases into strain-induced martensite in a multilayer deformed band architecture. Shear latent strains and operation hardness were also induced by harsh shot peening in the topmost coating layers. Extreme shot peening also significantly improved wettability and abrasion, both of which favorably influence how materials interface with their biological environments.

Salahinejad et al. [50] examined the interface properties of medical-grade stainless steel covered using nano-structured inorganic zirconium titanate ( $ZrTiO_4$ ) and composite  $ZrTiO_4$ -polymethyl methacrylate (PMMA) thin coatings in terms of bioactivity. Following one day of cultivation, the stability of mature human mesenchymal stem cells over the substrates was also evaluated statistically and graphically. The findings show that both coverings enhanced the substrate's hydrophilic nature, corrosion resistance, and therefore excellent biocompatibility. The specimen covered with the inorganic thin layer demonstrates a stronger cell response; although, the mixed coating's greater corrosion prevention points to the dominance of hydrophilicity. In conclusion,  $ZrTiO_4$ -based sol-gel coatings may be taken into consideration to enhance the bioactivity of metal implants. Additionally, Rezaei et al. [51] investigated double-layer coverings comprised of HA and HA-Mg that were placed over 316 LVM stainless steel. The sprayed coverings were composed of a thick coating of HA that was plasma-sprayed and a topmost part of HA-Mg composite covering that was cold-sprayed (Mg = 10 and 30 wt.%). After submerging the covered specimens in an SBF, the physiological behaviors of the specimens were assessed using 3-(4,5-Dimethylthiazol-2-yl) (MTT), inductively coupled plasma (ICP) spectroscopy, and electrochemical assays. Following corrosion experiments, micro-structural analyses of the covered specimens revealed that the topmost layer's magnesium content deteriorated in SBF fluid and created high porosity, which could serve as growth opportunities for bone cells. The use of double-layer covering solutions avoided the discharge of harmful ions in the platform, such as nickel, according to the findings of the ICP spectroscopic investigation. The double-layer covering technology increased the biocompatibility and bioactivity of 316 LVM stainless steel, according to the findings of MTT and SBF immersed experiments.

Furthermore, utilizing a microwave device, Ou et al. [40] plasma nitrided samples of AISI grade 303 austenitic SS. When microwave plasma was used to create samples of type 303, the plasma power had an impact on the morphology and content of the nitrided coatings. As the plasma strength increased, it was discovered that the morphology alteration process went from the  $\gamma$  phase to the  $\gamma_N$  phase. It was discovered that there was a positive correlation between plasma intensity and the depth and toughness of the nitrided coating. While Gram-negative *E. coli* came into encounter with the nitrided sort 303 SS samples, the bacteria's vitality was significantly diminished after 24 h. Plasma nitriding enhanced the physicochemical characteristics of type 303 SS. The aforementioned findings may help clarify the correlation among corrosion, attrition, and bio-compatibility of grade 303 stainless steel that has been nitrided so that more research into the possibility of this steel's usage as a biomedical component can be conducted.

## 2.2. Co–Cr Alloys

Compared to Ti alloys and stainless steels, Co–Cr alloys have much superior resistance to abrasion, temperature resistance, and rigidity. Additionally, Co–Cr alloys are more resistant to corrosion than 316 L stainless steel [52–56]. Because of this, Co–Cr alloys are frequently utilized for bone replacements, which are typically encircled by Cl-rich body fluids. If 316 L stainless steel were utilized rather than Co–Cr alloy, stress and corrosion-related fracturing might occur. Co–Cr alloys have been strengthened by Cr, which generates a persistent  $\text{Cr}_2\text{O}_3$  layer that shields the alloy against Cl-ion assaults. In an experiment, Amanov et al. [57] worked on gradient nanostructure (GN) and harmonic structure (HS) materials' physical characteristics, which ultrasonic nanocrystal surface modification (UNSM) effectively customized at 25 and 500 °C, correspondingly. The physical characteristics of additive-manufactured (AM) components, including yields and tension capabilities, were improved by the UNSM temperatures, and outperformed those of the as-AM Cr–Co–Mo alloy. The as-AM Cr–Co–Mo alloy yielded and ultimate tensile improved after treatment with UNSM at 25 °C, and then further improved following UNSM at 500 °C. Therefore, the pretreatment of UNSM to the as-AM Cr–Co–Mo alloy at 500 °C resulted in critical tensile enhancements for the medicinal and space industry. As a consequence, it could be thought to heavily depend on offering a convenient means of enhancing the structural characteristics of materials made using additive manufacturing. Similarly, Liu et al. [58] used plasma interface alloying using nitrogen or carbon at relatively reduced temperatures (around 300 and 400 °C) to enhance the toughness, hardness, corrosive, and corrosion-wear characteristics of pharmaceutical quality Co–Cr. The findings revealed that the optimal processing parameters developed certain attractive surface layers on Co–Cr alloy for biological purposes. The metallurgical, physical, toxicological, and wear surface characteristics of alloyed layers were evaluated. Low-temperature plasma surface alloying created a hard S-phase layer that ranged in depth from 0.8 to 2.7  $\mu\text{m}$  and was temperature dependent. Plasma carbonitriding generated a higher hard exterior than plasma nitriding when handled at the same temperature for the same period of time. Plasma nitriding (PN) and plasma carbonitriding (PCN) considerably increased the wear endurance of the Co–Cr alloy. While PCN specimens exhibit superior corrosion protection than PN specimens, low-temperature (350 °C) plasma surface alloyed Co–Cr exhibits resistance to corrosion that is comparable to an unprocessed substance. PCN and low-temperature PN successfully increased the corrosion-wear resistance of the Co–Cr alloy. Additionally, in his study, Valkov et al. [59] explored the prospect of employing the electron-beam surface engineering approach to change the composition and characteristics of Co–Cr–Mo alloys. The technical variables were adjusted to achieve the fastest cooling rate possible without scorching the surface. Figure 5 displays 3D atomic force microscopy (AFM) pictures of the surface features of the samples. It is clear that the electron beam treatment (EBT) procedure has a significant impact on substrate morphology.

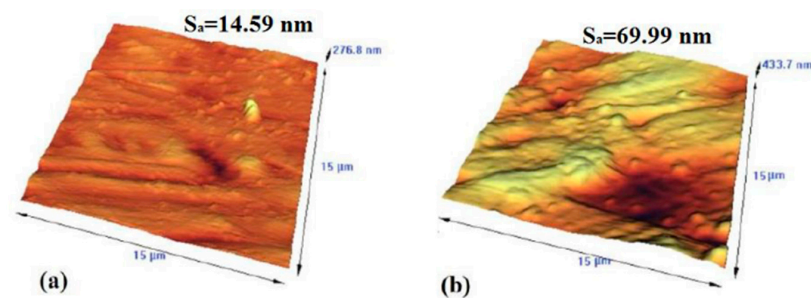


**Figure 5.** Three-dimensional AFM pictures of (a) untreated Co–Cr–Mo alloy and (b) treated Co–Cr–Mo alloy with an electron beam. Reprinted with permission from [59]. Copyright 2021 IOP publishing. Distributed under Creative Commons Attribution-based license (CCBY 4.0.).

Amanov et al. [60] investigated the heat effect of alteration of the Co-Cr-Mo alloy's interface after AM affected its interfacial and tribocorrosion capabilities. In order to produce a femoral head for metal-on-metal (MOM) joints, a Co-Cr-Mo alloy was processed using UNSM at both high temperature (HT) and ambient temperature (AT). Through the use of UNSM, this research sought to improve the specific wear rate (SWR), tribocorrosion resistance (TCR), and coefficient of friction (COF) of the AM-based Co-Cr-Mo alloy. In comparison to UNSM at AT and the Co-Cr-Mo alloy specimens that were produced as-is, the UNSM at HT specimen showed superior tribo and tribocorrosion capabilities. Depending on the alterations in surface topography, composition, and mechanical performance following UNSM at AT and HT, a thorough discussion of the COF and SRW decrease and TCR augmentation processes was conducted. The improvement in TCR of the Co-Cr-Mo alloy produced by AM, and the substitution of cast/wrought with an AM-based one, should be explored. Numerous biomedical activities that now employ a cast/wrought Co-Cr-Mo alloy could advantage from the decrease in COF and SRW.

### 2.3. Ti Alloys

Ti is a special component of the biomedical alloy class because of its better bioactivity, nontoxicity to biological surroundings, significant protection from corrosion, excellent stiffness, reduced percentage of elongation, and other desirable properties. Ti-based alloys have a lower density than Co-Cr alloys and stainless steel and Co-Cr-based alloys may rust or experience corrosion degradation, releasing some hazardous substances [61–66]. Therefore, by creating an extremely inert surface passivation TiO<sub>2</sub> coating, such degradation in Ti alloys can be completely minimized. By examining several Ti alloys, a team of scientists used electrochemistry to demonstrate that superior corrosion resistance is correlated with the existence and characteristics of the protective film. Additionally, the issue of stress insulation can be avoided by Ti alloys' lower elastic modulus. Ti alloys are the greatest option for resolving a range of biomedical issues. There are four categories of economically sheer Ti, numbered G1 through G4. Ti G4 treated with acid scratches showed improved surface structures and mechanical characteristics, making it the perfect implantation for use in dental. There are numerous Ti-based implants available in binaries and various alloy forms in addition to these economically sheer Ti implants. Ti-Nb alloy is a classic example of a binary Ti alloy. The most suitable substance for biomedical purposes is suggested to be permeable Ti-Nb alloys produced by electro-deoxidation. Maleki-Ghaleh et al. [67] used the plasma spray technique to deposit a sol-gel-produced tricalcium magnesium silicate powder on Ti-6Al-4V alloys. In this research, Ti-6Al-4V alloys were coated with nanoscale tricalcium magnesium silicate powder using the plasma spray technique. The 40 m thick coating film that was deposited was homogeneous in thickness. While the corrosion current density of the Ti-6Al-4V alloy specimen decreased from 1.84 to 0.31  $\mu\text{A}/\text{cm}^2$ , the inclusion of the tricalcium magnesium silicate layer significantly enhanced the corrosion resistance. The distribution and multiplication of cells incubated on the Ti-6Al-4V alloy following treatment with tricalcium magnesium silicate bioceramic were enhanced as an outcome, leading to a noticeable increase in biological behavior.

In an experiment, Celesti et al. [68] created Ti-AEMAC, Ti-GTMAC, Ti-AUTEAB, and Ti-OA specimens, complexed Ti plates using quaternary ammonium salts (QAS) and oleic acid (OA). These specimens were then examined for their abrasion and aqueous behavior using FTIR and SEM analysis. The surface characteristics of the metallic interfaces and, consequently, their bio-interaction, were demonstrated to be significantly impacted by the chemical changes. The Ti-AUTEAB and Ti-OA specimens, which include a lengthy alkyl chain across the silicon atom and the ammonium activity, demonstrated excellent anti-adhesion action towards Gram-negative *Escherichia coli* and Gram-positive *Staphylococcus aureus* at 1.5 and 24 h of bacterial interaction. Particularly, following 1.5 h, the Ti-AUTEAB specimen demonstrated an approximately one-step reduction in bacterial adherence to *Escherichia coli* compared to the other specimens. The findings of this research demonstrated the significance of chemical modification in resolving the antibacterial activities of

the metallic substrate and may provide fresh ideas for the production of medical equipment with built-in antibacterial properties. In this research, Ti metal coatings having built-in antibacterial properties were created by functionalizing silanized materials containing bioactive chemicals. The metallic substrates' free nucleophilic amino group and the QASs' reactive groups reacted to chemically bond the QASs under investigation, notably GTMAC, AEMAC, and AUTEAB, to the Ti-APTES specimen. In specific, the Michael additional step interaction among the amino group and the terminal double bond existing in the QASs allowed AEMAC and AUTEAB to be attached to the plates, whereas the ring-opening response among GTMAC's epoxide features and the amino group of Ti-APTES allowed GTMAC to be grounded to the exterior of the identical specimen. The natively occurring OA in the halogen-free Ti-OA sample was created by simply reacting the OA's carboxyl activity using the dimethylamino functionality disclosed on the TI-DAPTES specimen to produce the matching ammonium salt (Figure 6).

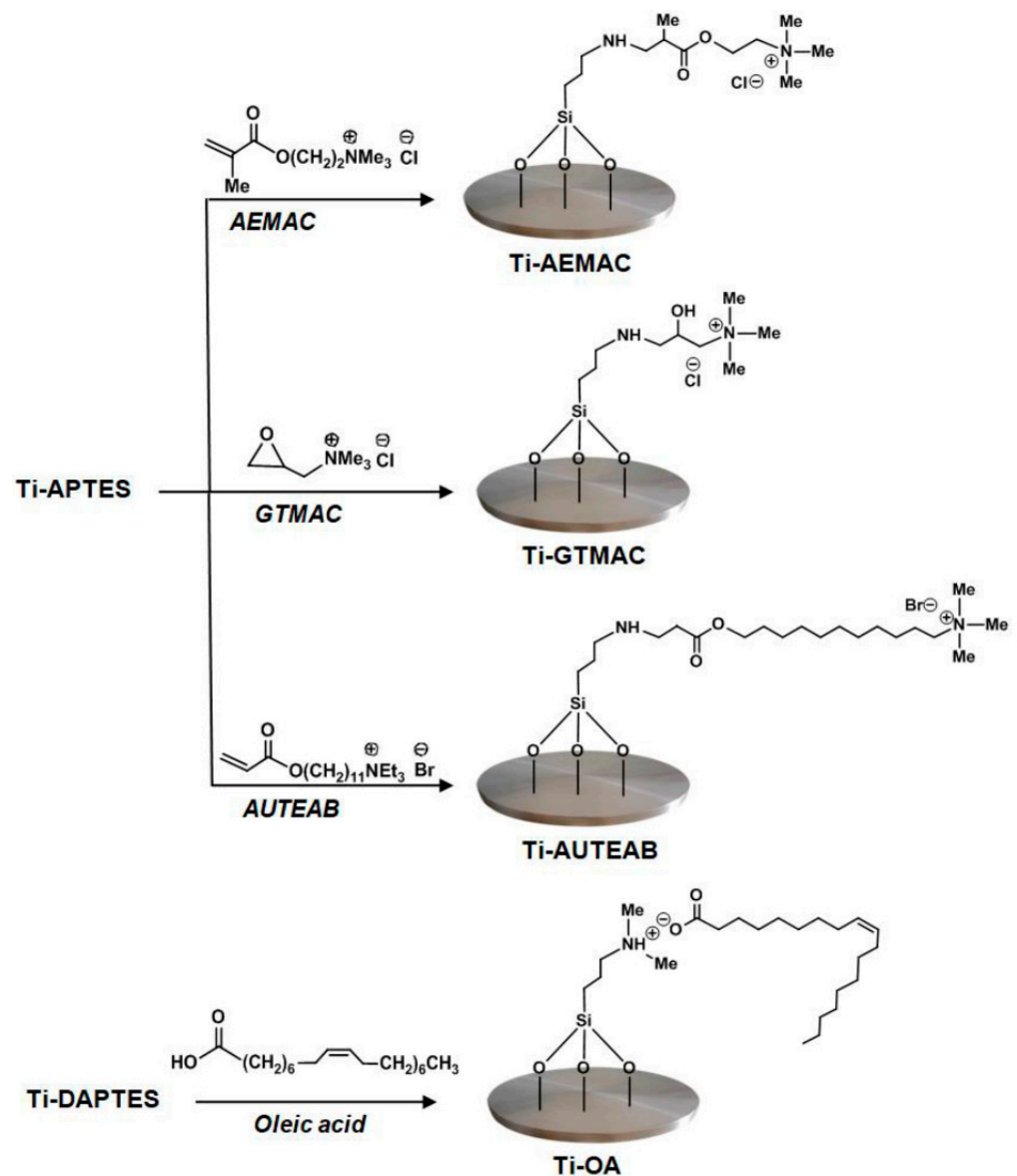


**Figure 6.** Diagram illustrating the synthetic pathways for functionalizing the surface of Ti. Reprinted with permission from [68]. Copyright 2021 MDPI. Distributed under Creative Commons Attribution-based license (CCBY 4.0).

After the research, FTIR studies verified the efficiency of the functionalization processes (Figure 7). Quaternary ammonium-functionalized specimens derived from Ti-APTES exhibit broadband at  $3000\text{--}2800\text{ cm}^{-1}$  attributed to the tension of the presented amine salt along with more peak intensity, in comparison to the Ti-APTES specimen, at  $2970\text{--}2960\text{ cm}^{-1}$ , caused by the C-H stretching of alkane functionalities (Figure 7). The Ti-GTMAC specimen exhibits two extra peaks at  $2750$  and  $1390\text{ cm}^{-1}$ , which were attributed to the alcohol function that was retained in this specimen following the opening of the epoxide group's ring. Owing to the C=O bond of the ester functionality, the Ti-AEMAC and Ti-AUTEAB T specimens exhibit a signal at  $1735$  and  $1730\text{ cm}^{-1}$ , correspondingly. Additionally, owing to the bending of C-O groups, these specimens exhibit maxima at  $1135\text{ cm}^{-1}$  for Ti-AEMAC and  $1130\text{ cm}^{-1}$  for Ti-AUTEAB.

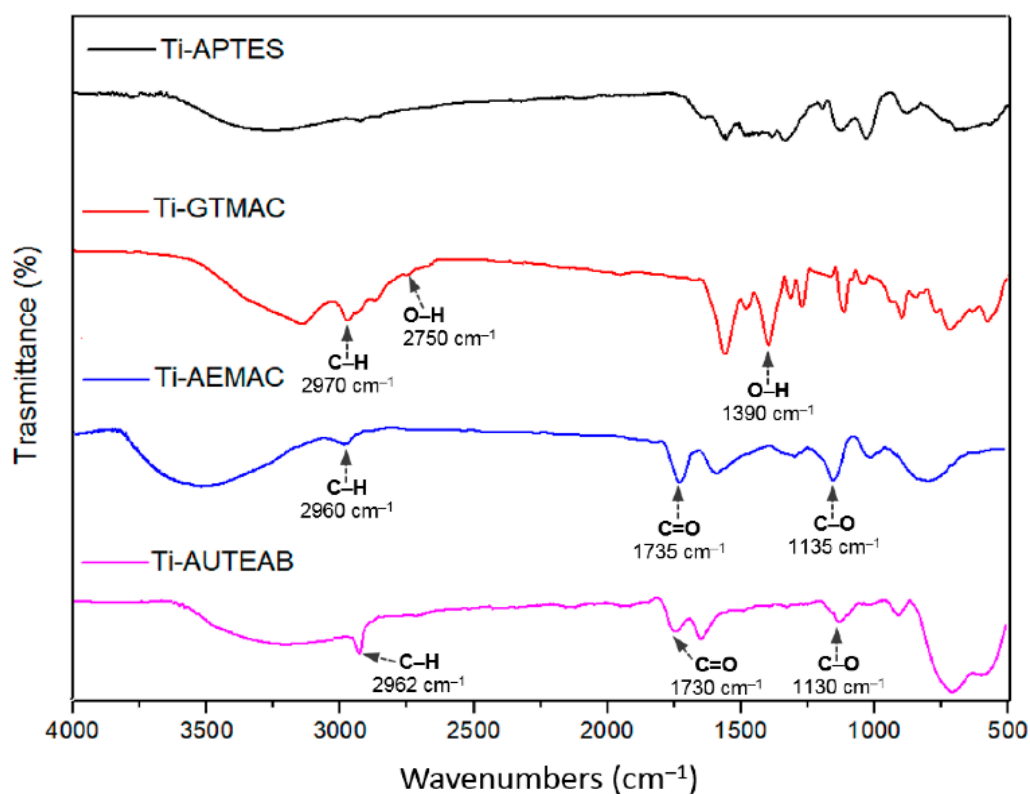


**Figure 7.** FTIR spectrum of Ti-AEMAC, Ti-GTMAC, and Ti-AUTEAB specimens, relevant with Ti-APTES specimens. Reprinted with permission from [68]. Copyright 2021 MDPI. Distributed under Creative Commons Attribution-based license (CCBY 4.0.).

Furthermore, all the materials under investigation had Wenzel contact angles that were consistently lower than 90 degrees when water drops were applied to the metallic top layer, showing that the coatings were hydrophilic (Figure 8). In comparison to the unprocessed specimen (contact angle of  $71.39^\circ$ ), the Ti discs treated with NaOH were significantly less alkaline, having a surface contact area of only 24.65. In comparison to the activated specimen Ti-OH, the specimens covalently to ammonium salts exhibit a distinct wettability behavior and a more hydrophobic characteristic. The contact angles for the Ti-AEMAC, Ti-GTMAC, Ti-AUTEAB, and Ti-OA samples are  $56.03^\circ$ ,  $63.02^\circ$ ,  $88.51^\circ$ , and  $87.50^\circ$ , correspondingly. The inclusion of a lipophilic alkyl chain in both of the functionalized specimens, Ti-AUTEAB and Ti-OA, could explain the lower hydrophilic nature seen for both materials. The shape of the interfaces and their inhomogeneities, which have an impact on the contact between the liquid and the substrate, determine the perceived static contact angle [69–72].

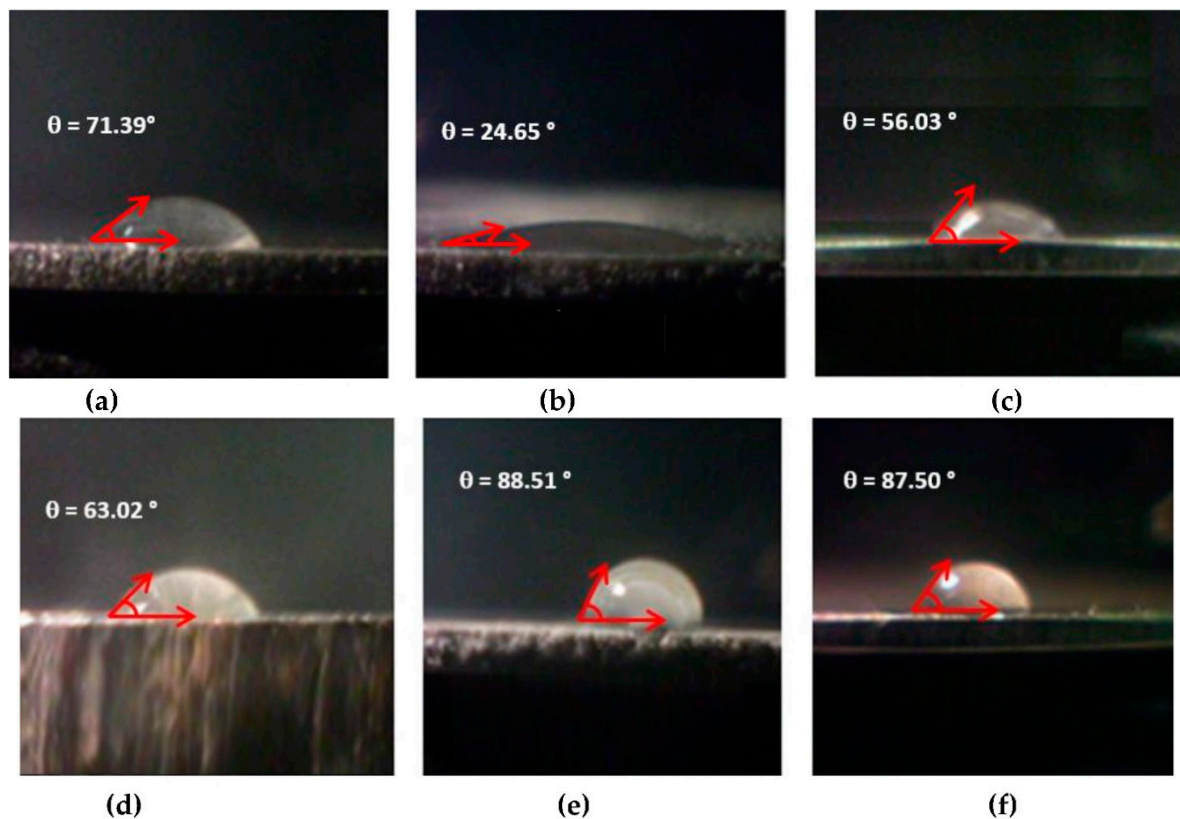


**Figure 8.** CA of  $\theta_w$  and  $\theta_Y$  of (a) Ti, (b) Ti-OH, (c) Ti-AEMAC, (d) Ti-GTMAC, (e) Ti-AUTEAB, and (f) Ti-OA specimens. Reprinted with permission from [68]. Copyright 2021 MDPI. Distributed under Creative Commons Attribution-based license (CCBY 4.0.).

### 3. Surface Modification Techniques for Biomedical Metals and Alloys

The necessity for innovative medical gadgets is increasing daily as a result of ongoing medical advancements, which have expanded the use of implantable devices. Regrettably, several events, such as surface-mediated activated thrombus, complement cascades, and device-centered infections can be induced by blood-contacting medical equipment, leading to a significant risk of refusal [73–78]. Tissue-contacting implants have the potential to cause bioinks “stress cracking,” fiber capsule development, localized implant-associated inflammatory, phagocyte-mediated oxidizing, and implantation degeneration. These result in decreased efficiency and inadequate device interaction with the neighboring structures. This has rendered it necessary to modify the hydrophilicity, wettability, barrier properties, and other surface functioning aspects of such biomaterials. The main process in the interface between biomaterials and organs is the sorption of proteins to the interface of the biocompatible material. Interface hydrophilicity, wettability, and surface charge can all be altered to alter the degree and nature of this sorption. The exterior of biomedical alloys made of SS, Ti, and Co usually experiences the first signs of deterioration. It has been demonstrated that raising the hydrophilic nature of a substance enhances its general bioactivity. Many surface modification technologies, including plasma treatment, laser treatment, PVD, several other coatings, and so on, are being used to overcome these challenges. Therefore, an appropriate surface modification strategy should be applied in order to enhance or enhance any of such materials’ attributes (particularly rust and impedances as well as bio-compatibility). The scientific studies on biomedical implant surface modification that have been released in the Web of Science Cluster during the past three years are additionally summarized in Figure 9. Over 1700 of the more than 2000 publications are involved with oxidation and corrosion characteristics, and approximately 200 and more documents, respectively, are devoted to strengthening biocompatibility and

antibacterial characteristics, indicating these are the crucial variables for strengthening the biomedical outcomes of Ti and Ti alloys, as exhibited in Figure 9. By applying Sida Acuta, Aloe Vera, and Terminalia Arjuna gel to various polymers, Shrivastava et al. [79] studied the surface alteration of polymers used in biomaterials. Their findings demonstrated that depositing these substances onto the interfaces of polymeric biomaterials may greatly lower their hydrophilic nature. Contact angle (CA) measurement was used to investigate the specimens' hydrophilicity modification. After the specimens refused to exhibit sufficient adhesion to cover when introduced under pressure by a flow apparatus that mimics the inner physiological circulation, they were treated with plasma. Plasma processing resulted in another decrease in the contact angle and high adherence of the layer to the substrates.

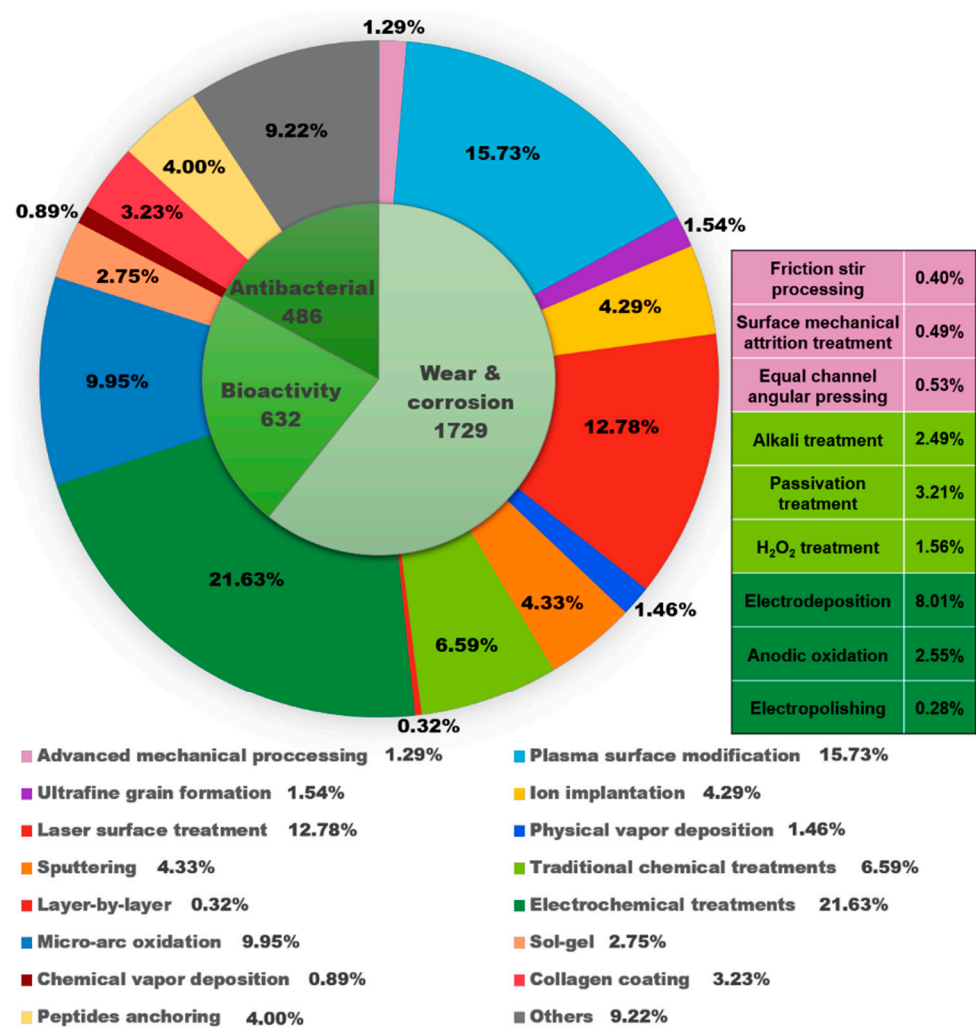
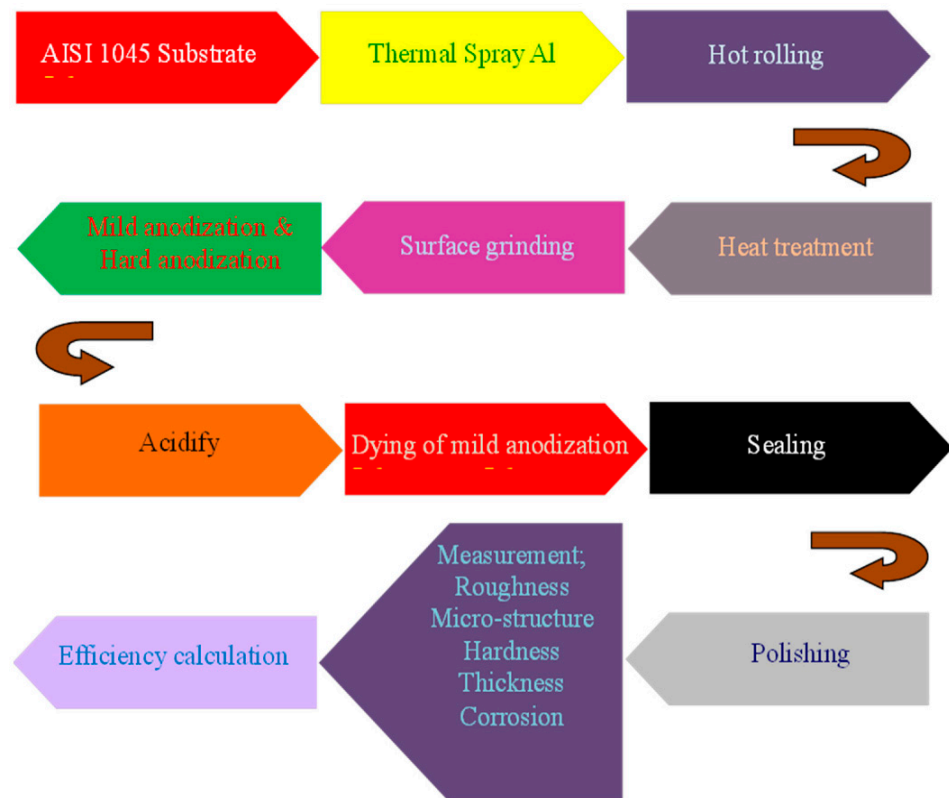


Figure 9. Diagrammatic representation of the analytical findings from three-year-old Web of Science Core Collection academic publications on the subject of surface modification of Ti alloys. Reprinted with permission from [80]. Copyright 2021 MDPI. Distributed under Creative Commons Attribution-based license (CCBY 4.0.).

### 3.1. Thermal Spraying

With the use of coatings, thermal spray is an efficient approach to increase abrasion resistance and bio-compatibility. Micrometers to many microns are the diameter span. High-speed oxygen fuel blasting, flame spray coating, plasma splashing, and other techniques comprise the principal thermal spraying techniques. These techniques may offer protection against corrosion, which is advantageous for biomedical purposes. The temperatures utilized in plasma spraying range from 2700 to 11,700 °C. Plasma arc heat is a common

source of energy for this technique. At these temperatures, metal and ceramic powders may dissolve, which can be utilized to create and deposit a range of coverings. In order to cover the alloy surfaces with plasma at rapid velocities, the source components are warmed or molten. In an experiment, the exterior properties of AISI 1045 intermediate carbon steel were improved by Chiang et al. [10] using two mass-produced commercial techniques, thermal spraying and anodization, for usage in unique devices or goods. The superficial qualities of carbon steel were significantly enhanced by the anodic layer. The carbon steel interface underwent a series of procedures to improve the integrity of the anodized coating, including sandblasting, coating the aluminum film, annealing, hot press, washing, polishing, and buffing. This study presented an anodization procedure to improve the resistance to corrosion, toughness, color variety, and electrical rigidity of carbon steel surfaces [81,82]. The surface's toughness, surface smoothness, coloration, and resistance to corrosion all increase, increasing between 170 and 524 HV and 1.26 and 0.15  $\mu\text{m}$ , respectively (from corroded to protection toward corrosion). The research on electrochemical corrosion on AISI 1045 steel surfaces having hard anodized films revealed that they had reduced corrosion current densities ( $105.9 \text{ A/cm}^2$ ) and greater impedances (9000 ohm) in HCl gas than bare AISI 1045 steel surfaces ( $104.2 \text{ A/cm}^2$  and 150 ohm). Figure 10 shows the relevant experimentation process.



**Figure 10.** Flowchart outlining each step of the research. Reprinted with permission from [10]. Copyright 2021 MDPI. Distributed under Creative Commons Attribution-based license (CCBY 4.0.).

The thick anodic coating on thermally coated Al/AISI 1045 carbon steel is depicted in Figure 11. In this image, the curled aluminum coating that had been coated is also visible. This coating prohibits the electrolyte from passing down the interface to the carbon substrate material. Figure 11a demonstrates the tough anodized coating's continued presence of numerous pores and flaws, whereas Figure 11b demonstrates the morphology of AISI 1045 carbon steel following 5% nitric acid + 5% alcohol solution etching and aluminum following 5% NaOH solution etching visibility. It is evident that both the hard anodized layer and the coated aluminum have numerous flaws: however, the hard anodized layer possesses a

greater quantity. Furthermore, the anodic coating's exceptional toughness and corrosion resistance are adequate to safeguard the exterior of carbon steel. A fine photomicrograph of the thermally sprayed aluminum over the hard anodized surfaces of an AISI 1045 carbon steel substrate is shown in Figure 11c. Following rolling, the aluminum spray had a layer of around 250  $\mu\text{m}$ . Following hard anodizing, the aluminum spray devoured 75  $\mu\text{m}$  of the original depth and expanded into a 175  $\mu\text{m}$  hard anodized layer. The overall film's width expanded by nearly 100  $\mu\text{m}$ , or 133%, in-depth. This resulted from the volume increase brought on by the anodized coating's cell architecture.

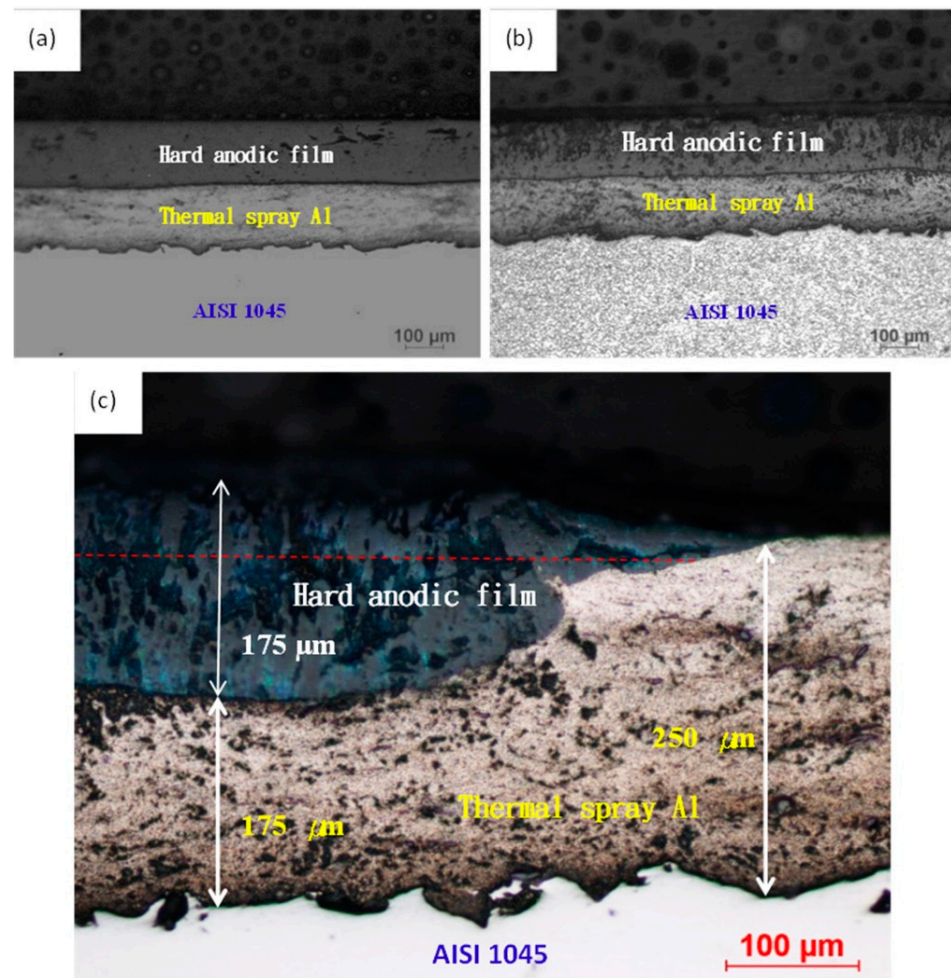


**Figure 11.** Following hard anodizing, optically micro-scans of thermally sprayed Al over AISI 1045 are shown in (a) prior etching, (b) post etching, and (c) a rather enlarged perspective. Reprinted with permission from [10]. Copyright 2021 MDPI. Distributed under Creative Commons Attribution-based license (CCBY 4.0.).

Similarly, Blum et al. [13] investigated a novel biologically generated coating used on substrates made of Ti alloy. Nanocrystalline HA was created and turned into an organic solution using a cheap feedstock of fish bones. Next, a high-velocity suspension flame spray method was used to create the covering. The suspending spray process enables the manufacture of fine and thick coatings with thickness values in the range of 23–33  $\mu\text{m}$  and roughness values in the range of  $R_z = 9\text{--}11$   $\mu\text{m}$  fulfilling the biomedical criterion. Additionally, the coverings demonstrated adequate chemical stability as observed by the minimal degradability behavior they exhibited after being submerged in SBF medium for up to 4 weeks. Throughout the specimen processing for nanoscale imaging, slicing, immersing, and refining procedures revealed no evidence of the HA covering spalling. The

coverings on flat specimens and rods contained some vertical fissures. On the TAN rods and demonstration bolts, though, the spray technique was significantly optimized, resulting in the fabrication of a thick, evenly distributed, and crack-free  $\beta$ -HA covering. It illustrates how the spray method may be modified to work with actual medical equipment. The *in vitro* analysis shows that the composite has adequate biocompatibility since it generated a bioactive stratum primarily constituted of HA and a tiny amount of  $\beta$ -TCP stage. The pH value seen following 4 weeks of exposure to SBF was equivalent to physiological pH standards.

Furthermore, utilizing the suspension high-velocity oxy-fuel (SHVOF) thermal spray method with 50 and 75 kW flame output, Bano et al. [12] created phosphate bio-glass (PBGs) films. The 50 kW film was significantly wider (24.6  $\pm$  2.3  $\mu$ m) than the 75 kW covering (16.0  $\pm$  3.4  $\mu$ m), but the 75 kW covering was rougher ( $R_a$  = 3.6  $\mu$ m) than the 50 kW covering ( $R_a$  = 2.7  $\mu$ m). The 75 kW covering displayed increased deterioration and ion discharge ratios as a result of the coarser interface. The preliminary glass composition had Q1 (phosphate tetrahedra having one oxygen) and Q2 (phosphate tetrahedra having two-bridging oxygen) components, and Raman's examination also showed compositional alterations. Furthermore, the coverings revealed a decrease in Q2 entities and an increase in Q1 and Q0 entities (phosphate tetrahedra having no oxygen), which resulted in slower rates of deterioration and altered ion discharge patterns in the glass covering in comparison to the original glass.

### 3.2. Glow Discharge Plasma

The interfaces of biomaterials and the associated implants are also modified by glow discharge plasma, which falls under the genres of plasma surface modification, deposition, and polymerization [43,81–88]. Native oxides on the substrates can be cleaned and eliminated. Glow discharge plasma can thus operate at a range of nanometers. This method creates an ionized gas, which indicates the type of substance being collected, in an ultra-high vacuum and a significant potential difference (1 kV with continuous or intermittent currents) across the respective electrodes. In an experiment, using the Radio-Frequency Chemical Vapor Deposition (RFCVD) technique on a NiTi alloy that had been oxidized under glow-discharge circumstances, Witkowska et al. [89] researched a short-term modification through low-temperature oxygen plasma that was suggested as an example of a technique for shaping the topographic features and surface area of the outer amorphous carbon coating. The molecular constitution of the upper layer's outer region was changed by this procedure. The interface hardness at the nanoscale also showed a small rise. Whereas the interface free energy fell by roughly 11%, it was found that the contact angles increased by around 20% for water and 30% for diiodomethane. The outcomes suggest possibilities for its usage in therapeutic purposes since they reveal that even brief interaction using low-temperature plasma could change the surface characteristics of the carbon covering. Microscale assessments of surface morphology (Figure 12) revealed an elevation in surface hardness following the hybrid procedure; although, the surface hardness at the nanometer was comparable to the NiTi alloy's original conditions. At the microscopic level, the oxygen plasma marginally smoothed the substrate in comparison to the specimens that had an a-C:N: H + TiO<sub>2</sub> coating prior to processing. Surface morphology was enhanced by plasma therapy at the nanometer, but the effects were substantially less. The majority of scientists found that plasma causes certain carbon materials such as fibers and nanotubes to have more surface flaws and hardness metrics. They also suggest that a prolonged therapy period may have the opposite impact, such as smoothing the texture [90,91].

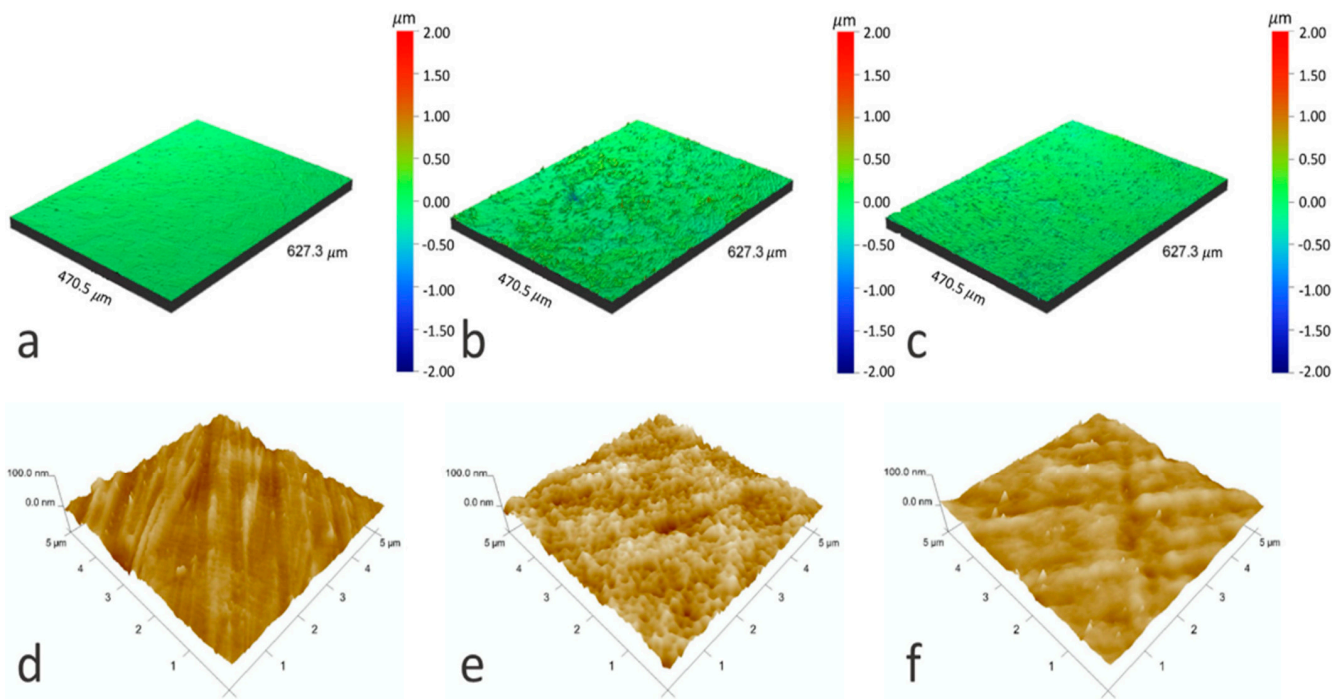


**Figure 12.** Photographs of the NiTi alloy texture taken with an optical profilometer (a–c) and an atomic force microscope (AFM) show the exterior in its initial condition, (d) AFM image of the plain metallic surface showing no fissures, (e) AFM images showing several corrosion pits and peaks (f) AFM images showing less amount of corrosion pits and peaks upon glow-discharge oxidation and RFCVD procedure. Reprinted with permission from [89]. Copyright 2021 MDPI. Distributed under Creative Commons Attribution-based license (CCBY 4.0.).

Yuvaraj et al. [92] used a DC moderate temperature plasma-based approach to successfully incorporate nano-carbon onto the interface of chemically generated nano-HA. It was found that HA's surface-integrated nano-carbon particulates have an overall particulate diameter of around 2–3 nm. Additionally, the high-resolution-transmission electron microscopy (HR-TEM) pictures showed that HA had a single-phase hexagonal geometry enclosed in a shell of homogeneous nanocarbon that was approximately 9 nm thick. The regular joint committee on powder diffraction standards (JCPDS) card no. 09–432 was determined to correspond closely to the XRD results of HA during plasma spraying. A minor coating of integrated carbon, as established by HR-TEM examination, was validated by the Raman research for the carbon-included HA specimen at 900 V, which revealed maxima about 1353 and 1578  $\text{cm}^{-1}$ . The X-ray photoelectron spectroscopy (XPS) technique was used to conduct a thorough elemental study on both sheer and plasma-processed specimens. With a raise in processing voltage (900 V), a considerable decrease in oxygen was observed, and it was discovered that the integration of carbon on HA increased. The expansion of the FT-IR pattern at 1096 and 1040  $\text{cm}^{-1}$  and the lowering of the intensity at 630  $\text{cm}^{-1}$  for sheer and plasma-treated HA specimens, respectively, showed the production of novel HA clusters in SBF. The FESEM investigation, which demonstrated the development of apatite particulate with a smooth interface on the HA interface, supported the FT-IR finding. The creation of homogeneous apatite granules was better for 900 V plasma-treated HA than in the other voltages, which might be because more carbon was effectively incorporated owing to increased acetylene depletion (900 V). The results of the research mentioned allow them to infer that more research is necessary to determine whether the HA interface formed by the incorporation of nano-carbon will be useful for biomedical, biomarker, and orthopedic biomedical implants.

In a study, Ponnusamy et al. [93] investigated the molecular processes by which radio frequency glow discharge treatments (RFGDT) mediate the sanitization of biomaterial

interfaces while also fostering cell adhesion and multiplication. Dentistry biomaterials were put through the RFGDT, and oral microbial organisms, including *Streptococcus mutants* (SM), *Moraxella catarrhalis* (MC), *Streptococcus gordonii* (SG), and *Porphyromonas gingivalis* (PG), were tested for vitality. Investigated were the cell adhesion and viability of the pre-odontoblast cell line MDPC-23. Furthermore, structural analyses of physiological signaling and redox production were conducted. Dentistry biomaterials caused reactive oxygen species (ROS) after dose-dependent RFGDT depending on the chemical constitution. The RFGDT-induced reduction in microbial vitality was more pronounced in the catalase-negative (SM and SG) species than in the catalase-positive (MC and PG) species. In cell adherence tests, MDPC 23 adherence and survivability were enhanced. N-acetylcysteine (NAC) and enzyme treatment processes eliminated these reactions. Immunoassays discovered that RFGDT was followed by redox-induced downstream transcription of the laminin receptors and ribosomal protein SA. Therefore, the redox that was produced by RFGDT facilitates antibacterial effects and enhances cell responses including adherence and reproduction. Collectively, their findings offered a molecular justification for the therapeutic applicability of RFGDT in conjunction with dentistry biomaterials for restorative therapeutic trials.

### 3.3. Ion Implantation

It is a sophisticated physical surface modification technique. Ion implantation is primarily used to increase wear, resilience, and high ductility. Ion implantation has a penetration spectrum of around 1  $\mu\text{m}$ . It is a low-temperature method that accelerates ions of a single component into a rigid substrate [94–99]. Ion implantation is frequently categorized as a hybrid process that combines beam-line and plasma absorption ion implantation techniques. To prevent infection, this technique needs a vacuum. In an experiment, Huang et al. [94] studied the Ti-25Nb-3Mo-2Sn-3Zr (wt.%) (titled TLM), a category of  $\beta$ -type Ti alloy, and found that the surface mechanical attrition treatment (SMAT) technique was an efficient direction to produce nano-grained (NG) texture. It was also discovered that the attained nanocrystalline exterior was proven to advertise favorable features of osteoblastic cells. Mg, Ag, or both ions were injected onto the NG TLM interface by ion implantation procedure in this study to additionally give the alloy superior osteogenic and antibacterial characteristics. For reference, the Mg and Ag ions were also co-implanted onto a coarse-grained (CG) TLM interface. The acquired findings demonstrated that further ion implantation does not significantly modify the surface hardness and topography of the SMAT-treated surfaces, nor does it significantly affect the morphology of the beta-Ti nanograins produced by SMAT. Additionally, it has been found that the transplanted Mg and Ag ions reside as MgO and metallic Ag nanoparticles (NPs) that are densely embedded in the  $\beta$ -Ti matrix and have grain sizes of approximately 15 and 7  $\mu\text{m}$ , correspondingly. *Staphylococcus aureus* (*S. aureus*) colonization on various substrates and the primary cell attachment and activities of rabbit bone marrow mesenchymal stem cells (rBMMSCs), comprising multiplication, osteo-differentiation, and extracellular remodeling, were examined. The outcomes of the in-vitro experiments show that the Mg and Ag single-ion transplanted NG texture substantially enhances the rBMMSCs reaction or impedes the expansion of *S. aureus*, whilst the Mg/Ag co-transplanted NG texture might simultaneously improve the rBMMSCs features and impede the growth of bacteria, certainly compared to the NG substratum, and this effectivity was more prominent as contrasted to the Mg/Ag co-transplanted NG. The co-implantation of Mg and Ag ions in the SMAT-achieved nanograins in the TLM interface covering was discovered to not only permit the construction of dual-functional surfaces having excellent osteoblastic and antimicrobial capabilities but also to perform a significant part in defining the fates of rBMMSCs. Their research offered a unique approach for creating clinically useful, high-efficacy Ti-based implants.

In their research, Malvi et al. [96] created high-intensity ion implantation that was used to attach a marker in an alloy. In this innovative method, SS316L was implanted with a persistent isotope of silver ( $^{109}\text{Ag}$ ) as a marker to identify and track the material's

deterioration. The ions can penetrate deeply into the substrate of the SS316 L material despite the high-intensity ion implantation of the  $^{109}\text{Ag}$  isotope. To replicate the superficial deterioration of the implant, rapid and regular dynamic immerse studies were conducted in 30%  $\text{H}_2\text{SO}_4$  and SBF. These findings demonstrated a link involving isotopic marker leaks and substance deterioration. According to electrochemical corrosion testing, the ion-implanted samples have a comparable level of corrosion protection to the untreated samples. Cell survival on SS316 L and  $^{109}\text{Ag}$  ion-implanted surfaces did not significantly vary, according to in vitro toxicity studies. When MG-63 osteoblast cells were cultivated on SS316 L that had  $^{109}\text{Ag}$  ions transplanted into it, the synthesis of osteocalcin was significantly increased.

Akpek et al. [95] centered on the outcomes of metal vapor vacuum arc (MEVVA) ion implantation of Ag and Ti ions on textiles. The investigation was carried out in three stages to help understand this. As the antibacterial capacities of Ag and  $\text{TiO}_2$  are widely recognized, the antibacterial efficacies of Ag and  $\text{TiO}_2$  were thoroughly examined in the initial half. Following the initial series of antibacterial experiments, these medical fabrics were rinsed 30 times, and the next series of antibacterial assessments were conducted to ascertain the implanted ions' ability to adhere to substrates. The outcomes were contrasted with medicinal fabrics impregnated with nanoparticles. The next section examined the rusting and abrasion properties of polyester fabrics infused using Ag and Ti at a concentration of  $5 \times 10^{-15}$  ion/ $\text{cm}^2$ . Last, but not least, the UV protection ability of Ag and Ti ion-implanted polyester fabrics, having a concentration of  $5 \times 10^{-15}$  ion/ $\text{cm}^2$ , was evaluated. The tests revealed that the  $\text{TiO}_2$  ion-implanted polyester cloth maintained over 85% antimicrobial effectiveness following 30 cleanings. Additionally, when contrasted with an unprocessed textile, Ti ion implantation decreased a polyester textile's resistance coefficient by about 50%. Last, but not least, the polyester textile with Ag-ion implantation offered a UV resistance value of 30, which is regarded as extremely exceptional shielding. The fibers of medical textiles coated with nanoparticles are shown in Figure 13. As previously indicated, as the solvent dissipates, the nanoparticles gathered on the interface and formed physical interactions with both the substrate and one another. In contrast, the thickness of ion implantation was typically around 0.1–2  $\mu\text{m}$ , based on the substrate, the kind of embedding component, and its kinetic energy. Therefore, at depths of 50–100  $\mu\text{m}$ , the modifications to the requirements could be seen. As a result, the textile materials' capability to expand and stretch remains unchanged because the impact of interface modification only affects the material's exterior and not its bulk.

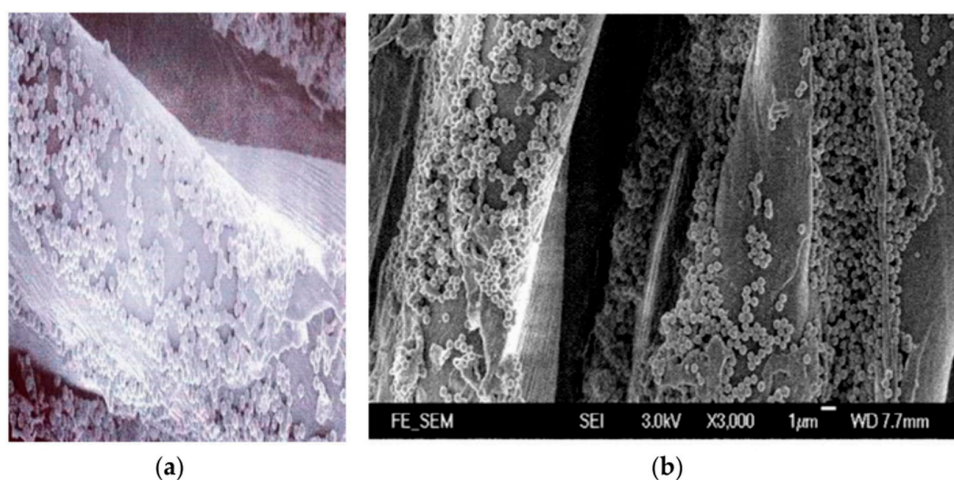


**Figure 13.** (a) Medical textile fibers coated with Ag nanoparticles. (b) Medical fabrics using  $\text{TiO}_2$ -nanoparticle-treated fibers. Reprinted with permission from [95]. Copyright 2021 MDPI. Distributed under Creative Commons Attribution-based license (CCBY 4.0.).

### 3.4. Ultrasonic Nanocrystal Surface Modification Techniques (UNSM)

In the domain of biomedical technologies, there is presently growing interest in a recently discovered UNSM technique. It can increase an alloy's wear resistance, abrasion resistance, and resistance to corrosion [100–105]. The UNSM procedure can modify the mechanical and physical characteristics down to a depth of roughly 750  $\mu\text{m}$ . Ultrasonic impacts are used in the UNSM process to create nanostructured substrates. High-frequency (20 kHz) ultrasonic waves are transmitted via a tungsten carbide tip throughout UNSM and then projected onto a specimen substrate. By precisely altering the operational variables, the UNSM is exceptional in that it can generate accurate hierarchical surface layouts. Another crucial factor is UNSM's temperature. For instance, a Co-Cr-Mo alloy generated by SLM was treated by UNSM at various temperatures. UNSM has a higher impact at hot temperatures as compared to room temperature. UNSM enhances the surface quality of the specimen and reduces its permeability, which results in enhanced biocompatibility, chemical resistance, and biomechanical qualities. Zhang et al. [97] investigated the effects of applying the heating process and ultrasonic polishing to a laser-clad Fe-based covering. In addition to ultrasonic burnishing (UB) at ambient temperature, two other mixtures of ultrasonic burnishing and thermal therapy were investigated. These were ultrasonic burnishing at a moderate temperature (UWB) and UWB combined by continual thermal treatment for a length of time (UWB/HT). Four specimens in total were created and put through an investigation. The superficial characteristics of the three differentially processed specimens were enhanced to variable levels as compared to the untreated (controlled) specimen, having the UWB/HT procedure specimen acquiring the best one. In comparison to the regulated specimen, the UWB/HT procedure reduced the hardness and permeability of the Fe-based covering by 87.86%, 65.41%, and 34.88%, accordingly. It also raised the coating's toughness. The UWB/HT sample's morphology and fatigue strength both saw significant improvements. The UWB/HT Fe-based covering additionally demonstrated the greatest fatigue rate. In conclusion, UWB/HT was thought to possess the ideal possibility of successfully treating laser cladding to superior exterior characteristics compared to the other two techniques, which was anticipated to promote the use of the laser cladding method, especially in the creation of some highly demanded products serving in harsh environments.

With respect to surface morphology, microstructure, the dispersion of tensile stress, fracture toughness, and tensile stress patterns, Dang et al. [98] examined the surface functionalization of 300 M steel produced by the ultrasonic surface rolling process (USRP). According to the data, USRP reduced surface roughness (Ra) by more least 1 magnitude (from 0.30 to 0.025 mm) with just one session. Additionally, a significant plastic distortion coating was seen at the upper surface, which increased compressive strain by about 190% and surface fracture toughness by around 17%. In USRP, it is possible to create a significant thermoplastic shear strain of 3 and a shear strain frequency of  $105\text{ s}^{-1}$  into the upper surface, which drives the formation of a dislocated tangle, walls, and cells. The USRP specimen exhibits a pronounced micro-structural development trend dominated by dislocated slippage and mechanical merging. The resilience to strong wear behavior was increased as a consequence of the excellent surface polish, strong micro-hardness, and large stiffness tensile stress. Additionally, the tensile stress increased by 3.8%, but the related yield strengths and elasticity decreased by 5.9% and 24.3%, correspondingly.

The interface characteristics of a nano-layered CrN/CrAlN coating, which was coated on the AISI D3 cold-work tool steel, were the subject of Pak et al.'s [106] research to investigate the impact of the ultrasonic peening pre-treatment. The layer was applied through cathodic arc physical vapor deposition (CAPVD). Rockwell-C and Vickers microhardness testing, potentiodynamic polarization, and pin-on-disk were used to assess the surface characteristics of the films. The findings demonstrate that the ultrasonic peening pre-treatment technique enhanced the hardenability of the untreated surface, decreased surface imperfection, and induced compression residual strain. Pre-treating D3 cold work steel materials with ultrasonic peening improved the wear resilience on the covered samples' surfaces by

a mean of 47%, with a 25% ultrasonic power producing the highest wear-resistant results. The attachment of the nano-layered CrN/CrAlN protective layer towards the substrate is also ideal (HF1 level) in the predrilled specimen to a strength of 20%. Additionally, its mean surface roughness has the least amount ( $R_a = 0.36 \mu\text{m}$ ), and its corrosion impedance was indeed enhanced by about 33.2% compared to the base-covered specimen in the 3.5 wt.% NaCl solution.

### 3.5. Physical Vapor Deposition

By altering the interface of alloy implants, physical vapor deposition (PVD) is another efficient method for enhancing the biofunctionality of biomedical implants [107–109]. PVD uses coatings to protect biomedical implants against corrosive conditions, much like the processes explored previously. PVD coverings are typically homogeneous and thick, but time consuming. Because PVD could readily regulate the Ca/Pa ratios and microstructure, Ca/Pa-based materials including HA, Si-HA, C-HA, and Mg-HA are frequently utilized in PVD. However, PVD's dissolution rate is insufficient for biological applications. Vacuum evaporation and magnetron sputtering are the two most popular PVD procedures and their operating depth limit can extend up to about  $4 \mu\text{m}$ . PVD's primary use in biomedicine is to increase materials' hardness, bio-compatibility, fatigue strength, and corrosion resistance. For instance, in their work, Oliveira et al. [99] utilized a conjugated reactor that employed the Plasma Enhanced Chemical Vapor Deposition method in conjunction with using an Ag hollowed cathode to produce silver nanoparticle-doped diamond-like carbon sheets on the interface of Ti6-Al-4V alloys to assess the flow of argon from 20 to 80 sccm and the effects of tribological properties and bio integration. The hollowed cathode's ability to provide a gradient of silver content from the substrates to the layer formed, which itself is desired in biological applications, was demonstrated by the layer thickness of the subsequent ion mass spectrometry. Through AFM, it was discovered that raising the argon circulation from 20 to 80 sccm resulted in a more acicular relieve and encouraged an increment in  $sp^3$  hybridization, which also characterizes coatings with good bonding and friction coefficients, as well as biomedical applications where the substance was confined to load-bearing and wear. The findings of in vivo testing demonstrated that silver loading in Diamond-like Carbon coatings accelerated bio-integration more quickly than in non-doped Diamond-like Carbon coatings, and they demonstrated the possibility of their use in medical prosthetic composites.

Several forms of silver (Ag)-based nanocomposite thin coatings were created by Alam et al. [110] by applying physical vapor deposition processes, addressing their synthesis, characterization, characteristics, and potential prospective commercial possibilities. Although distinguishably noticeable diameters of nanoparticles were not seen in the elevated temperature (over  $300^\circ\text{C}$ ) heat-treated composite film, suggesting that this novel-produced composite substance could be suitable for many surface coatings. The findings of the morphology investigation performed on bare Ag and nanocomposite (Ag+SiC) sheets are shown in Figure 14. Figure 14a,b show that the bare Ag film transformed into nanoparticles, which were quite enormous in dimension and structure. In contrast, the composite coating showed resistance to transforming into nanoparticles of distinctively observable size (Figure 14c,d). According to these findings, this composite substance could tolerate temperatures that are relatively greater than those required for the production of increased conventional optical coating. The coated chamber temperature in the coatings industry is over  $180^\circ\text{C}$ , in which a pristine metal coating could quickly oxidize or become nanoparticles attributed to the dominance of the covering structure's neighboring oxide layer.

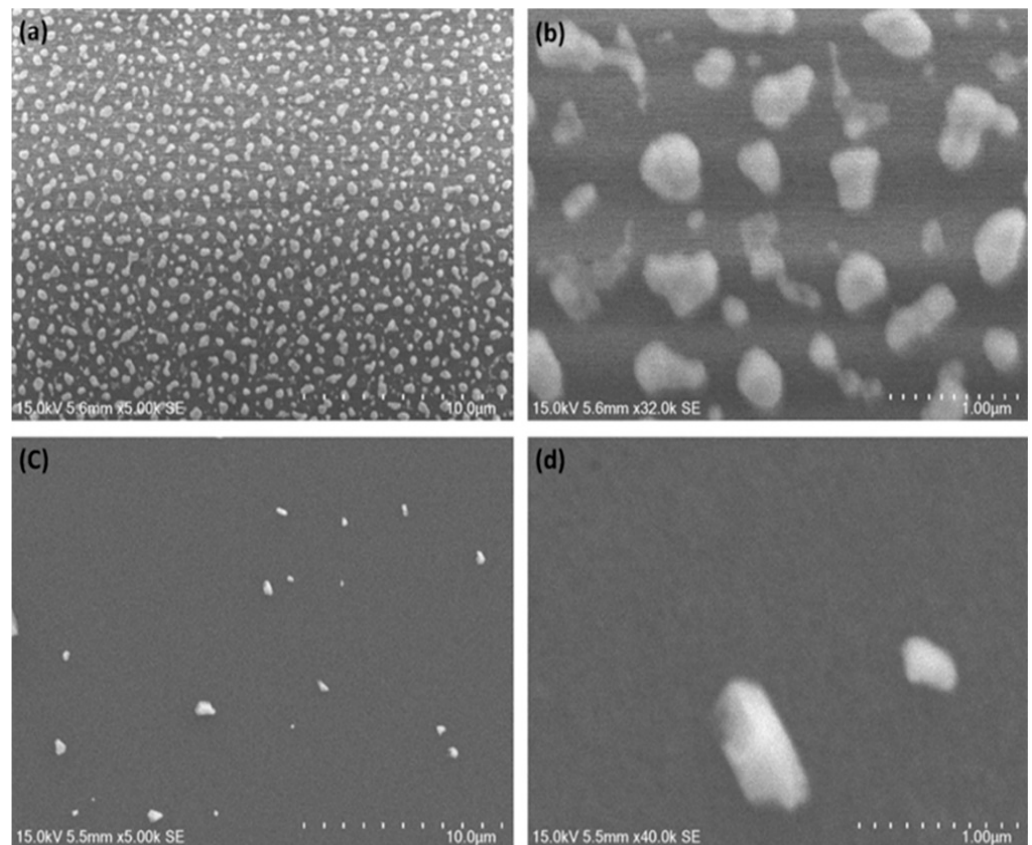


**Figure 14.** An analysis of the morphology of pristine Ag and pristine Ag with 5% SiC. Following annealing at 350 °C for 1 h, SEM pictures of an Ag thin coating were produced (see **a,b**), and an Ag + SiC composite thin coating was recorded following irradiation to the same temperature (**c,d**). Surface flaws in photos (**c,d**) could be caused by contaminants on the surface or light precipitation. Reprinted with permission from [110]. Copyright 2021 MDPI. Distributed under Creative Commons Attribution-based license (CCBY 4.0.).

Vignesh R. et al. [111] improved the surface modification of pristine Mg to make it more viable as a biodegradable substance for cardiovascular purposes. On pristine Mg substrates, sheer Fe and HA were covered. Their mechanical and biological features were examined. An Fe and HA covering on Mg enhanced its tensile rigidity by around 45 and 21%, correspondingly, from its original value of 80 MPa. For purest Mg, a maximal deterioration rate of roughly 5.4 mm/year was noted. The HA layer reduced the rate of deterioration by nearly 73%. Furthermore, galvanic corrosion increased the rate of deterioration for the Fe covering by a factor of six. All three substrates were shown to be nonhemolytic during a hemolysis experiment, and the cell vitality for untreated, Fe, and HA-covered substrates using the MTT cytotoxic testing is 96.24%, 94.8%, and 97.13%, correspondingly. Sheer Mg has no cytotoxic or carcinogenic characteristics, thus covering Fe and HA improves mechanical stability without changing their physiological characteristics. As a result, this research validates a modified Mg substrate as a useful substance for cardiovascular activities.

### 3.6. Plasma-Assisted Surface Treatments

A constrained ionized gas called plasma can have its pressure and temperature adjusted across a diverse variety. These factors allow for the identification of low or high-pressure plasmas as well as hot or cold plasmas. Plasmas are created by separating electrons from their parent atoms or molecules, which are still in an ionized state. An electric field is typically applied to a neutral gaseous precursor in order to produce and maintain low-

temperature plasmas for industrial purposes. As a consequence of the interplay of the gas with high-energy photons caused by cosmic radiation or naturally occurring radioactive deterioration, any area of a neutral gas constantly includes some molecules that have been dissociated into ionic species. Ions and electrons are accelerated by the supplied electric field, and when these electric charges hit the neutral organic precursors, they produce additionally charged entities and cause their disintegration. These charged particles and extremists can interact with a substrate more readily, changing the substrate's framework.

These coatings are designed to enhance the substrate's inherent qualities while maintaining its physical qualities. These plasma procedures can be used to create a variety of different components and structures, including biocompatible materials, antibacterial equipment, drug delivery, biofilms, the upcoming creation of nano bioactive components, corrosion protection lubricants, surface coating to improve tribological behavior, and others [112–117]. In rapid harvesting conditions, Okazaki et al. [72] tested three Ti-Zr alloys for biomedical compatibility. Additionally, they examined the histopathology of rats that had received long-term implants of virgin vanadium (V), Al, nickel (Ni), Zr, Nb, and Ta metals and also Ni-Ti and Ti-15V-3Al-3Sn alloys enriched in V. Utilizing rabbits allowed researchers to examine how the form of the dental implant (screw) affected morphometrical variables. Additionally, they looked at the grit-blasted Ti-Zr alloys' maximal extraction characteristics following being implanted in rabbits. Three Ti-Zr alloys—Ti-15Zr-4Nb, Ti-15Zr-4Nb-1Ta, and Ti-15Zr-4Nb—had their biological stability evaluated, and neither regular nor rapid removal had any unfavorable consequences. Above the sheer V and Ni implants, no bone developed. Mature bone encircled the Al, Zr, Nb, and Ni-Ti implantation. In comparison, the new bone created around Ti-Zr and Ti-6Al-4V alloys, in contrast to the bone created around Ti-Ni, increased Ti alloys that appeared to be thin. The Ti-15Zr-4Nb-4Ta dental implant's thread part promoted bone resorption at the same rate as a single layer. The implant duration in rabbits improved exponentially along with the maximal withdrawal stresses of the grit and shot-blasted Ti-Zr alloys. Shot-blasted Ti-Zr alloy shafts had a lower pull-out strain than grit-blasted ones. The Ti-15Zr-4Nb alloy interface that had been grit-blasted using  $\text{Al}_2\text{O}_3$  particles had the identical surface roughness (Ra) and area ratio of remaining  $\text{Al}_2\text{O}_3$  particles as the grit-blasted Alclassic stem surfaces. It was made clear that the Ti-15Zr-4Nb alloy may be employed to create the stems of prosthetic hip joints, as seen in Figure 15.

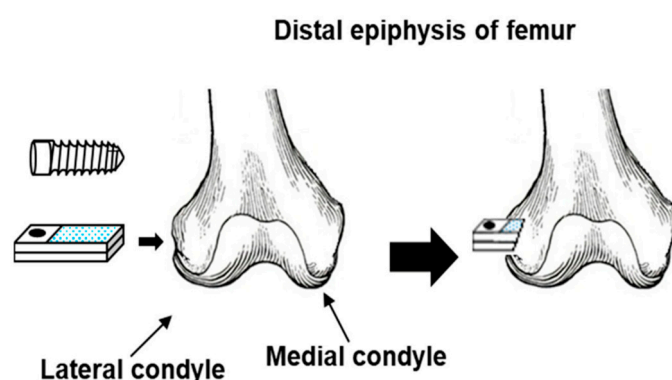


**Figure 15.** Illustration in diagrammatic form of rabbits' femurs after implantation. Reprinted with permission from [72]. Copyright 2021 MDPI. Distributed under Creative Commons Attribution-based license (CCBY 4.0.).

Figure 16 displays optical microstructures of the undecalcified bone segments stained using bare V, Ni, Al, Zr, and Nb metals and Ni-Ti alloy 52 weeks after transplantation. Surrounding the bare V and Ni implantation, no bone was developed, whereas a thin coating of new bone developed around the Al implant. Mature bone encircled the Al, Zr, Nb, and Ni-Ti implants.

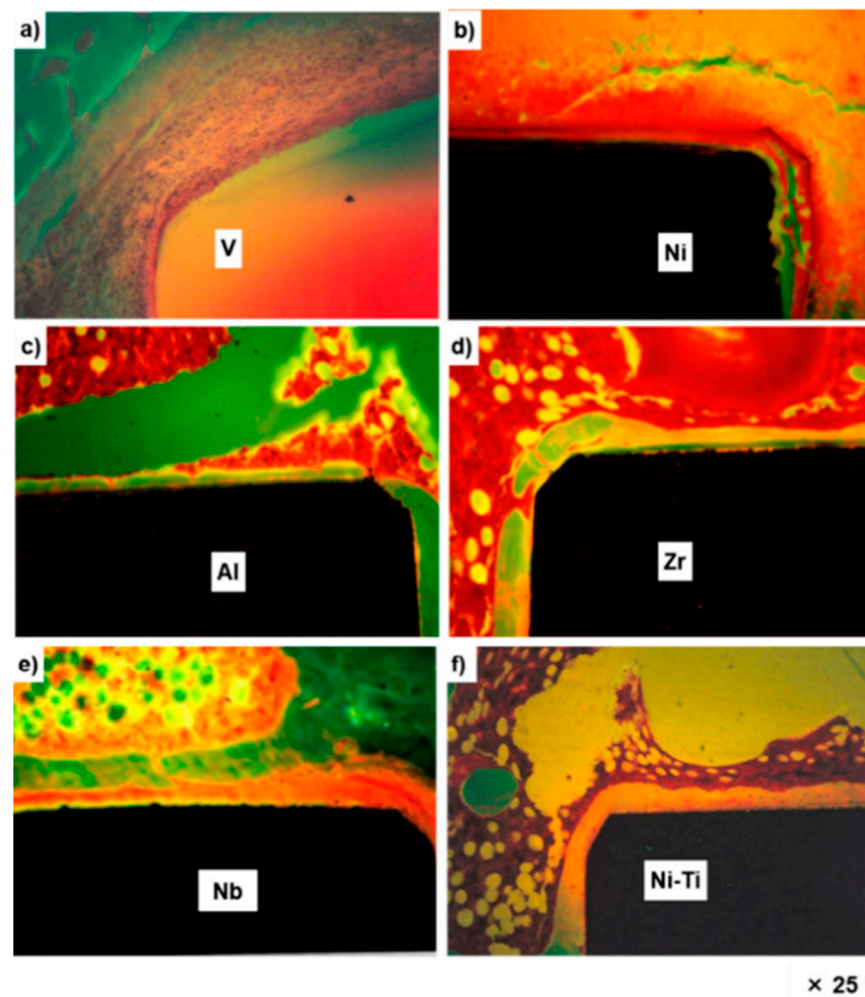


**Figure 16.** Following 52 weeks, optical microstructures of bone developed surrounding bare V, Ni, Al, Zr, and Nb metals and Ni-Ti alloy (a–f). Metal implants are visible as black shadows. The transplanted sample for V was discarded while the section was being prepared. Reprinted with permission from [72]. Copyright 2021 MDPI. Distributed under Creative Commons Attribution-based license (CCBY 4.0.).

Additionally, the medical device sector currently uses some of the plasma-based surface treatment approaches that Bencina et al. [22] discussed, while others are still in the early stages of research and/or commercialization. The most widely used plasma therapy methods are centered on plasma covering technology, but there is also a considerable possibility for treating metallic surfaces directly with gaseous plasma. Biomimetic surface-based methods have a lot of possibilities because it has been demonstrated that they can promote desirable cell-type adherence and growth while inhibiting bacterial adherence on the nanoscale scale.

### 3.7. Photon Irradiation

Despite one major benefit, the ability to modify very tiny and confined surface areas, photon irradiation surface modification is employed in several biomedical applications [88,118,119]. Based on the intensity selected, the processed polymer substrate may experience ablation or physical and chemical modifications. As an illustration, UV laser irradiation in air, water, and ozone causes the production of oxygen functional groups such as C-O and C=O on a PP surface. The production of contact lenses is an intriguing use of photon irradiation. As the hard exterior of contact lenses produces physical distress, regulated irreversible surface softness of thermoplastic materials without compromising

the bulk qualities that might be obtained by CO<sub>2</sub> laser irradiation provides a special benefit [120–122]. Several materials might undergo chemical or physical changes when exposed to excimer laser light. To quickly increase pressure and disrupt connections at the surface of the material, the method uses brief, powerful bursts of light. The bond breakdown raises the local particulate concentration in a limited region (i.e., pressure). The shockwave that results from the concomitant quick increase in pressure rapidly discharges material pieces as particles and gases. Because there is minimal extra heat that is passed to the adjacent object during the procedure, substances including biological tissues, ceramics, composite, crystalline, glass, sheets, and polymers could all benefit greatly from its utilization. The most effective way to treat materials utilizing excimer lasers is typically to use a suitable mask put into the beam. The images of the mask trends are then projected onto the work item via a lens in a typically reduced form. The intricacy of the imaging optical equipment could be determined by the necessary image quality and dimensions. For extremely precise tiny part milling, multi-component lenses could provide images having a precision of 1 µm. In addition to surface morphology, photochemically induced surface reactions employing excimer laser as UV emitters could change the surface properties of polymers. Polar surface functional groups could be produced through regulated surface photo-oxidation, changing the surface's hydrophilicity and hydrophobicity. The modified material's bio and hemocompatibility may then be impacted by this [123]. To improve cytocompatibility, Tavakoli and colleagues first examined the possibilities of modifying polymer surfaces utilizing lasers. Additionally, polymer surfaces were treated with excimer lasers to enhance ensuing adherence for adhesion binding. Implantable grade polyester ether ketone (PEEK) that has had surface modification with an ArF laser change surface morphology to create distinct surface characteristics, which affect the type of osteoblast cell attachment, conformation, and alignment onto the processed PEEK specimens. In the acetabular portion of a hip replacement, PEEK is generally researched as a possible substitute for ultra-high molecular mass polyethylene. Due to PEEK's high wear endurance, aseptic slippage could be prevented by reducing wear particulates at the articulation interface. The polymer's strong rigidity and hardness are further characteristics. Furthermore, the substance is simple to sterilize due to its great resilience to chemicals, heat, humidity, and cosmic rays. PEEK's biocompatibility is influenced by the surface's proximity to the physiological surroundings. The PEEK surface modification and morphology are altered by the excimer laser treatments, which also affects the polymer's therapeutic efficacy. The transplantation of acrylamide (AAm) and 2-hydroxyethyl methacrylate (HEMA) to the interface of a thermoplastic material, such as ethylene propylene rubber (EPR), could be started using a CO<sub>2</sub> pulse laser as a generator of IR radiation. The mounted biomaterial with poly(AAm) and poly(HEMA) exhibits a fractal architecture. Due to the availability of both hydrophilic and hydrophobic areas on fractal surfaces, biomaterial treated with photon irradiation is particularly well suited as a biomaterial [124].

### 3.8. Ion-beam Modification

Ion beams are utilized to alter the hydrophilic/hydrophobic nature, bioadhesion, and other properties of polymer surfaces. The ion beam energy and beam concentration have a considerable impact on the pattern created on a polymer substrate. The endurance of the altered polymer interface (as opposed to the surface modified with plasma, when surface "reconstruction" occurs) is a notable benefit of ion-beam modifications. Based on the kind of ions utilized, the kind of polymer, the ion energy, and the beam intensity, several sorts of biochemical processes, including oxidation, reduction, crosslinking, ion implantation, removal of hetero atoms, and ring formation, take place during in the ion beaming of various polymers. The conclusion of the ion beam alteration depends significantly on the composition of the polymer. The identical processing of various polymers may give rather varied effects. As a dentistry biomaterial formed by vacuum low-temperature ejection of hydrogenated–dehydrogenated Ti powder combined with graphite flakes, Sugar et al. [125] investigated the surface modification of a novel form of Ti–graphite

composite. By introducing varying degrees of incident energy from the fiber nanosecond laser operating at 1064 nm wavelength, two testing substrates were created. The quality of the machined surfaces was evaluated, and surface roughness variables were measured using confocal laser scanning microscopy and contact profilometry. Through the use of SEM and XRD investigations, the phase and chemical constitution were thoroughly assessed. In order to examine the effects of the laser treatment variables employed on the cell's cultivation and osteo-differentiation, *in vitro* assays utilizing human mesenchymal stem cells were carried out. The bioactivity analysis indicates that in comparison to the exterior characteristics with deleterious kurtosis correlation, leptokurtic distribution curve, and lower peaks spacing, the exterior account with optimistic kurtosis coefficient, platykurtic distribution curve, and a significant increase in spectra spacing demonstrated superior bioactivity. Figure 17 depicts the exploratory configuration of the device, which includes the major components of the laser devices, including the pulse method system, illuminating the workstation, the discharge, the laser scanner outcome, the Z-axis measuring probe, situating the CCD camera, the cooler, the fixture for placing samples, the nozzle of protecting gas, the work surface, and laser beam radius.

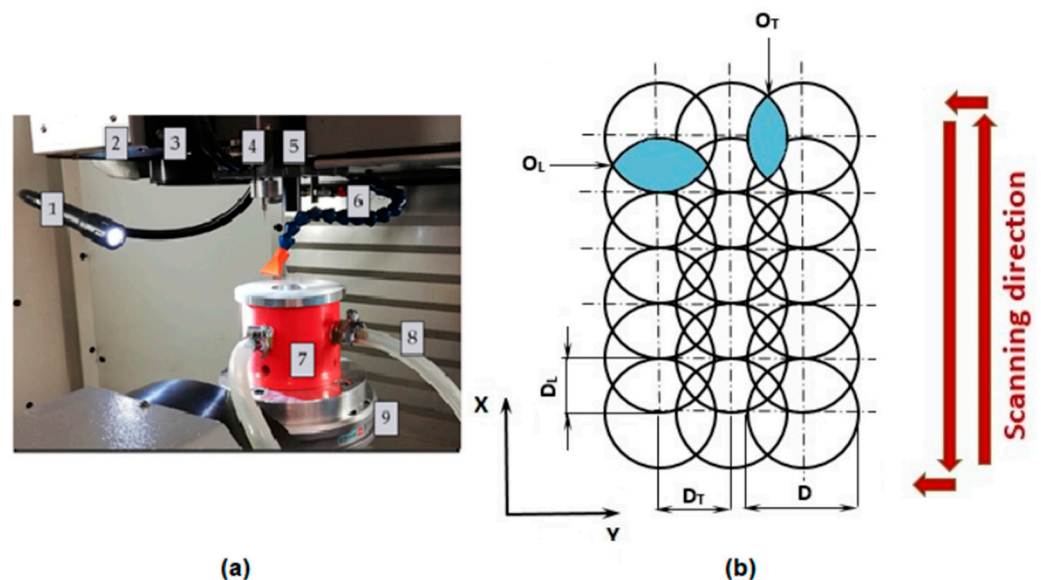


**Figure 17.** Experiment initiation. (a) The primary components of a laser system: a pulse mode design, Illuminating the workstation, first 2—exhaust, 3—output from a laser scanning, the Z-axis measurement probe, Setting the CCD camera, the chiller, the attachment for placing samples, (b) the shielding gas input, the work surface, and the laser beam width  $D_T$ —transverse pulse distance (m),  $O_T$ —transverse pulse overlap,  $O_L$ —lateral pulse distance (m), and  $D_L$ —lateral pulse overlap. Reprinted with permission from [125]. Copyright 2021 MDPI. Distributed under Creative Commons Attribution-based license (CCBY 4.0).

The interfaces following laser machining and the interfaces as received have different surface geometries, as shown in Figure 18. On both machined substrates, significantly fragmented wavy forms of the reprocessed and hardened material appeared visible. Surface B has a roughness that seems a little bit finer than Surface A since it was machined using a larger quantity of energy supplied to the substance ( $ET = 5 \text{ mJ}$ ). When the incident intensity is increased, the square-shaped pattern produced by the cross-hatching approach of laser beam motion can be seen. Both machined substrates showed voids with sizes varying from 1 to 5 nm when seen at a greater resolution (1500). These minute flaws were presumably caused by the melting substance interacting with the flow of the shielding gas. Due to the intense laser energy or unpredictable processing circumstances, these porosity and permeability are typically brought on by confined gases in the molten substrate. In our example, the inherent permeability of the machined substance created by powder

metallurgy and the permeability produced by laser irradiation combined to produce the ultimate shape and size of the permeability. This mixture makes it feasible to create interconnected holes on the interfaces and subsurface regions, which will encourage cell growth there.

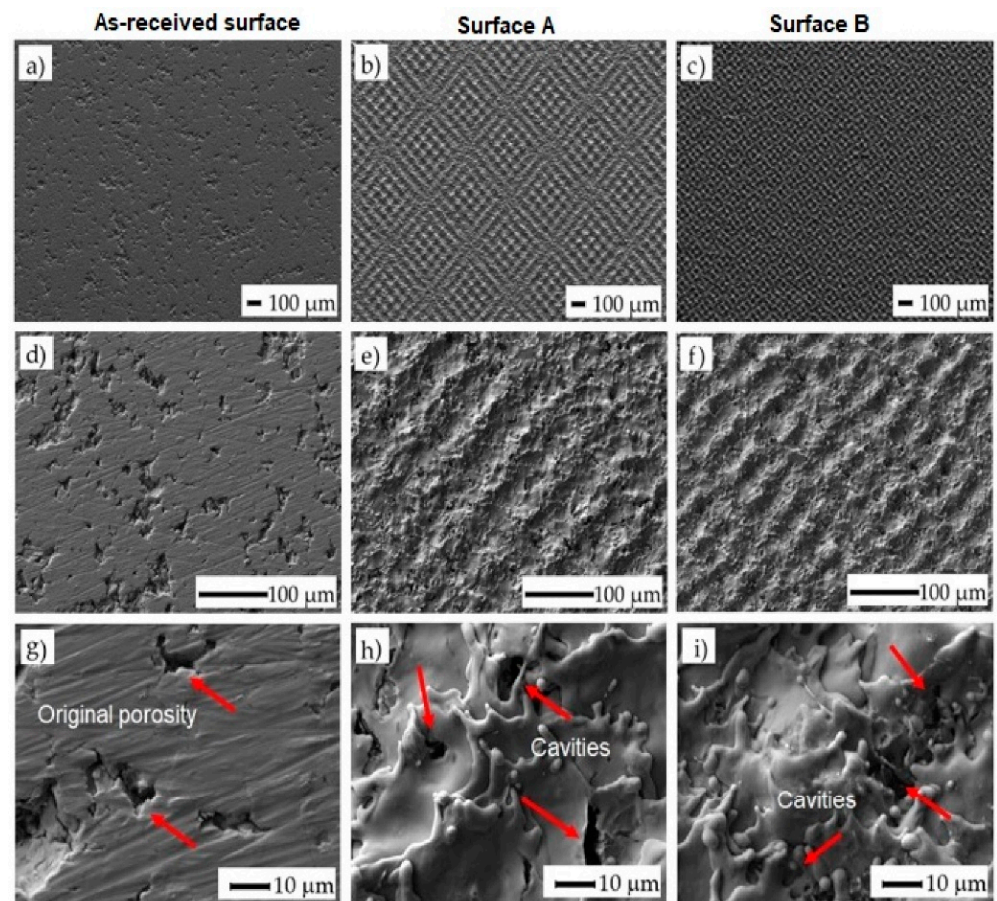


**Figure 18.** SEM illustrations of treated substrates: (a) as-received surface at a resolution of 50; (b) surface A at ET of 0.5 mJ and a resolution of 50; (c) exterior B at ET of 5 mJ and a resolution of 50; (d) surface prior to laser machining at a resolution of 250; (e) exterior A at ET of 0.5 mJ and resolution of 250; (f) exterior B at ET of 5 mJ; (g) SEM scan showing original porosity; while (h) showing greater amounts of cavities as a result of corrosive ion invasion and (i) showing reduced amount of cavities which restrict the invasion of corrosive ions on the surface of metal. Reprinted with permission from [125]. Copyright 2021 MDPI. Distributed under Creative Commons Attribution-based license (CCBY 4.0.).

#### 4. Surface Modification Coatings for Biomedical Metals and Alloys

The surface of biomedical alloys comprised of Ti, Co, and stainless steel usually experiences the initial symptoms of deterioration. Therefore, a competent surface modification methodology must be applied in order to modify or enhance any of these materials' attributes (particularly corrosion and stress resistance as well as biocompatibility) [126–131]. Implementations intend the choice of protective coatings, and the desired tensile, biochemical, and thermo qualities frequently define the coating technique and preparation methods [132–134]. The entire procedure illustrated in Figure 19 shows some significant coating qualities that are typically required of biomedical coatings, including strong biocompatibility of the intended stage and crystalline nature, acceptable coating stability, and appropriate permeability [43]. To maintain the coating's stability, it is important to make sure that the required structural properties are maintained. The several phases that could be typically distinguished in the discharge of successively packed multilayered coatings

are shown in Figure 20 (steps 1, 2, and 3) [43]. Owing to the identified limited durability of multilayer complexes and the overall reduced efficiency to maintain active molecules across the multilayers, especially in cases of robust and particular drug–polymer correlations, a maximal active agent discharge is often obtained around 24–48 h. (e.g., hydrogels). First (step 1), a quick and abrupt discharge happens as a result of the loosely adherent outermost layer degrading, showing that this phase is controlled by the decomposition processes instead of the process of diffusion. Then, a second stage could be distinguished once active agents have been depleted (step 2). Distribution is postponed at this phase because active agent deterioration surpasses discharge. In step 3, a mixture of active substance dispersion and coating deterioration releases nearly all of the preloaded active agents. Since kinematic characteristics and discharged quantities vary depending on the location of the packed sheets inside the multilayered, the multilayered filling also enables an additional discharge regulation. Whenever external surfaces are loaded, the discharged quantity increases in contrast to intermediary or inner coatings [135].

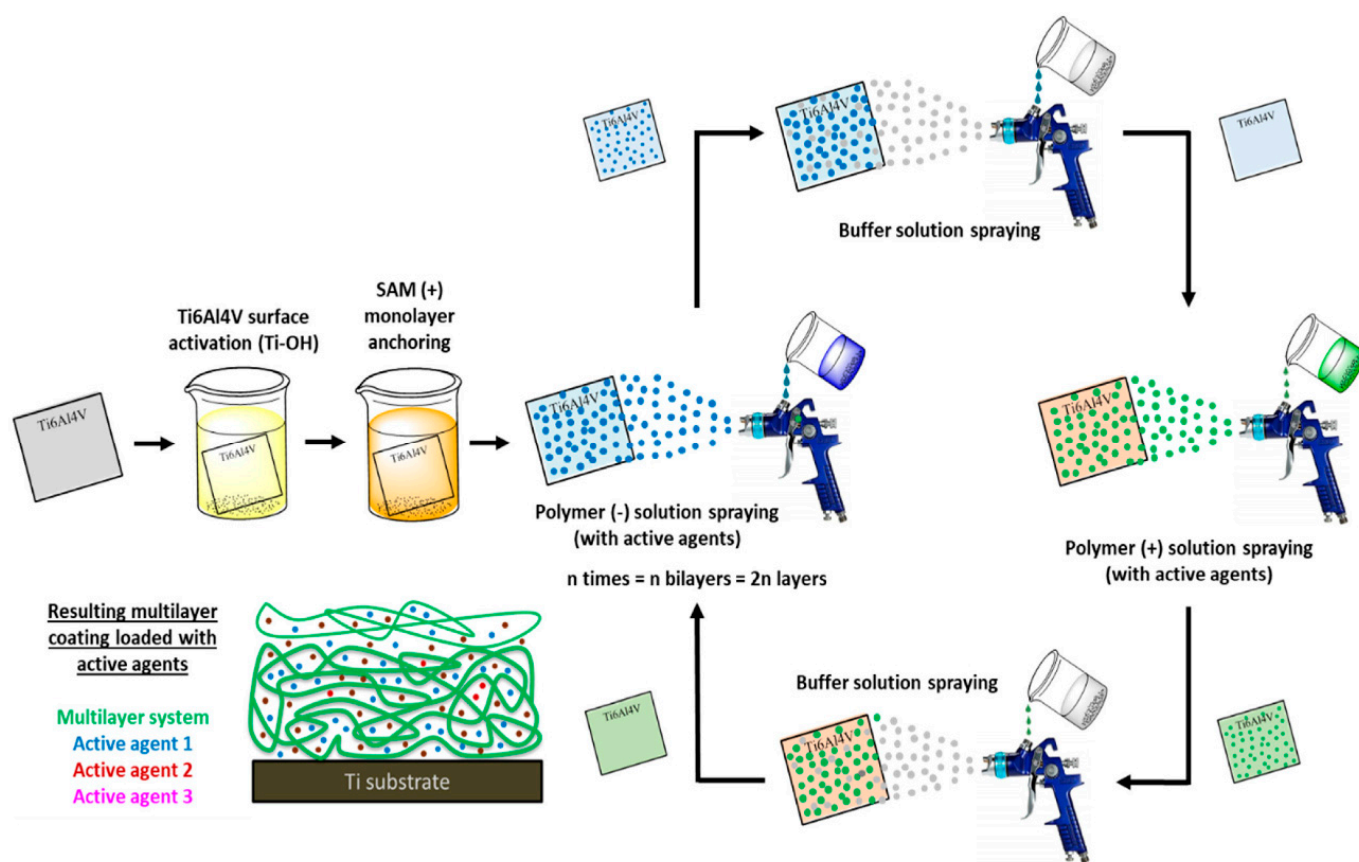


**Figure 19.** A generalized illustration of the LbL assembly technique using positively and negatively charged polymers to cover the Ti6–Al–4V substrate using preloaded active agents. Adapted with permission from [43] (MDPI) (2021). Distributed under Creative Commons Attribution-based license (CCBY 4.0.).

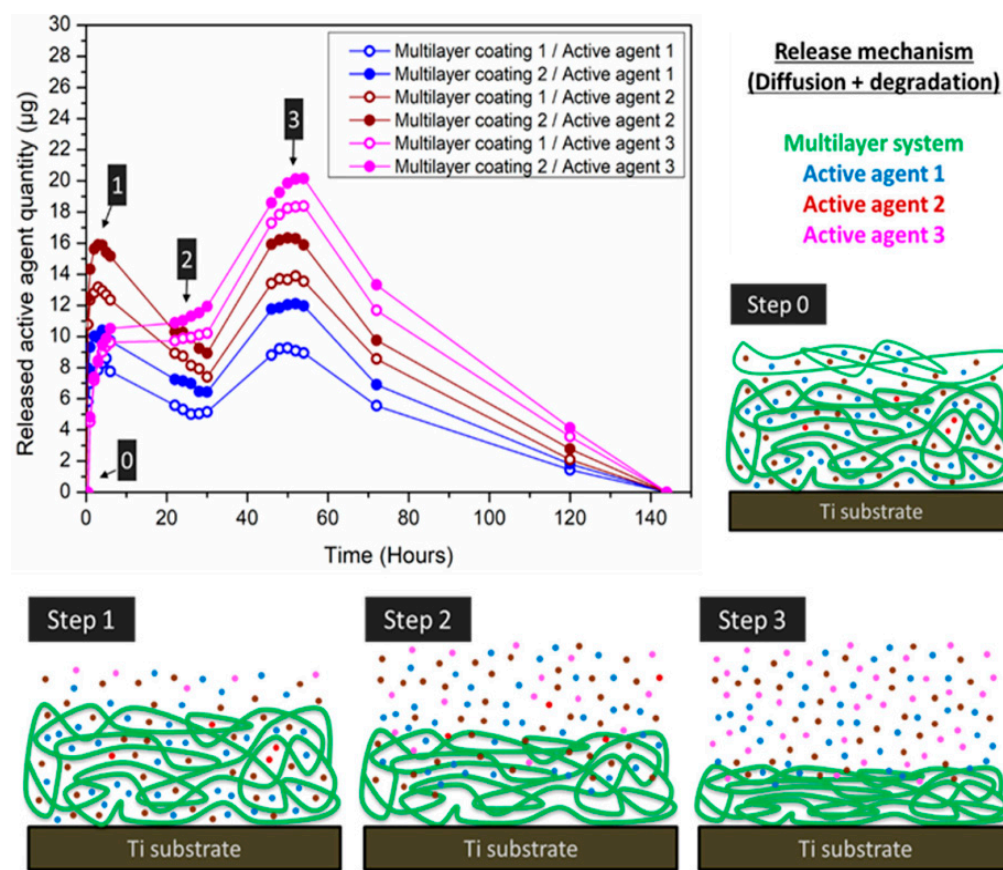


**Figure 20.** The accumulated controlled release pattern of active agents following 140 h, shown as an instance of a release-based multilayered covering on a Ti substrate. The discharge process via multilayer devices involves drug transport and multilayer breakdown mechanisms. Reprinted with permission from [43]. Copyright 2021 MDPI. Distributed under Creative Commons Attribution-based license (CCBY 4.0.).

#### 4.1. Nanostructure Coatings

The development of a novel understanding of cellular reactions at the cellular spectrum in the twenty-first century coincided with the emergence of nano-scale covering technologies for biomaterials. It was thought that the nano-scaled films improved cell adhesion and interface spreading, and also physiological activity. Additionally, it was hypothesized that nano-structured interfaces encourage osteoblast activities due to their capacity to mimic the structural components of naturally occurring body proteins that resemble bone. As proteins found in the extracellular matrix (ECM) of bones are made up of nanosized organics comparable to collagen fibrils, interfaces with nano physiognomy possess significantly changed cellular and subcellular functions in the body. While two generally categorized groups, namely, Carbon nanotubes (CNTs) and TiO<sub>2</sub> nanotubes, are mentioned beneath and offer the ability to imitate the interface of biomaterials to an acceptable extent. The recently discovered CNT possess a remarkable tenacity and stiffness and are chemically durable. Thin graphite cylinders called CNT are made of active sheets of carbon atoms arranged in a hexagonal matrix. CNTs were introduced, and CNTs show high values for mechanical parameters, such as Young's modulus, which is significantly greater than strong-strength steel. CNTs could therefore be used to improve the mechanical characteristics of coverings. Through an experiment, Esteban et al. [136] presented the antibiotic-loaded nanotube surface treatments of Ti alloys as shown in Figure 21.

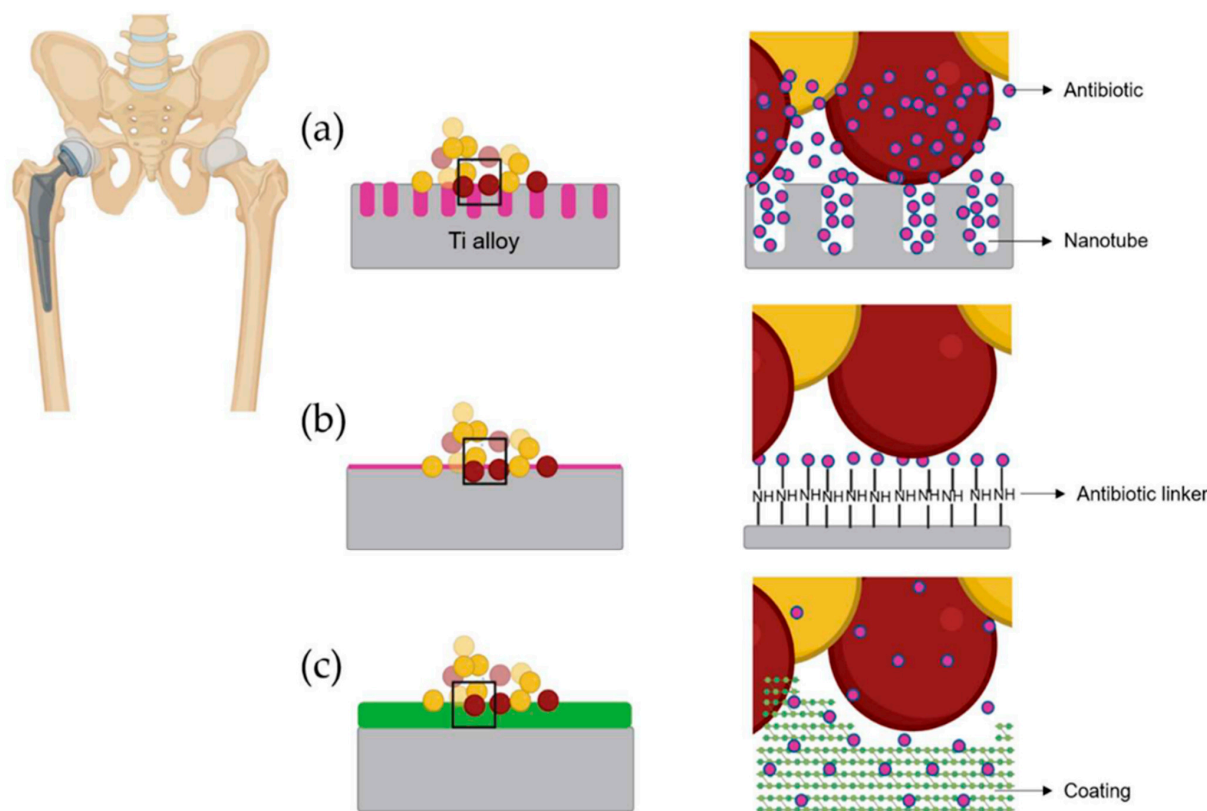


**Figure 21.** Several local antibiotic therapeutic techniques: (a) Nanotubes filled with antibiotics. (b) Ti alloy is covalently attached to an antibiotic. (c) Coating with antibiotics. Yellow denotes a living bacterium. Red indicates dead bacteria. Reprinted with permission from [136]. Copyright 2021 MDPI. Distributed under Creative Commons Attribution-based license (CCBY 4.0.).

Similarly, to enhance the *in vitro* osteoblastic reaction, Lee et al. [137] investigated the nano-topographical characteristics of titanium–niobium–zirconium (TNZ) alloy surfaces created utilizing the TIPS process. TIPS is a novel method for exfoliating the substrate of metallic bio-implants by bombarding them with targeted metal cations that were enhanced by an exceptionally high negative bias voltage that was given to the surfaces. The ion etching energy and the kind of substrate or target material of TIPS were two empirical factors that could be modulated to effectively regulate the nano-topography of the TNZ substrates. As a consequence, several nanopatterns (diameter: 10–210 nm) were created on the TNZ alloy surfaces. Test groups with nanopattern widths between 130 and 210 nm (the 130 and 210 nm groups) were matched to the control group. Experimental sets having nanopattern diameters of 130 and 210 nm outperformed the control group in terms of cell attachment, multiplication, and differentiation. Their research showed that TIPS is a potential technique that could offer the substrate of metallic bio-implants brilliant biological functionalities. To verify the cytocompatibility of the nanostructured TNZ surfaces, osteoblastic cell attachment, multiplication, and differentiation were monitored (Figure 22). The actin filament (red) and cell nuclei (blue) of the osteoblastic cell adhesion test (see Figure 22A) were dyed, and a confocal laser scanning microscope (CLSM) and FE-SEM observations of the cells were conducted. Even following receiving Nb-TIPS exposure, the morphologies of osteoblasts attached to the TNZ surfaces were barely different from those of the comparison group (Figure 22A CLSM 80 pictures). Furthermore, the Ta-TIPS-treated TNZ groups exhibited considerable morphology alterations. The 130 and 210 nm groups were distinguished from Flat TNZ, particularly, by a greater region of connected osteoblasts and an activated cytoskeleton. The volume of osteoblast cells adhered to each substrate was measured using the surface coverage rate of the osteoblasts, which was

calculated using CLSM images. The outstanding osteoblastic cell attachment levels were observed in the experiment sets having nanopattern thicknesses of less than 130 nm (Ta-TIPS TNZ 130 and 210 nm groups), which were 3.5 and 3.4 times greater than that of Flat TNZ (Figure 22B). A cell proliferation assay was used to gauge the cells' vitality. Following 3 days of cell culture, there was no discernible enhancement in the cytocompatibility of the Nb-TIPS-treated TNZ compared to Flat TNZ. The improved proliferation capabilities of the 130 and 210 nm groups, in contrast, were 157 and 146% higher, correspondingly, than those of the comparison group (Figure 22C). Cells were grown for 14 days in physiological conditions to assess osteoblast cell development. For the groups having nanopattern thicknesses of less than 100 nm, there was no improvement in cytocompatibility relative to that of Flat TNZ (Nb-TIPS 10, 50, and 90 nm and Ta-TIPS 40 nm). Furthermore, the 130 and 210 nm groups' cytocompatibility. Furthermore, compared to the control group, the cytocompatibility of the 130 and 210 nm groups was more than twice as significant (Figure 22D).

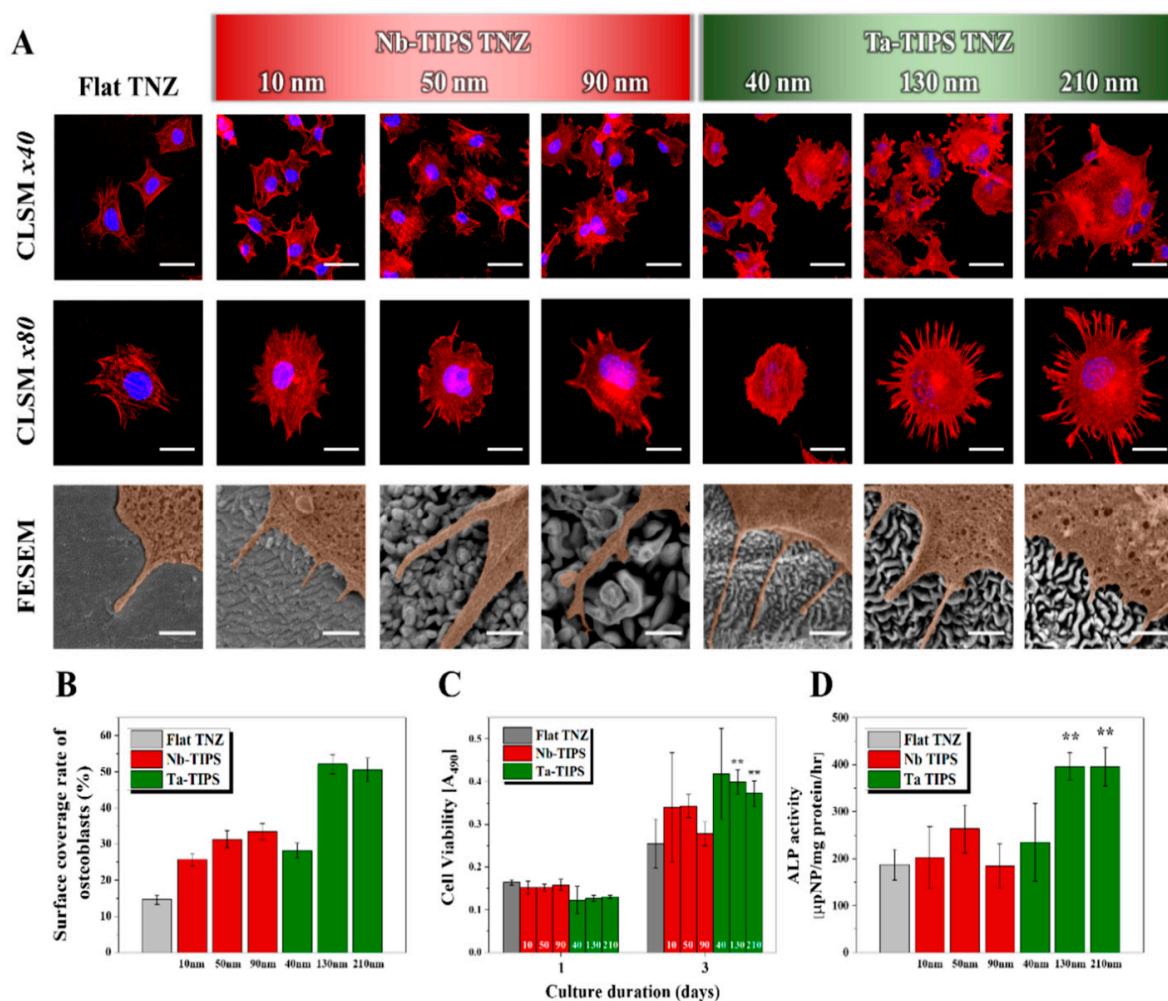


**Figure 22.** Experiments on Flat, Nb- (10, 50, and 90 nm), and Ta-TIPS (40, 130, and 210 nm)-coated TNZ were performed in vitro on osteoblast cells: (A) CLSM images of adherent cells on the substrates at low and high magnifications. (B) Quantitative measurement of the osteoblast cells' interface covering ratio. Osteoblast cells' differentiation (ALP activity) and cell proliferation (C) following 1, 3, 6, and 14 days, correspondingly (\*\*  $p < 0.005$ ) The white scale bars in the top, middle, and bottom lines, correspondingly, represent 50 nm, 25 nm, and 500 nm. (D) illustrates the cytocompatibility of the 130 and 210 nm groups was over two times higher than that of the control group. Reprinted with permission from [137]. Copyright 2021 MDPI. Distributed under Creative Commons Attribution-based license (CCBY 4.0).

#### 4.2. Bio-inert Material Coatings

Bio-inert materials were initially only developed with the slightest negative impact on host tissue following transplantation in consideration. Traditionally, stainless-steel implants were utilized to quicken the healing process after a dislocation. Additionally, alloys based on Co and Cr are generally employed as appropriate metallic biomaterials. The usage of bone cement (PMMA) prostheses with a core composed of stainless steel was pioneered in the 1950s as an innovation for bone retention. The procedure gave the joints the necessary core stability and surface barrier properties. Additionally, owing to the existence of Cr > 12 wt.%, stainless steel is employed as an inert material. These Cr levels enable the production of chromium oxide ( $\text{Cr}_2\text{O}_3$ ) films, which have exceptional corrosion resistance, robust adhesion, and self-healing capabilities. Figure 23 shows a graphical representation of the osseointegration pathway for both bioinert and bioactive implants. The surgical implantation interface is covered in blood instantly. Over several weeks following the treatment, regeneration continues. Throughout this period, the callus develops as the new bone was created from the residual hematoma. Both implant forms are present during these procedures. The extra ions on the exterior of the bioactive implants, on the other hand, expedite and favor the production of stronger bone tissue. The phosphate coating also creates a coarser implant interface, increasing the implant's surface interaction with the bone.

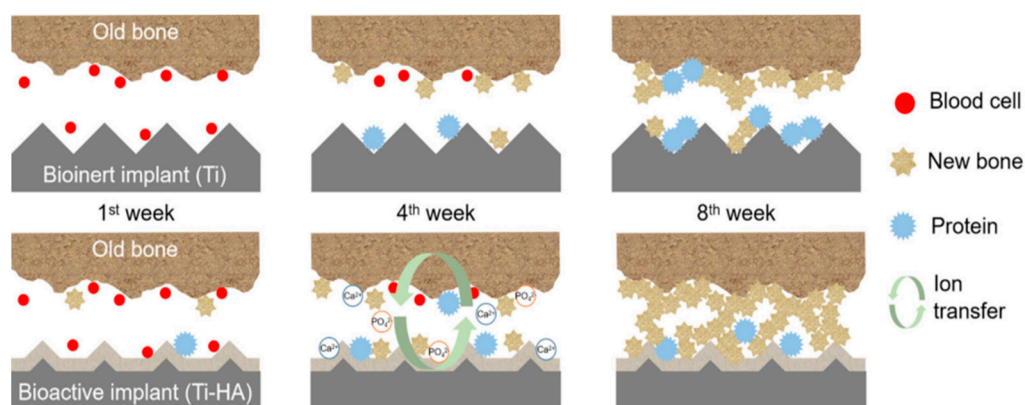


**Figure 23.** Implant osseointegration involving bioactive and inert prostheses shown schematically. Adapted with permission from [64] (MDPI) (2021). Distributed under Creative Commons Attribution-based license (CCBY 4.0.).

In an experiment, hyaluronic acid was used by Chico et al. [138] to enhance the properties of electrochemically reduced graphene oxide (ErGO) on CoCr (ErGOHA). A 24 h immersion in a phosphate buffer saline (PBS) solution comprising 3 g/L of hyaluronic acids was used to functionalize the material. The electrochemical impedance spectroscopy (EIS) was used to examine the erosion resistance of CoCrErGO and CoCrErGOHA substrates for 7 days in PBS. Mitochondrial function (WST-1 assay) and plasma membrane disruption were measured in the mouse macrophage J774A.1 cell line to examine biocompatibility and lethality (LDH assay). TNF- and IL-10 cytokines, which serve as markers of pro- and anti-inflammatory reactions were found in macrophage culture supernatants and utilized to assess the inflammatory reaction. Two-time variables were found in the CoCrErGOHA EIS diagrams: the first, which was related to the hydration and dispersion of the HA coating adsorbed on ErGO; and the second, which was related to the corrosion resistance of the ErGOHA/CoCr interaction. Depending on the biocompatibility, cytotoxicity, and inflammatory processes of the macrophage tests, CoCrErGOHA surfaces exhibited improved behavior in comparison to the CoCr and CoCrErGO interfaces. An increase in inflammatory behavior was suggested by the quantitative examination of IL-10, which revealed that functionalization using hyaluronic acids causes greater levels of anti-inflammatory cytokines. Comparable optical microscopy photographs of macrophages cultivated for 72 h

on a sheet comprised of CoCrErGOHA, CoCrErGO, and CoCr are shown in Figure 24. Following surface treatment, the dispersion of cells on each interface revealed variations in the biocompatibility of the materials. The macrophages have a heterogeneous dispersion across the CoCr interfaces, with cell clumping in some regions of the substance (Figure 24a). The dispersion of the cells was altered by ErGO alteration on the CoCr substrates (Figure 24b), even though macrophages are dispersed relatively evenly. An elevation in the number of macrophages is seen after further hyaluronic acid functionalization of CoCrErGO interfaces (Figure 24c), which may indicate that the material's biocompatibility has been enhanced. On this surface, cells are distributed fairly uniformly, albeit some aggregate in clusters.

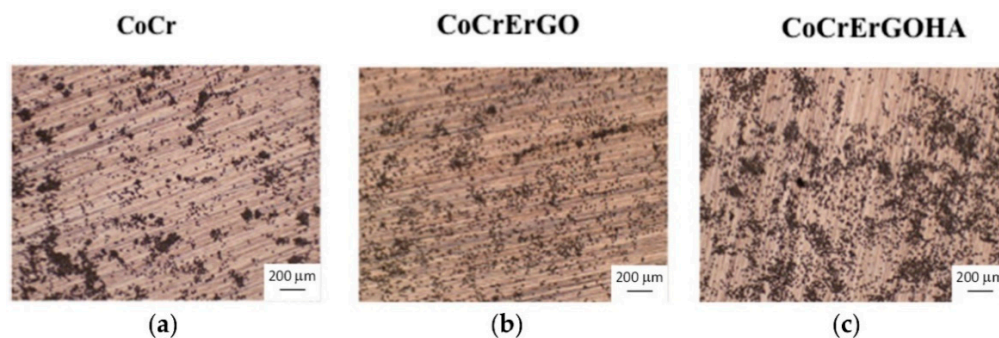


**Figure 24.** Following 72 h of cultivation, the pattern dispersion of the macrophage J774A.1 on the (a) CoCr, (b) CoCrErGO, and (c) CoCrErGOHA discs can be seen using optical imaging. Reprinted with permission from [138]. Copyright 2021 MDPI. Distributed under Creative Commons Attribution-based license (CCBY 4.0.).

#### 4.3. Bioactive Glass Coatings

The University of Florida was the first to propose a group of substances having a significant bioactivity index under the name “bioglass”. The bioactive glasses quickly disseminate a thin coating of hydroxycarbonate-apatite in contact with biological fluids forming a strong link with human bone. Bioactive materials including silica, calcium, phosphorus, and sodium ions are released when bioactive glass surfaces interact, activating intracellular and extracellular reactions, which lead to fast bone growth. In an experiment, Rojas et al. [139] investigated the influence of atmospheric plasma spraying variables on the production of permeability in coatings produced from 45S5 bioglass powder. The Jets&Poudres software's numerical simulation was used to define the spraying variables. An Oerlikon Metco F4 MB gun featuring a 6 mm diameter interior nozzle was used to spray plasma. Three Ar/H<sub>2</sub> blends (95/5, 88/12, and 84/16 vol.%) were employed as plasma-forming gases; the current intensity was adjusted from 450 to 650 A, and the spray range was adjusted from 60 to 100 mm. The air jet pressure was used to regulate the rapidness that the specimens cooled down while being sprayed. Na<sub>2</sub>O and P<sub>2</sub>O<sub>5</sub> volatilization, which increased with the plasma jet enthalpy utilized to liquefy the feedstock powder and declined with both the spray range and the pressure of air jets employed to cool the produced specimens, were the main sources of porosity development in the sprayed bioglass coatings. The Ca/P proportion improved when phosphorus pentoxide concentrations declined in certain coatings, which may influence the HCA formation rate and bioglass degradation rate. The regulation of the globular permeability in the framework of the 45S5 Bio-glass coatings produced by APS was possibly due to the regulation of the plasma enthalpy, the spraying range, and the air jet pressure employed to cool them. The BG6 coating was produced by utilizing a plasma jet with an enthalpy of 436 kJ/mol, at a spraying range of 100 mm, including air jets (forward) with a pressure of 0.2 MPa. In contrast, the BG12 coating was produced utilizing a plasma jet with an enthalpy of 640 kJ/mol, at a spraying range of 60 mm, and using air jets (behind) having a pressure of 0.6 MPa revealed the optimum porosity. Similarly, Zhang et al. [140] investigated the in vivo efficacy of Ti-6Al-4V alloy coated with a CaO-MgO-SiO<sub>2</sub>-based bioactive glass-ceramic for

bone repair. By using atmospheric plasma spraying (APS) to manufacture the M2-coated Ti-6Al-4V cylinders, these were implanted into New Zealand rabbits for 1, 2, and 3 months, correspondingly, with commercially available HA-coated Ti-6Al-4V serving as the reference. The efficacy of the CaO-MgO-SiO<sub>2</sub>-based bioactive glass–ceramic M2-coated Ti-6Al-4V implant was assessed in this study using a New Zealand rabbit femoral defect paradigm with the conventional HA coating/Ti6Al4V serving as the reference. Following treatment, the lesion in the operation region was cured properly, illustrating no evidence of a toxic or external body reaction, substance contamination, or tissue demise. The neighboring muscle tissue proved biocompatible with the M2-coated Ti6Al4V alloy. Around the implants, a significant quantity of new bone grew, and intense bone assimilation occurred at the interface, showing exceptional osteointegration characteristics. In conclusion, the findings showed that the M2-coated Ti6Al4V had superior biological activity in vivo and could eventually replace HA-coated Ti6Al4V in treating load-bearing bone defects. This unique implant has a substantially superior capability to stimulate osteogenesis than the reference, and it may also stimulate the production of new bone in the bone marrow.

In a solvent, Dudek et al. [141] combined HA powder to a chemically produced silicon dioxide/silver (nSiO<sub>2</sub>/Ag) nanocomposite in distinct mass ratios (1:1, 5:1, and 10:1), which were electrophoretically accumulated on the exterior of the NiTi alloy under distinct period and voltage conditions. In order to strengthen their bond with the NiTi substrate, homogeneous coatings were then heated at 700 °C for two hours in an argon environment. The co-deposited components' diagonal dimension modifications throughout the smelting procedure were also investigated. The coverings were generated by a colloidal dispersion of nSiO<sub>2</sub>/Ag nanocomposite powder in 96% ethanol and 0.1 wt.% HA powder utilizing the electrophoretic deposition (EPD) process. The approach outlined in the research was followed to produce the silver–silica nanosystem. The suspension spent two hours in the ultrasonic bath prior to adsorption. The cathode was made of a NiTi alloy, and the counter electrode was made of platinum. Cataphoretic implantation was carried out at voltages ranging from 5 to 50 V and durations ranging from 0.5 to 5 min. The green coverings were then allowed to dry for 24 h at ambient temperature. The uniform sheets were then heated for two hours at 700 °C in an argon environment to sinter the ceramic particulates and improve the coating's adherence to the NiTi metallic substrate. The 1:1 ratio covering was observed to exhibit shear failure, whilst the others were determined to be crack-free, well-adhered, and susceptible to bending to 3.5%. Increasing nanocomposite concentrations resulted in coarser coverings. The experiments using EIS in Ringer's solution showed that the substance with the highest corrosion resistance exhibited capacitive behavior. The NiTi electrode covered using a 5:1 ratio HA/nSiO<sub>2</sub>/Ag hybrid coating exhibited the maximum kinetics and sensitivity to pitting corrosion. Additionally, ten Raman spectra from various areas of the covering were gathered, similar to the initial coatings. Their great resemblance made it possible to analyze them as a representation of the entire body of work. The spectra for both coatings, which were prepared in mutual ratios of 5:1 and 10:1 among HA and nSiO<sub>2</sub>/Ag, were identical (Figure 25b). Following heat treatment, the point Raman's investigation showed several intriguing structural changes that were unanticipated, challenging to understand, and invisible in the X-ray data. The symmetric bending of the P-O v<sub>1</sub> vibration inside the (PO<sub>4</sub>)<sub>3</sub> tetrahedra was linked to one low-intensity wave having a center of roughly 967 cm<sup>-1</sup>, and this band was a typical marker band that distinguishes HA. This line's location is quite near to the HA band's location in the specimen that has not undergone thermal treatment. An additional theory involving silica carriers is that following covering sintering, typical silica bands, which are seen at about 460 and 400 cm<sup>-1</sup>, become more intense (Figure 25b). Currently, no published data are addressing this issue; however, the other bands that were distinguished by very intense strength are highly challenging to understand. The stretching vibrations of Ti-O, which are normally a feature of the hematite composition, however, are linked to two bands having centers at about 600 and 450 cm<sup>-1</sup> (Figure 25a). Other severely disorganized or even amorphous

composite substances might well have formed, according to other strong-intensity bands with quite significant whole width at half-maximal intensities.

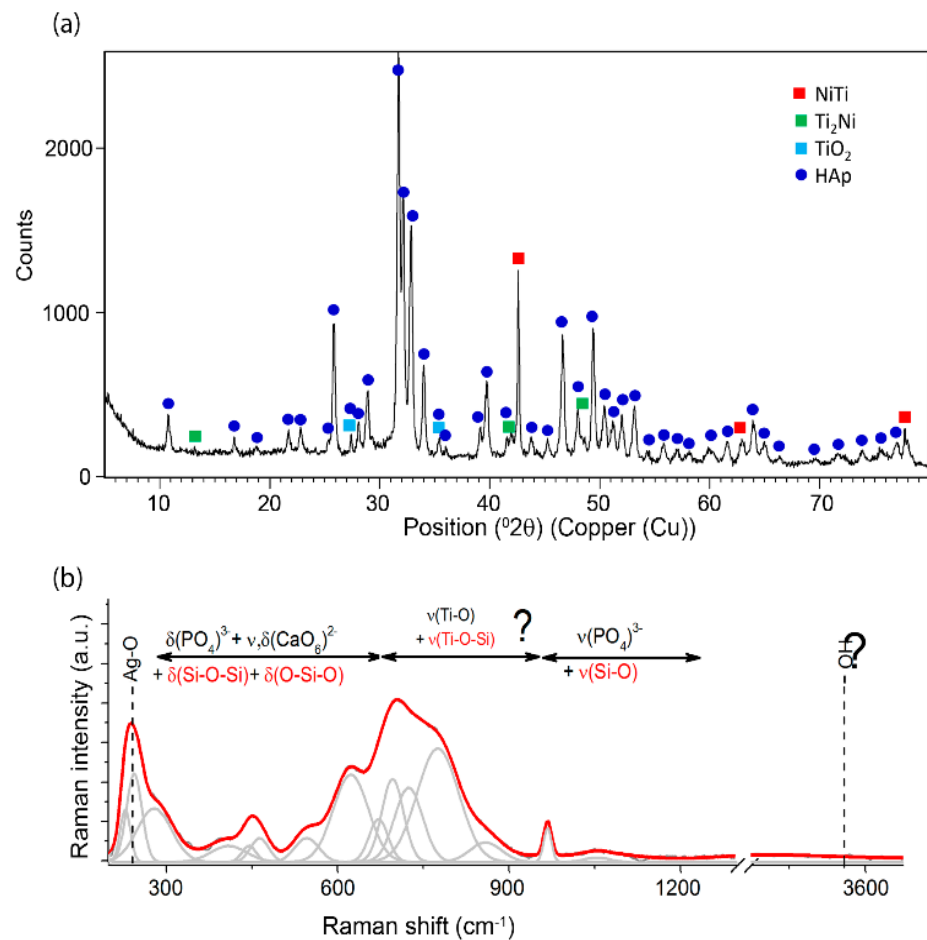


**Figure 25.** Following thermal treatment, an XRD signal was obtained for coating 5:1 (50 V, 120 s), along with an example Raman spectrum (a). The Voigt function was used to fit the bands with the fewest possible components (b). Reprinted with permission from [141]. Copyright 2021 MDPI. Distributed under Creative Commons Attribution–based license (CCBY 4.0).

#### 4.4. Hydroxyapatite (HA) Coatings

Bioactive substances including hydroxyapatite  $\{(Ca_{10}(PO_4)_6(OH)_2, HA\}$ , calcium phosphates (CaP) are widely utilized for effective bone prenovation and bone in-growth at the tissue–implant interface owing to their superior adaptation under in vivo conditions. These ceramic coatings are extensively used to boost the biocompatibility of metal implants without affecting their structural performance owing to the equivalent chemical composition or straight attachment of the HA layer to fibrous tissue. Furthermore, there is a positive association between the HA covering and the uncovered bone that similarly showed an increase in the rate of adhesion. As a result, HA covering helps the implant remain stably fixed to the bone while minimizing side effects by perhaps reducing the release of metallic ions from the implantation. The processing issues related to plasma spraying hydroxyapatite films were overcome by Cheang et al. [142]. This research discusses a few issues concerning plasma spray coating of HA and makes the case for customizing the morphology and characteristics of the powder input via appropriate precondition methods to improve deposition effectiveness and provide a satisfactory coating architecture. The main issues with thermally squirted HA films are that they are insufficient to melt, repeatability, and exceed biological standards. The usage of HA-wrapped implants has had inconsistent results, which raises the possibility that the substance was unexpected. From a

strictly operational standpoint, this analysis implies that effective powder conditions may reduce some of the inconsistency that results from an absence of operational parameter consistency. Thermal spraying HA feedstocks exist in a wide range of compositions, phases, crystallinities, particulate diameters, shapes, and structures. The majority of HA powders are flocculated spray-dried products. Regrettably, these powders possess a propensity to disintegrate in turbulent plasma, resulting in a covering that is composed of droplets with a length scale that is a combination of the initial range of sizes and disintegrated shards. This broad variety of particulate sizes produced a coating, but it lacked the requisite degree of reliability. Given that the covering microstructure is strongly reliant on the properties of the powder, this is enough to lead to significant variance. Without taking the crucial particulate diameter into account, choosing a particulate shape will inevitably result in the production of undesirable stages, amorphous, and structurally deficient microstructures. Thermal spraying has trouble meeting the demand for pore diameters in the 200–400 pm region. There must be further post-treatment procedures. The conflicting, conditionally incompatible parameters were covering durability and biocompatibility. The consistency of the covering may be compromised for greater biocompatibility in short-term applications of HA film if the covering is only present momentarily. Furthermore, post-treatment procedures are essential to reestablishing biocompatibility, which is generally lacking in a mechanically adhesive and amorphous as-sprayed film for more long-term, irreversible uses wherein an extremely crystalline HA state is essential.

Similarly, Mavis et al. [143] concentrated on developing formulas for suitable solvents for dip coating HA on Ti-6Al-4V surfaces, utilizing granules made from chemically precipitated HA precursors. In this work, formulas for coating Ti-6Al-4V substrates with calcium HA dip-coating solutions were established. These solutions contained poly(ethylene glycol), glycerol, and/or gelatin as the organic ingredients. A unique device that might deliver consistent dipping and extraction speeds (such as 100 mm/min) was used to carry out the dip-coating procedure. The green, coated strips did not need to be dried in regulated humid situations according to the HA dip-coating solution formulations created in this investigation. Calcination of the HA dip-coated Ti-6Al-4V sheets was carried out at 840 °C in a nitrogen-gas environment. The HA films were quite permeable and had bonding constants greater than 30 MPa.

Furthermore, using a recently created production method called powder mixed-electro discharge machining (PM-EDM), Amin et al. [144] explained the processing and spraying tactics on biomaterials. Materials that migrated were removed from the machined edge as a result of heating and biochemical processes using thermoelectric methods. In order to create biocompatible coverings, HA powder, which yields Ca, P, and O, was frequently utilized. According to reports, the HA added-EDM technique considerably enhances biomaterials' coating qualities, corrosion and abrasion resistance, and bio functions. Since both the mobility and the accumulation of the corroded materials rely solely on the relevant conditions and physical properties of the additional powders, samples, and electrodes, the basic underlying mechanisms of the movement and accumulation of the melded components that are presumed to happen all through the PM-EDM method were stochastic in behavior. The heat energy generated throughout the machining was sufficient to merge the surface components of the electrodes and the sample, the dispersed powders, and the insulator. Additional components from both the active component and the electrode were heated and degraded instead of flushed away as a result of the retention of a small machining gap and the production of a quite elevated temperature. This caused a few of the degraded materials to collect on the machined component. The dispersed particulates in the active fluid that acted as a coolant were simultaneously slightly dissolved and electrified as a result of passing via the small discharge space. The deposition on the modified section occurs quickly where the charged particulates create chain-like connections due to the electromagnetic interactions, electrophoresis pressure drops, and electrostatic interaction. Additionally, the opposing device polarity causes oxide to develop owing to chemical interactions between the molten and charged particulates, and the ionized debris scraped

off the electrodes and the instrument surface. Over the machined substrate, the produced oxide alloys were applied and hardened. Furthermore, C and OH were fed into the decomposing active liquid to produce carbides and oxide alloys.

#### 4.5. Electrophoretic Deposition (EPD)

EPD is gaining more attention in the materials research community and a multitude of novel opportunities for the technique are developing in the treatment of both conventional and cutting-edge materials. EPD is a cost-effective approach that typically only needs basic manufacturing equipment, which contributes to its high adaptability in the usage of diverse materials and blends of materials. EPD could be adaptable to a range of equipment and component configurations and has a significant capability for scaling up to massive product dimensions, varying from micrometers to meters. EPD is typically performed in a two-electrode cell wherein particle aggregation is principally accountable for the development and evolution of solid formations on the electrode, while electrophoresis is used to move charged particles distributed in a liquid to the working electrode. EPD could be used with a wide range of materials that are accessible as colloidal suspensions or as micro powders (often with particle sizes less than or equal to 30  $\mu\text{m}$ ). EPD may deposit materials such as polymers, metals, ceramics, glasses, and their composites. In an experiment, Maleki-Ghaleh et al. [145] used the EPD method and the reaction bond sintering procedure to cover a NiTi alloy with a composite coating made of HA, multi-walled carbon nanotubes (MWCNTs, 1 wt.%), and titanium (Ti, 20 wt.%). The microstructure and phase analyses of the HA, HA-Ti (20 wt.%), and HA-Ti (20 wt.%)-MWCNTs (1 wt.%) coatings were characterized using the XRD and FE-SEM, correspondingly. The adhesion and micro-indentation testers were used to assess the mechanical properties of the coatings. By observing the formation of the apatites, the bioactivity behavior of the coatings was evaluated in a simulated body fluid (SBF). Furthermore, the biological activity of the coatings was assessed using osteoblast-like MG63 cells. According to the FE-SEM analysis's findings, adding Ti significantly enhanced the smelting of the HA coating. Additionally, the HA coating's hardness and adhesion intensity increased after being combined with Ti and CNT (HA-Ti(20 wt.%)-MWCNTs(1 wt.%) coating), increasing from 72 HV and 17.2 MPa to 405 HV and 32.1 MPa, accordingly. The biological experiments also showed a remarkable enhancement in the formation of bone cells and apatite on the Ti and MWCNT-based HA coatings. Using the EPD method, the same group covered a NiTi alloy substrate with an HA-Ti (Ti, 20 wt.%) composite coating [146]. The HA powder was combined with Ti powder utilizing a ball milling technique before the coating was applied. The HA-Ti composite powders were combined with Ti and then deposited on the NiTi substrate using the EPD technique in n-butanol for two minutes with an induced voltage of 60 V. The micro-scratch, micro-indentation, and polarization tests were used to evaluate the electrochemical and mechanical properties of coatings. The findings showed that the milling procedure duration provided a substantial impact on reaction bonds and that 4 h was the ideal mixing period. The HA-Ti composite coating's (304 HV) micro-hardness was significantly greater than that of the HA coating's (72 HV). Additionally, because the HA coating contained Ti particles, more energy was needed to separate it from the NiTi substrate in the micro-scratch test, increasing from 7.1 to 17.8 N. The electrochemical resistivity of the HA-Ti composite coating was greater than that of the HA coating, according to the polarization data. After being combined with Ti particles, the NiTi alloy's corrosion resistance improved from 133 to 2720  $\text{k}\Omega\text{ cm}^2$ .

Utilizing a mixture of EPD and reactive bonding throughout the sintering, Khalili et al. [147] generated various composite coatings containing 20 wt.% silicon and 1 wt.% MWCNT of HA on NiTi substrate. As a reactive bonding material, silicon was utilized. A steady voltage of 30 V was used during the EPD process for 60 s. Following deposition, specimens were dehydrated before being annealed in a vacuum furnace for 1 h at 850  $^{\circ}\text{C}$ . MWCNTs serve as reinforcing fibers in the HA-20%Si-1%MWCNTs composite coating, holding the matrices intact and forming a bridge architecture that promotes coating uniformity. Additionally,

the inclusion of Si particles functions as a reaction bonding reagent, catalyzing dispersion processes and causing the development of some biocompatible phases, such as  $\text{Ca}_3\text{SiO}_5$  and  $\text{CaSiO}_3$ , which fill the spaces within the HA particles. Furthermore, using the EPD approach, Maleki-Ghaleh et al. [148] covered the NiTi alloy with a composite made of HA-titanium (Ti, 20 wt.%) and MWCNTs (1 wt.%). In an SBF, the EIS and PDP tests were used to examine the corrosion behaviors of the coated NiTi specimens. In the SBF, the quantities of Ni ions liberated from the coated NiTi were measured. According to the EIS findings, the MWCNTs and Ti were added to the HA coating to further enhance the corrosion resistance of the NiTi coated with the agent. Upon being coated with the HA-Ti-MWCNTs composite coating, the current density and corrosion resistance of the NiTi alloy decreased from  $2.52 \mu\text{A}\cdot\text{cm}^{-2}$  and  $24.13 \text{ k}\Omega$  to  $0.91 \text{ nA}\cdot\text{cm}^{-2}$  and  $5.92 \text{ M}\Omega$ , respectively. Additionally, after being coated with HA-Ti-MWCNTs, the amount of Ni ions discharged from the surface of the NiTi alloy into the SBF media decreased from  $11.8$  to  $0.08 \mu\text{gr}\cdot\text{L}^{-1}$ . Additionally, the cellular multiplication in the culture media formed from NiTi alloy coated with HA-Ti-MWCNTs increased greatly when contrasted to that of pure NiTi alloy, and the cell culture media itself showed no toxicity.

#### 4.6. Bio-mimetic Coating (Smart Biomaterials)

The ability of a substance to respond to external and internal stimuli, including pH, temperature, and ionic intensity, distinguishes it as a smart substance. The scaffold morphological analysis of a smart substance, which was given by Holzapfel et al., revealed the morphological features, chemical properties, and morphology that significantly impacted tissue rejuvenation. For instance, some permeable substances may be used by precisely choosing the permeability, pore diameter, and pore interconnectivity of interfaces with great biocompatibility. Additionally, Kim et al. [84] used a variety of Ti surface-treatment techniques, including micro-arc oxidation, anodic oxidation, acid etching, and HA blasting. These approaches' effects on sample surfaces were examined in terms of their architecture, chemical constitution, and water sorption. For the covered samples, the coated layer's adhesive ability was also evaluated. In this experiment, the conventionally accessible Ti plates (conventionally sheer Ti G4) having sizes of  $10 \text{ mm} \times 10 \text{ mm} \times 2 \text{ mm}$  were manufactured. P400, P1000, and P2000 SiC papers were used to polish Ti plates in order. Ti sheets were polished, rinsed in ethanol using a sonic cleaner to eliminate dirt, and then allowed to dry at a temperature around  $70 \text{ }^\circ\text{C}$  before pre-treatment with a protective coating. Ti plates were struck by jetted HA particulates during the manufacture of HA-blasted Ti sheets, and the surfaces were then washed in nitric acid to remove any leftover HA sandblasting particulates. Before the subsequent post-treatment, a similar HA-blasting operation was carried out. Nitric acid-treated Ti sheets were first submerged in a 5 M NaOH medium for 24 h at  $60 \text{ }^\circ\text{C}$ , followed by 24 h at  $80 \text{ }^\circ\text{C}$  in distilled water. Then, samples were heated for one hour at  $600 \text{ }^\circ\text{C}$  after being oxidized in an oven overnight at  $40 \text{ }^\circ\text{C}$ . Upon the sandblasting and acid etching (SLA)-Ti substrate, a  $\text{TiO}_2$  coating was created using AO and MAO techniques. The AO method employed a mixture of 98 vol.% ethylene glycol (Sigma-Aldrich) and 2 vol.% distilled water, while the MAO method utilized an electrolytic solution comprising 0.25 wt.% ammonium fluoride (Sigma-Aldrich, Saint Louis, MO, USA). Ti plates that had undergone SLA treatment were immersed in the electrolytic solutions before being exposed to a DC field (HD-9001D, FinePower, Seoul, Korea) of 60 V for 30 min. Manufactured SLA/AO-Ti surfaces were washed with ultrasonography in ethanol, acetone, and distilled water in that order. In electrolytic aqueous solutions of 0.15 M calcium acetate monohydrate (Sigma-Aldrich) and 0.02 M glycerol phosphate calcium salt, MAO therapy was carried out. The stainless-steel counter electrode and the samples received electrical power via a pulsed DC field for two minutes at 350 V, 660 Hz, and 60% activity. In order to avoid temperature increases during the procedure, a cooling bath set at  $10 \text{ }^\circ\text{C}$  was used. SLA/MAO-Ti substrates were once again cleaned with purified ethanol and water following processing. Figure 26 shows FE-SEM analysis of the surface features of Ti samples that have been subjected to surface treatment. In the Ti sample, the distinctive polishing

structure is apparent (Figure 26a). Figure 26b,c, on the other hand, depict surfaces that have been abraded by the blasted and acid processing method on the HA-blasted samples and SLAs. The greatly magnified picture shows surface characteristics that have been precisely sculpted through blowing and etching. On the other hand, distinct patterns were seen in the two experiment sets that received extra electro-oxidation polishing. Figure 26d based on low-magnification images shows no significant changes identified among SLA/AO samples and HA and SLA samples. Although this phenomenon is characteristic of AO therapy, nanoporous rods were created on the SLA-treated Ti surfaces, as shown in the inset picture. The SLA/MAO samples, however, showed no signs of SLA therapy (Figure 26e), and a characteristic crater-like permeable morphology developed on the substrate. The arrangement and its geometries are similar to patterns reported in many MAO investigations, and they were produced by the multiple arcs on the Ti surface throughout the MAO treatment procedure. This result showed that further processing of SLA-treated Ti surfaces can result in a more abrasive structure or the development of a protective coating.

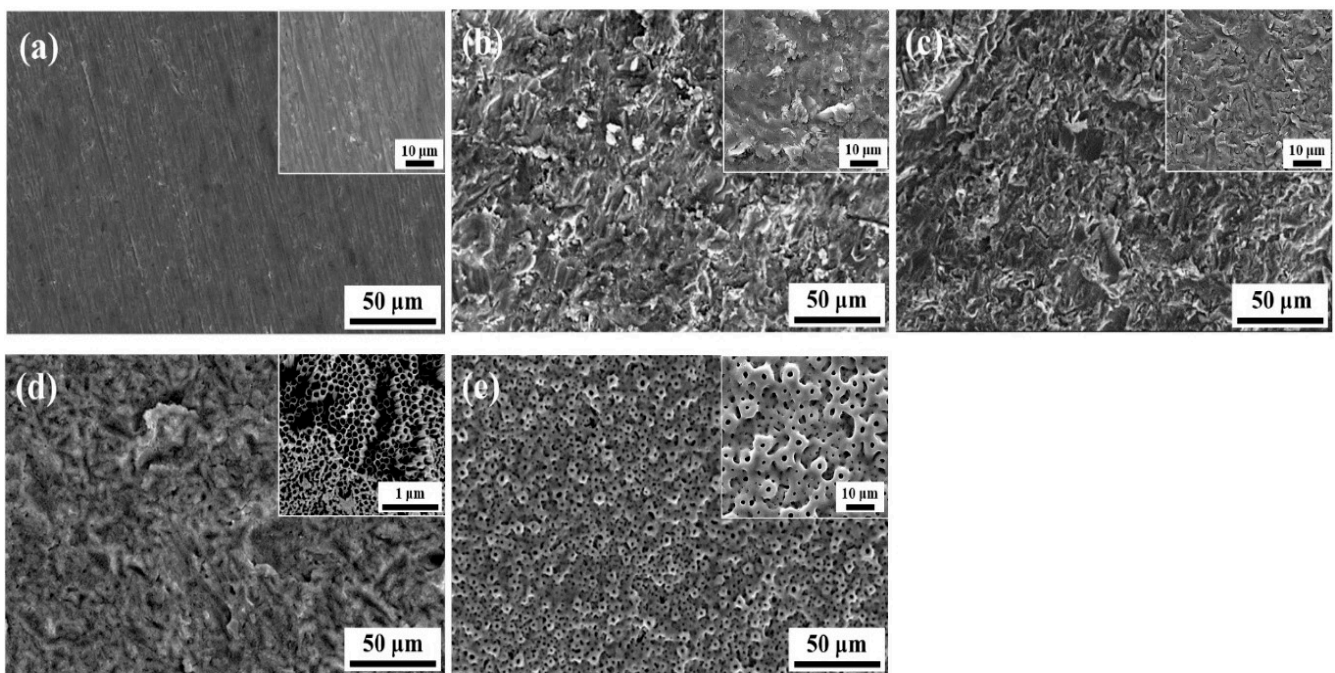


**Figure 26.** The surface texture of (a) Ti has been subjected to a variety of processes, including (b) HA blasting, (c) SLA, (d) AO, and (e) MAO. Reprinted with permission from [84]. Copyright 2021 MDPI. Distributed under Creative Commons Attribution-based license (CCBY 4.0.).

Target-ion-induced plasma sputtering (TIPS) was used by the team of researchers to alter the nano-morphological characteristics of Ti, Nb, and Zr (TNZ) alloy interfaces to enhance the *in vitro* osteoblastic activity. The TIPS approach is a revolutionary method for cleaning metal bio-implants by bombarding the surface with targeted metal cations that were enhanced by an exceptionally large negative bias voltage given to the surfaces. By adjusting empirical TIPS parameters (such as the ion etching energy and the kind of surface or target substances), the nano-micrography of the TNZ interfaces was effectively regulated. As a consequence, several nanopatterns (diameter: 10–210 nm) were created on the TNZ alloy surfaces. Wu and Kuromoto state that the anodizing duration and quantity affect the depth of the coating film of AO, and the parameters used here produced a depth of about 1 µm as shown in Figure 27 [84]. As the imposed bias voltage during MAO therapy (350 V) was substantially greater than it was during AO therapy (60 V), samples handled with MAO showed a denser coating thickness than those exposed with AO (60 V). Due to this distinction, MAO had a significantly stronger electric reaction on the Ti layer in the electrolyte than AO.

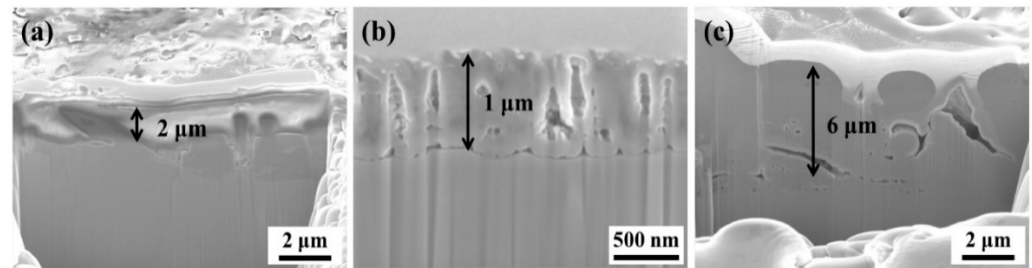


**Figure 27.** Surface-modified Ti pictures obtained using a focused ion beam (FIB) in (a) HA, (b) SLA/AO, and (c) SLA/MAO. Reprinted with permission from [84]. Copyright 2021 MDPI. Distributed under Creative Commons Attribution-based license (CCBY 4.0.).

### 5. Challenges and Future Perspectives

The main criteria for choosing biomaterials in this domain are their physiological, structural, biochemical, and microstructural abilities. Moreover, the main areas of incapacity linked to incendiary issues with bio-implants are poor tensile integrity, excessive strain ratio, poor bio-stability, and poor resistance to corrosion. As observed, the HA is a bone implant substance that shows outstanding adhesion properties and could be readily deposited on substrates while preserving inherent bulk components qualities. Additionally, the bioglass coatings may eventually arise in terms of the material's bio-inertness and bio-activity. Similarly, a nano-functionalized substrate offers potential biologic characteristics such as cell adherence, rejuvenation, and dispersion across the interface, which encourage osteoblastic progenitor cells to use different proliferation agents to accelerate the healing cycle. Furthermore, it is widely recognized that interface stimulation improves a variety of biological properties of Ti-based biomaterials, including biological properties and resilience to biocorrosion. In actuality, the oxide layer (mostly  $\text{TiO}_2$ ) is in charge of preventing air corrosion and the discharge of toxic ions through prostheses in the body that may have negative physiological effects. Furthermore, the current article has demonstrated that the activation of Ti surfaces alone may improve certain desired bioactive characteristics, including tissue rejuvenation and osseointegration for prospective cardiac, dentistry, and orthopedic purposes. However, transplantation techniques and the post-implantation phase include numerous intricate biological reactions, which might render the aforementioned bioactive qualities of oxidized Ti substrates unsatisfactory. Active -OH molecules of the hydroxylated area also play a significant role at this phase as they allow Ti substrates the flexibility needed for additional chemical modification to bioactive bio(macro)molecules, pharmaceuticals, or other substances. Consequently, surface modification techniques facilitate us to acquire significant hydroxylation (Ti-OH) levels, which enable a larger proportion of crosslinking areas using the reactive substances in addition to generating the effective oxide layer ( $\text{TiO}_2$ ) upon the Ti interfaces. Figure 28 illustrates how chemical and physical techniques are typically used to modify Ti surfaces to activate them. All of the drawbacks of physical and chemical treatments, including their high costs, modest energy requirements, hazardous complications, waste disposal, and other issues, are very significant and need to be acknowledged by all as depicted in Figure 28. Consequently, new methods to impart positive characteristics including antimicrobial, self-healing, anti-inflammatory, drug carriers, and wound healing must be more evaluated in an effort to improve the efficacy of biomaterials and biomedical implants.

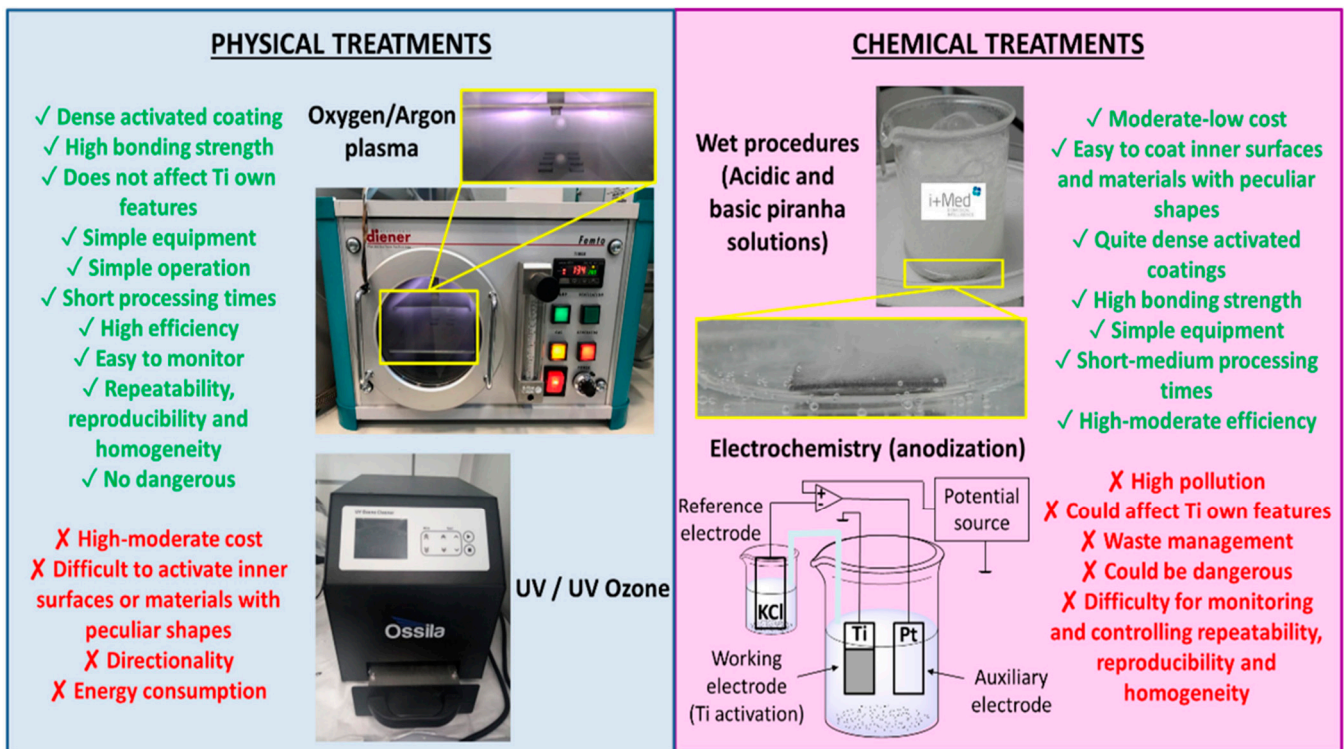


**Figure 28.** Several physical and chemical treatments for the surface modifications of biomedical metals such as Ti surface along with their advantages (green) and disadvantages (red). Reprinted with permission from [43]. Copyright 2021 MDPI. Distributed under Creative Commons Attribution-based license (CCBY 4.0.).

## 6. Conclusions

Several metals such as Ti, Zr, Co, Cr, Ni, etc., and their alloys perform a crucial function as fundamental components of dental and orthopedic everlasting implantation. Unfortunately, malfunctioning of these biomaterial implants may frequently be attributed to infections induced by corrosion, extreme stress, or osteogenesis dearth. Several surface modification-based techniques such as ion implantation, thermal spraying, ultrasonic nanocrystal surface modification, glow discharge plasma, electrophoretic deposition, and physical vapor deposition and coatings are significantly employed and help to prevent the corrosion of biomedical implants, satisfying the extremely strict standards of biomaterials surfaces for a particular biomedical purpose by strengthening interfacial adhesion and encouraging proactive behavior. Acute immobilization or prolonged discharge of the relevant engaged substance has been shown to effectively perform this intentional action, which possesses strong osteogenesis and antimicrobial capabilities. Several compelling sets of studies that have been reviewed in this article such as Bodon et al. [43], Yan et al. [25], and Salahinejad et al. [50], and many more with potent findings have demonstrated that the discussed physical surface modifications are reliable and efficient approaches for improving the surface bio functionality, biocompatibility, antibacterial activity, and anti-corrosion property of biomedical implants, such as Ti alloys, stainless steel, Co-Cr alloys, etc., by examining the interface properties of biomedical implants with the integration of nano-structured inorganic zirconium titanate ( $ZrTiO_4$ ) and composite  $ZrTiO_4$ -polymethyl methacrylate (PMMA) thin coatings. The future of surface modification techniques would be to form and advance multifunctional and nanoparticle surface coatings that can integrate the merits of several coatings and offer a more advantageous approach to surface modification. The association between the human cell and biomedical implant surface must be extensively explored and comprehended as it has been discovered that the implants are consistently in contact with the cells. This insight will be crucial in manufacturing new implants that will

resolve the current issue. Surface modification has the potential to significantly enhance the functionality of biomedical implants; therefore, more research is needed to evolve innovative surface modification techniques that will result in implants with superlative antimicrobial activity, biocompatibility, and wear and corrosion resistance.

**Author Contributions:** Conceptualization, A.T. and A.K.; Validation, A.K., L.G. and R.M.; Formal Analysis, R.M. and F.Z.; Writing—Original Draft Preparation, A.T.; Writing—Review and Editing, A.T., A.K., L.G. and R.M.; Visualization, S.K. and F.Z.; Supervision, A.K. and L.G.; Funding Acquisition, R.M. and L.G. All authors have read and agreed to the published version of the manuscript.

**Funding:** This research was funded by Deanship of Scientific Research at King Khalid University grant number RGP. 2/175/43.

**Institutional Review Board Statement:** Not applicable.

**Informed Consent Statement:** Not applicable.

**Data Availability Statement:** Not applicable.

**Conflicts of Interest:** The authors declare no conflict of interest.

## References

1. Molino, G.; Bari, A.; Baine, F.; Fiorilli, S.; Vitale-Brovarone, C. Electrophoretic Deposition of Spray-Dried Sr-Containing Mesoporous Bioactive Glass Spheres on Glass–Ceramic Scaffolds for Bone Tissue Regeneration. *J. Mater. Sci.* **2017**, *52*, 9103–9114. [[CrossRef](#)]
2. Barfeie, A.; Wilson, J.; Rees, J. Implant Surface Characteristics and Their Effect on Osseointegration. *Br. Dent. J.* **2015**, *218*, E9. [[CrossRef](#)] [[PubMed](#)]
3. Baine, F.; Fiorilli, S.; Vitale-Brovarone, C. Composite Biomaterials Based on Sol-Gel Mesoporous Silicate Glasses: A Review. *Bioengineering* **2017**, *4*, 15. [[CrossRef](#)] [[PubMed](#)]
4. Kačiulis, S.; Mattogno, G.; Pandolfi, L.; Cavalli, M.; Gnappi, G.; Montenero, A. XPS Study of Apatite-Based Coatings Prepared by Sol-Gel Technique. *Appl. Surf. Sci.* **1999**, *151*, 1–5. [[CrossRef](#)]
5. Sreekanth, D.; Rameshbabu, N. Development and Characterization of MgO/Hydroxyapatite Composite Coating on AZ31 Magnesium Alloy by Plasma Electrolytic Oxidation Coupled with Electrophoretic Deposition. *Mater. Lett.* **2012**, *68*, 439–442. [[CrossRef](#)]
6. Schindhelm, K.; Milthorpe, B.K. An Overview of Biomaterials. *Australas. Phys. Eng. Sci. Med.* **2003**, *9*, 29–32.
7. Dos Santos, G.A. The Importance of Metallic Materials as Biomaterials. *Adv. Tissue Eng. Regen. Med. Open Access* **2017**, *3*, 300–302. [[CrossRef](#)]
8. Yadav, S.; Gangwar, S. An Overview on Recent Progresses and Future Perspective of Biomaterials. *IOP Conf. Ser. Mater. Sci. Eng.* **2018**, *404*, 012013. [[CrossRef](#)]
9. Martinez-Boubeta, C.; Simeonidis, K.; Oró, J.; Makridis, A.; Serantes, D.; Balcells, L. Finding the Limits of Magnetic Hyperthermia on Core-Shell Nanoparticles Fabricated by Physical Vapor Methods. *Magnetochemistry* **2021**, *7*, 49. [[CrossRef](#)]
10. Chiang, P.C.; Chen, C.W.; Tsai, F.T.; Lin, C.K.; Chen, C.C. Hard Anodization Film on Carbon Steel Surface by Thermal Spray and Anodization Methods. *Materials* **2021**, *14*, 3580. [[CrossRef](#)]
11. Liu, R.; Yuan, S.; Lin, N.; Zeng, Q.; Wang, Z.; Wu, Y. Application of Ultrasonic Nanocrystal Surface Modification (UNSM) Technique for Surface Strengthening of Titanium and Titanium Alloys: A Mini Review. *J. Mater. Res. Technol.* **2021**, *11*, 351–377. [[CrossRef](#)]
12. Bano, S.; Rincon Romero, A.; Islam, M.T.; Grant, D.M.; Ahmed, I.; Hussain, T. Development and Characterization of Phosphate-Based Glass Coatings via Suspension High-Velocity Oxy-Fuel (SHVOF) Thermal Spray Process. *J. Therm. Spray Technol.* **2021**, *30*, 1862–1874. [[CrossRef](#)]
13. Blum, M.; Sayed, M.; Mahmoud, E.M.; Killinger, A.; Gadow, R.; Naga, S.M. In Vitro Evaluation of Biologically Derived Hydroxyapatite Coatings Manufactured by High Velocity Suspension Spraying. *J. Therm. Spray Technol.* **2021**, *30*, 1891–1904. [[CrossRef](#)]
14. Sharma, S.; Ganjoo, R.; Saha, S.K.; Kang, N.; Thakur, A.; Assad, H.; Kumar, A. Investigation of Inhibitive Performance of Betahistine Dihydrochloride on Mild Steel in 1M HCl Solution. *J. Mol. Liq.* **2021**, *347*, 118383. [[CrossRef](#)]
15. Kumar, A.; Thakur, A. *Encapsulated Nanoparticles in Organic Polymers for Corrosion Inhibition*; Elsevier Inc.: Amsterdam, The Netherlands, 2020; ISBN 9780128193594.
16. Sandilya, S.; Thakur, A.; Suresh Singh, S.; Kumar, A. Recent Advances, Synthesis and Characterization of Bio-Based Polymers from Natural Sources. *Plant Cell Biotechnol. Mol. Biol.* **2021**, *22*, 70–93.
17. Sharma, S.; Ganjoo, R.; Saha, S.K.; Kang, N.; Thakur, A.; Assad, H.; Sharma, V.; Kumar, A. Experimental and Theoretical Analysis of Baclofen as a Potential Corrosion Inhibitor for Mild Steel Surface in HCl Medium. *J. Adhes. Sci. Technol.* **2021**, *36*, 2067–2092. [[CrossRef](#)]

18. Kaur, M.; Thakur, A.; Sharma, V.; Kumar, A. Tricine as An Effective Corrosion Inhibitor For Aluminium In Acidic Medium. *Think India J.* **2019**, *22*, 3200–3219.
19. Parveen, G.; Bashir, S.; Thakur, A.; Saha, S.K.; Banerjee, P.; Kumar, A. Experimental and Computational Studies of Imidazolium Based Ionic Liquid 1-Methyl- 3-Propylimidazolium Iodide on Mild Steel Corrosion in Acidic Solution Experimental and Computational Studies of Imidazolium Based Ionic Liquid 1-Methyl- 3-Propylimidazolium. *Mater. Res. Express* **2020**, *7*, 016510. [[CrossRef](#)]
20. Bashir, S.; Lgaz, H.; Chung, I.M.; Kumar, A. Effective Green Corrosion Inhibition of Aluminium Using Analgin in Acidic Medium: An Experimental and Theoretical Study. *Chem. Eng. Commun.* **2020**, *8*, 1121–1130. [[CrossRef](#)]
21. Thakur, A.; Kumar, A. Sustainable Inhibitors for Corrosion Mitigation in Aggressive Corrosive Media: A Comprehensive Study. *J. Bio-Tribo-Corros.* **2021**, *7*, 67. [[CrossRef](#)]
22. Benčina, M.; Resnik, M.; Starič, P.; Junkar, I. Use of Plasma Technologies for Antibacterial Surface Properties of Metals. *Molecules* **2021**, *26*, 1418. [[CrossRef](#)] [[PubMed](#)]
23. Singh, D.; Singh, R.; Boparai, K.S. Development and Surface Improvement of FDM Pattern Based Investment Casting of Biomedical Implants: A State of Art Review. *J. Manuf. Process.* **2018**, *31*, 80–95. [[CrossRef](#)]
24. Khor, K.A.; Gu, Y.W.; Pan, D.; Cheang, P. Microstructure and Mechanical Properties of Plasma Sprayed HA/YSZ/ Ti-6Al-4V Composite Coatings. *Biomaterials* **2004**, *25*, 4009–4017. [[CrossRef](#)] [[PubMed](#)]
25. Yan, X.; Cao, W.; Li, H. Biomedical Alloys and Physical Surface Modifications: A Mini-Review. *Materials* **2022**, *15*, 66. [[CrossRef](#)]
26. Umoren, S.A.; Solomon, M.M.; Obot, I.B.; Suleiman, R.K. A critical review on the recent studies on plant biomaterials as corrosion inhibitors for industrial metals. *J. Indus. Eng. Chem.* **2019**, *76*, 91–115. [[CrossRef](#)]
27. Zhang, L.C.; Chen, L.Y.; Wang, L. Surface Modification of Titanium and Titanium Alloys: Technologies, Developments, and Future Interests. *Adv. Eng. Mater.* **2020**, *22*, 1901258. [[CrossRef](#)]
28. Huang, S.; Liang, N.; Hu, Y.; Zhou, X.; Abidi, N. Polydopamine-Assisted Surface Modification for Bone Biosubstitutes. *Biomed Res. Int.* **2016**, *2016*, 2389895. [[CrossRef](#)] [[PubMed](#)]
29. Liu, Y.; Bao, C.; Wismeijer, D.; Wu, G. The Physicochemical/Biological Properties of Porous Tantalum and the Potential Surface Modification Techniques to Improve Its Clinical Application in Dental Implantology. *Mater. Sci. Eng. C* **2015**, *49*, 323–329. [[CrossRef](#)]
30. Jaganathan, S.K.; Supriyanto, E.; Murugesan, S.; Balaji, A.; Asokan, M.K. Biomaterials in Cardiovascular Research: Applications and Clinical Implications. *Biomed Res. Int.* **2014**, *2014*, 459465. [[CrossRef](#)]
31. Izman, S.; Rafiq, M.; Anwar, M.; Nazim, E.M.; Rosliza, R.; Shah, A.; Hass, M.A. Surface Modification Techniques for Biomedical Grade of Titanium Alloys: Oxidation, Carburization and Ion Implantation Processes. *Titan. Alloy. Towar. Achiev. Enhanc. Prop. Divers. Appl.* **2012**, *42*, 201–228. [[CrossRef](#)]
32. Thakur, A.; Kaya, S.; Abousalem, A.S.; Sharma, S.; Ganjoo, R.; Assad, H.; Kumar, A. Computational and Experimental Studies on the Corrosion Inhibition Performance of an Aerial Extract of Cnicus Benedictus Weed on the Acidic Corrosion of Mild Steel. *Process Saf. Environ. Prot.* **2022**, *161*, 801–818. [[CrossRef](#)]
33. Schäfer, E. Effect of Physical Vapor Deposition on Cutting Efficiency of Nickel-Titanium Files. *J. Endod.* **2002**, *28*, 800–802. [[CrossRef](#)] [[PubMed](#)]
34. Zhou, S.J.; Bai, Y.; Ma, W.; Chen, W. Plasma-Sprayed Fluoridated Hydroxyapatite/Calcium Silicate Composite Coatings for Biomedical Applications. *J. Therm. Spray Technol.* **2019**, *28*, 1025–1038. [[CrossRef](#)]
35. Hacking, S.A.; Zuraw, M.; Harvey, E.J.; Tanzer, M.; Krygier, J.J.; Bohn, J.D. A Physical Vapor Deposition Method for Controlled Evaluation of Biological Response to Biomaterial Chemistry and Topography. *J. Biomed. Mater. Res. Part A* **2007**, *82*, 179–187. [[CrossRef](#)] [[PubMed](#)]
36. Wang, L.; Zhao, X.; Ding, M.H.; Zheng, H.; Zhang, H.S.; Zhang, B.; Li, X.Q.; Wu, G.Y. Surface Modification of Biomedical AISI 316L Stainless Steel with Zirconium Carbonitride Coatings. *Appl. Surf. Sci.* **2015**, *340*, 113–119. [[CrossRef](#)]
37. Yang, S.; Dillon, O.W.; Puleo, D.A.; Jawahir, I.S. Enhancement of Wear Resistance for Improved Functional Performance of Co-Cr-Mo Hip Implants through Cryogenic Surface Treatment: A Case Study. *Mach. Sci. Technol.* **2021**, *25*, 455–476. [[CrossRef](#)]
38. Bagherifard, S.; Slawik, S.; Fernández-Pariente, I.; Pauly, C.; Mücklich, F.; Guagliano, M. Nanoscale Surface Modification of AISI 316L Stainless Steel by Severe Shot Peening. *Mater. Des.* **2016**, *102*, 68–77. [[CrossRef](#)]
39. Chikarakara, E.; Naher, S.; Brabazon, D. Process Mapping of Laser Surface Modification of AISI 316L Stainless Steel for Biomedical Applications. *Appl. Phys. A Mater. Sci. Process.* **2010**, *101*, 367–371. [[CrossRef](#)]
40. Ou, K.L.; Chou, H.H.; Liu, C.M.; Peng, P.W. Surface Modification of Austenitic Stainless Steel with Plasma Nitriding for Biomedical Applications. *Surf. Coat. Technol.* **2011**, *206*, 1142–1145. [[CrossRef](#)]
41. Demirci, S.; Dalmuş, R.; Dikici, T.; Tünçay, M.M.; Kaya, N.; Güllüoğlu, A.N. Effect of Surface Modifications of Additively Manufactured Ti-6Al-4V Alloys on Apatite Formation Ability for Biomedical Applications. *J. Alloys Compd.* **2021**, *887*, 161445. [[CrossRef](#)]
42. González, J.E.; de Armas, G.; Negrin, J.; Beltrán, A.M.; Trueba, P.; Gotor, F.J.; Peón, E.; Torres, Y. Influence of Successive Chemical and Thermochemical Treatments on Surface Features of Ti6Al4V Samples Manufactured by SLM. *Metals* **2021**, *11*, 313. [[CrossRef](#)]
43. Sánchez-Bodón, J.; Del Olmo, J.A.; Alonso, J.M.; Moreno-Benítez, I.; Vilas-Vilela, J.L.; Pérez-Álvarez, L. Bioactive Coatings on Titanium: A Review on Hydroxylation, Self-Assembled Monolayers (SAMs) and Surface Modification Strategies. *Polymers* **2022**, *14*, 165. [[CrossRef](#)]

44. Hu, C.; Ashok, D.; Nisbet, D.R.; Gautam, V. Bioinspired Surface Modification of Orthopedic Implants for Bone Tissue Engineering. *Biomaterials* **2019**, *219*, 119366. [[CrossRef](#)]
45. Fox, K.E.; Tran, N.L.; Nguyen, T.A.; Nguyen, T.T.; Tran, P.A. *Surface Modification of Medical Devices at Nanoscale-Recent Development and Translational Perspectives*; Elsevier Inc.: Amsterdam, The Netherlands, 2018; ISBN 9780128134771.
46. Hasan, A.; Saxena, V.; Pandey, L.M. Surface Functionalization of Ti6Al4V via Self-Assembled Monolayers for Improved Protein Adsorption and Fibroblast Adhesion. *Langmuir* **2018**, *34*, 3494–3506. [[CrossRef](#)]
47. Lin, M.; Zhao, Y.; Wang, S.Q.; Liu, M.; Duan, Z.F.; Chen, Y.M.; Li, F.; Xu, F.; Lu, T.J. Recent Advances in Synthesis and Surface Modification of Lanthanide-Doped Upconversion Nanoparticles for Biomedical Applications. *Biotechnol. Adv.* **2012**, *30*, 1551–1561. [[CrossRef](#)]
48. Hanawa, T. Titanium-Tissue Interface Reaction and Its Control with Surface Treatment. *Front. Bioeng. Biotechnol.* **2019**, *7*, 170. [[CrossRef](#)] [[PubMed](#)]
49. Singh, R.; Martin, M.; Dahotre, N.B. Influence of Laser Surface Modification on Corrosion Behavior of Stainless Steel 316L and Ti-6Al-4V in Simulated Biofluid. *Surf. Eng.* **2005**, *21*, 297–306. [[CrossRef](#)]
50. Salahinejad, E.; Hadianfard, M.J.; Macdonald, D.D.; Sharifi, S.; Mozafari, M.; Walker, K.J.; Tahmasbi Rad, A.; Madihally, S.V.; Vashae, D.; Tayebi, L. Surface Modification of Stainless Steel Orthopedic Implants by Sol-Gel ZrTiO<sub>4</sub> and ZrTiO<sub>4</sub>-PMMA Coatings. *J. Biomed. Nanotechnol.* **2013**, *9*, 1327–1335. [[CrossRef](#)] [[PubMed](#)]
51. Rezaei, A.; Goleji, R.B.; Alipour, F.; Hadavi, M.M.; Mobasherpour, I. Hydroxyapatite/Hydroxyapatite-Magnesium Double-Layer Coatings as Potential Candidates for Surface Modification of 316 LVM Stainless Steel Implants. *Ceram. Int.* **2020**, *46*, 25374–25381. [[CrossRef](#)]
52. Lu, T.; Qiao, Y.; Liu, X. Surface Modification of Biomaterials Using Plasma Immersion Ion Implantation and Deposition. *Interface Focus* **2012**, *2*, 325–336. [[CrossRef](#)]
53. Noqta, O.A.; Aziz, A.A.; Usman, I.A.; Bououdina, M. Recent Advances in Iron Oxide Nanoparticles (IONPs): Synthesis and Surface Modification for Biomedical Applications. *J. Supercond. Nov. Magn.* **2019**, *32*, 779–795. [[CrossRef](#)]
54. Lee, J.Y.; Aguilar, L.E.; Park, C.H.; Kim, C.S. UV Light Assisted Coating Method of Polyphenol Caffeic Acid and Mediated Immobilization of Metallic Silver Particles for Antibacterial Implant Surface Modification. *Polymers* **2019**, *11*, 1200. [[CrossRef](#)]
55. Moxon, K.A.; Kalkhoran, N.M.; Markert, M.; Sambito, M.A.; McKenzie, J.L.; Webster, J.T. Nanostructured Surface Modification of Ceramic-Based Microelectrodes to Enhance Biocompatibility for a Direct Brain-Machine Interface. *IEEE Trans. Biomed. Eng.* **2004**, *51*, 881–889. [[CrossRef](#)]
56. Variola, F.; Brunski, J.; Orsini, G.; De Oliveira, P.T.; Nanci, A. Nanoscale Surface Modifications of Medically-Relevant Metals: State-of-the Art and Perspectives. *Nanoscale* **2012**, *3*, 335–353. [[CrossRef](#)] [[PubMed](#)]
57. Amanov, A. A Promising Post-Additive Manufacturing Surface Modification for Tailoring Gradient Nanostructure and Harmonic Structure in Co–Cr–Mo Alloy. *Vacuum* **2020**, *182*, 109702. [[CrossRef](#)]
58. Liu, R.; Li, X.; Hu, X.; Dong, H. Surface Modification of a Medical Grade Co–Cr–Mo Alloy by Low-Temperature Plasma Surface Alloying with Nitrogen and Carbon. *Surf. Coatings Technol.* **2013**, *232*, 906–911. [[CrossRef](#)]
59. Valkov, S.; Parshorov, S.; Andreeva, A.; Nikolova, M.; Petrov, P. Surface Modification of Co–Cr–Mo Alloys by Electron-Beam Treatment. *IOP Conf. Ser. Mater. Sci. Eng.* **2021**, *1056*, 012008. [[CrossRef](#)]
60. Amanov, A. Effect of Post-Additive Manufacturing Surface Modification Temperature on the Tribological and Tribocorrosion Properties of Co–Cr–Mo Alloy for Biomedical Applications. *Surf. Coatings Technol.* **2021**, *421*, 127378. [[CrossRef](#)]
61. Mahapatro, A. Bio-Functional Nano-Coatings on Metallic Biomaterials. *Mater. Sci. Eng. C* **2015**, *55*, 227–251. [[CrossRef](#)]
62. Chauhan, S.; Upadhyay, L.S.B. Biosynthesis of Iron Oxide Nanoparticles Using Plant Derivatives of Lawsonia Inermis (Henna) and Its Surface Modification for Biomedical Application. *Nanotechnol. Environ. Eng.* **2019**, *4*, 8. [[CrossRef](#)]
63. Song, C.; Sun, W.; Xiao, Y.; Shi, X. Ultrasmall Iron Oxide Nanoparticles: Synthesis, Surface Modification, Assembly, and Biomedical Applications. *Drug Discov. Today* **2019**, *24*, 835–844. [[CrossRef](#)]
64. Prodana, M.; Stoian, A.B.; Burnei, C.; Ionita, D. Innovative Coatings of Metallic Alloys Used as Bioactive Surfaces in Implantology: A Review. *Coatings* **2021**, *11*, 649. [[CrossRef](#)]
65. Xue, T.; Attarilar, S.; Liu, S.; Liu, J.; Song, X.; Li, L.; Zhao, B.; Tang, Y. Surface Modification Techniques of Titanium and Its Alloys to Functionally Optimize Their Biomedical Properties: Thematic Review. *Front. Bioeng. Biotechnol.* **2020**, *8*, 603072. [[CrossRef](#)]
66. Florea, D.A.; Albuleț, D.; Grumezescu, A.M.; Andronescu, E. Surface Modification—A Step Forward to Overcome the Current Challenges in Orthopedic Industry and to Obtain an Improved Osseointegration and Antimicrobial Properties. *Mater. Chem. Phys.* **2020**, *243*, 122579. [[CrossRef](#)]
67. Maleki-Ghaleh, H.; Hafezi, M.; Hadipour, M.; Nadernezhad, A.; Aghaie, E.; Behnamian, Y.; Abu Osman, N.A. Effect of Tricalcium Magnesium Silicate Coating on the Electrochemical and Biological Behavior of Ti-6Al-4V Alloys. *PLoS ONE* **2015**, *10*, e0138454. [[CrossRef](#)]
68. Celesti, C.; Gervasi, T.; Cicero, N.; Giofrè, S.V.; Espro, C.; Piperopoulos, E.; Gabriele, B.; Mancuso, R.; Lo Vecchio, G.; Iannazzo, D. Titanium Surface Modification for Implantable Medical Devices with Anti-Bacterial Adhesion Properties. *Materials* **2022**, *15*, 3283. [[CrossRef](#)]
69. Schweitzer, L.; Cunha, A.; Pereira, T.; Mika, K.; Do Rego, A.M.B.; Ferraria, A.M.; Kieburg, H.; Geissler, S.; Uhlmann, E.; Schoon, J. Preclinical in Vitro Assessment of Submicron-Scale Laser Surface Texturing on Ti6Al4v. *Materials* **2020**, *13*, 5342. [[CrossRef](#)]

70. Miranda, I.; Souza, A.; Sousa, P.; Ribeiro, J.; Castanheira, E.M.S.; Lima, R.; Minas, G. Properties and Applications of PDMS for Biomedical Engineering: A Review. *J. Funct. Biomater.* **2022**, *13*, 2. [[CrossRef](#)]
71. Tortorella, S.; Buratti, V.V.; Maturi, M.; Sambri, L.; Franchini, M.C.; Locatelli, E. Surface-Modified Nanocellulose for Application in Biomedical Engineering and Nanomedicine: A Review. *Int. J. Nanomedicine* **2020**, *15*, 9909–9937. [[CrossRef](#)]
72. Okazaki, Y.; Katsuda, S.I. Biological Safety Evaluation and Surface Modification of Biocompatible Ti–15Zr–4Nb Alloy. *Materials* **2021**, *14*, 731. [[CrossRef](#)]
73. Delfi, M.; Ghomi, M.; Zarrabi, A.; Mohammadinejad, R.; Taraghdari, Z.B.; Ashrafizadeh, M.; Zare, E.N.; Agarwal, T.; Padil, V.V.T.; Mokhtari, B.; et al. Functionalization of Polymers and Nanomaterials for Biomedical Applications: Antimicrobial Platforms and Drug Carriers. *Prosthesis* **2020**, *2*, 117–139. [[CrossRef](#)]
74. Ravichandran, R.; Sundarrajan, S.; Venugopal, J.R.; Mukherjee, S.; Ramakrishna, S. Applications of Conducting Polymers and Their Issues in Biomedical Engineering. *J. R. Soc. Interface* **2010**, *7*, S559–S579. [[CrossRef](#)] [[PubMed](#)]
75. Yoshida, S.; Hagiwara, K.; Hasebe, T.; Hotta, A. Surface Modification of Polymers by Plasma Treatments for the Enhancement of Biocompatibility and Controlled Drug Release. *Surf. Coatings Technol.* **2013**, *233*, 99–107. [[CrossRef](#)]
76. Govindarajan, T.; Shandas, R. A Survey of Surface Modification Techniques for Next-Generation Shape Memory Polymer Stent Devices. *Polymers* **2014**, *6*, 2309–2331. [[CrossRef](#)]
77. Raval, N.; Kalyane, D.; Maheshwari, R.; Tekade, R.K. *Surface Modifications of Biomaterials and Their Implication on Biocompatibility*; Elsevier Inc.: Amsterdam, The Netherlands, 2019; ISBN 9780128144282.
78. Kyzioł, K.; Kaczmarek, Ł.; Brzezinka, G.; Kyzioł, A. Structure, Characterization and Cytotoxicity Study on Plasma Surface Modified Ti-6Al-4V and  $\gamma$ -TiAl Alloys. *Chem. Eng. J.* **2014**, *240*, 516–526. [[CrossRef](#)]
79. Shrivastava, V.P.; Subedi, D.P. Surface Modification of Polymeric Biomaterials by Coating Herbal Extracts. *J. Nano Res. Adv. Mater. Polym. Sci.* **2020**, *1*, 1–10.
80. Xu, J.; Zhang, J.; Shi, Y.; Tang, J.; Huang, D.; Yan, M.; Dargusch, M.S. Surface Modification of Biomedical Ti and Ti Alloys: A Review on Current Advances. *Materials* **2022**, *15*, 1749. [[CrossRef](#)]
81. Bouazizi, N.; Vieillard, J.; Samir, B.; Derf, F. Le Advances in Amine-Surface Functionalization of Inorganic Adsorbents for Water Treatment and Antimicrobial Activities: A Review. *Polymers* **2022**, *14*, 378. [[CrossRef](#)]
82. Sikdar, S.; Menezes, P.V.; Maccione, R.; Jacob, T.; Menezes, P.L. Plasma Electrolytic Oxidation (Peo) Process—Processing, Properties, and Applications. *Nanomaterials* **2021**, *11*, 1375. [[CrossRef](#)]
83. Saberi, A.; Bakhsheshi-Rad, H.R.; Abazari, S.; Ismail, A.F.; Sharif, S.; Ramakrishna, S.; Daroonparvar, M.; Berto, F. A Comprehensive Review on Surface Modifications of Biodegradable Magnesium-Based Implant Alloy: Polymer Coatings Opportunities and Challenges. *Coatings* **2021**, *11*, 747. [[CrossRef](#)]
84. Kim, J.; Lee, H.; Jang, T.S.; Kim, D.; Yoon, C.B.; Han, G.; Kim, H.E.; Jung, H. Do Characterization of Titanium Surface Modification Strategies for Osseointegration Enhancement. *Metals* **2021**, *11*, 618. [[CrossRef](#)]
85. Feng, L.; Liu, Z. Biomedical Applications of Carbon Nanomaterials. In *Biomedical Applications and Toxicology of Carbon Nanomaterials*; Wiley-VCH: Hoboken, NJ, USA, 2016; pp. 131–162. [[CrossRef](#)]
86. Prakasam, M.; Locs, J.; Salma-Ancane, K.; Loca, D.; Largeteau, A.; Berzina-Cimdina, L. Biodegradable Materials and Metallic Implants-A Review. *J. Funct. Biomater.* **2017**, *8*, 44. [[CrossRef](#)] [[PubMed](#)]
87. Bekmurzayeva, A.; Duncanson, W.J.; Azevedo, H.S.; Kanayeva, D. Surface Modification of Stainless Steel for Biomedical Applications: Revisiting a Century-Old Material. *Mater. Sci. Eng. C* **2018**, *93*, 1073–1089. [[CrossRef](#)] [[PubMed](#)]
88. Civantos, A.; Martínez-Campos, E.; Ramos, V.; Elvira, C.; Gallardo, A.; Abarrategi, A. Titanium Coatings and Surface Modifications: Toward Clinically Useful Bioactive Implants. *ACS Biomater. Sci. Eng.* **2017**, *3*, 1245–1261. [[CrossRef](#)]
89. Witkowska, J.; Tarnowski, M.; Choińska, E.; Kulpa, M.; Szade, J.; Raugh, G.; Świążkowski, W.; Wierzchoń, T. Plasma Modification of Carbon Coating Produced by Rf Cvd on Oxidized Niti Shape Memory Alloy under Glow-Discharge Conditions. *Materials* **2021**, *14*, 4842. [[CrossRef](#)] [[PubMed](#)]
90. Devgan, S.; Sidhu, S.S. Evolution of Surface Modification Trends in Bone Related Biomaterials: A Review. *Mater. Chem. Phys.* **2019**, *233*, 68–78. [[CrossRef](#)]
91. Chu, P.K.; Chen, J.Y.; Wang, L.P.; Huang, N. Plasma-Surface Modification of Biomaterials. *Mater. Sci. Eng. R Rep.* **2002**, *36*, 143–206. [[CrossRef](#)]
92. Yuvaraj, S.; Muthukumarasamy, N.; Flores, M.; Rajesh, G.; Paraskevopoulos, K.M.; Pouroutzidou, G.K.; Theodorou, G.S.; Ioannidou, K.; Lusvardi, L.; Velauthapillai, D.; et al. Incorporation of Nanosized Carbon over Hydroxyapatite (HAp) Surface Using DC Glow Discharge Plasma for Biomedical Application. *Vacuum* **2021**, *190*, 110300. [[CrossRef](#)]
93. Ponnusamy, S.; Ali, H.H.; Dutt, F.; Rahman, S.U.; Salah, A.A.; Pipalia, M.; Baier, R.E.; Arany, P.R. Redox Signaling Induces Laminin Receptor Ribosomal Protein-SA Expression to Improve Cell Adhesion Following Radiofrequency Glow Discharge Treatments. *Sci. Rep.* **2022**, *12*, 7742. [[CrossRef](#)]
94. Huang, R.; Liu, L.; Li, B.; Qin, L.; Huang, L.; Yeung, K.W.K.; Han, Y. Nanograins on Ti-25Nb-3Mo-2Sn-3Zr Alloy Facilitate Fabricating Biological Surface through Dual-Ion Implantation to Concurrently Modulate the Osteogenic Functions of Mesenchymal Stem Cells and Kill Bacteria. *J. Mater. Sci. Technol.* **2021**, *73*, 31–44. [[CrossRef](#)]
95. Akpek, A. Analysis of Surface Properties of Ag and Ti Ion-Treated Medical Textiles by Metal Vapor Vacuum Arc Ion Implantation. *Coatings* **2021**, *11*, 102. [[CrossRef](#)]

96. Tel, G. Ion Implantation of  $^{109}\text{Ag}$  Stable Isotope as a Tracer in SS316L Biomedical Implant for Failure Detection. Failure Detection. In *Introduction to Distributed Algorithms*; Cambridge University Press: Cambridge, UK, 2012; pp. 505–519. [[CrossRef](#)]
97. Zhang, C.; Shen, X.; Wang, J.; Xu, C.; He, J.; Bai, X. Improving Surface Properties of Fe-Based Laser Cladding Coating Deposited on a Carbon Steel by Heat Assisted Ultrasonic Burnishing. *J. Mater. Res. Technol.* **2021**, *12*, 100–116. [[CrossRef](#)]
98. Dang, J.; An, Q.; Lian, G.; Zuo, Z.; Li, Y.; Wang, H.; Chen, M. Surface Modification and Its Effect on the Tensile and Fatigue Properties of 300M Steel Subjected to Ultrasonic Surface Rolling Process. *Surf. Coat. Technol.* **2021**, *422*, 127566. [[CrossRef](#)]
99. de Oliveira, A.; Placias, F.G.; Sobrinho, A.S.d.S.; Leite, D.M.G.; Miyakawa, W.; Neto, J.J.; Koh, I.H.J.; Liberatore, A.M.A.; dos Santos, M.A.; Matieli, J.E.; et al. Secondary Ion Mass Spectrometry and Atomic Force Microscopy Analysis of Silver-Doped Diamond-like Carbon Films on Titanium Alloy (Ti6Al4V) for Possible Biomedical Application. *Thin Solid Films* **2021**, *719*, 138487. [[CrossRef](#)]
100. Kandasamy, K.; Surendhiran, S.; Syed Khadar, Y.A.; Rajasingh, P. Ultrasound-Assisted Microwave Synthesis of CdS/MWCNTs QDs: A Material for Photocatalytic and Corrosion Inhibition Activity. *Mater. Today Proc.* **2020**, *47*, 757–762. [[CrossRef](#)]
101. Zhao, H.Z.; Du, Q.; Li, Z.S.; Yang, Q.Z. Mechanisms for the Direct Electron Transfer of Cytochrome c Induced by Multi-Walled Carbon Nanotubes. *Sensors* **2012**, *12*, 10450–10462. [[CrossRef](#)]
102. Montemor, M.F.; Ferreira, M.G.S. Analytical Characterisation and Corrosion Behaviour of Bis-Aminosilane Coatings Modified with Carbon Nanotubes Activated with Rare-Earth Salts Applied on AZ31 Magnesium Alloy. *Surf. Coat. Technol.* **2008**, *202*, 4766–4774. [[CrossRef](#)]
103. Chen, S.; Wang, X.; Zhu, G.; Lu, Z.; Zhang, Y.; Zhao, X.; Hou, B. Developing Multi-Wall Carbon Nanotubes/Fusion-Bonded Epoxy Powder Nanocomposite Coatings with Superior Anti-Corrosion and Mechanical Properties. *Colloids Surfaces A Physicochem. Eng. Asp.* **2021**, *628*, 127309. [[CrossRef](#)]
104. Prasannakumar, R.S.; Chukwuike, V.I.; Bhagyaraj, K.; Mohan, S.; Barik, R.C. Electrochemical and Hydrodynamic Flow Characterization of Corrosion Protection Persistence of Nickel/Multiwalled Carbon Nanotubes Composite Coating. *Appl. Surf. Sci.* **2020**, *507*, 145073. [[CrossRef](#)]
105. Dalla, P.T.; Tragazikis, I.K.; Exarchos, D.A.; Dassios, K.G.; Barkoula, N.M.; Matikas, T.E. Effect of Carbon Nanotubes on Chloride Penetration in Cement Mortars. *Appl. Sci.* **2019**, *9*, 1032. [[CrossRef](#)]
106. Pak, A.; Masoudi, M.; Elmkhah, H. Effect of Ultrasonic Peening on the Surface Properties of Nano-Layered CrN/CrAlN Coating Deposited by CAPVD Method on D3 Tool Steel. *Surf. Interfaces* **2022**, *28*, 101618. [[CrossRef](#)]
107. Zare, E.N.; Lakouraj, M.M.; Moosavi, E. Poly (3-Aminobenzoic Acid) @ MWCNTs Hybrid Conducting Nanocomposite: Preparation, Characterization, and Application as a Coating for Copper Corrosion Protection. *Compos. Interfaces* **2016**, *23*, 571–583. [[CrossRef](#)]
108. Yin, Y.; Lü, Y.; Wu, P.; Cai, C. Direct Electrochemistry of Redox Proteins and Enzymes Promoted by Carbon Nanotubes. *Sensors* **2005**, *5*, 220–234. [[CrossRef](#)]
109. Hong, J.; Zhao, Y.X.; Xiao, B.L.; Moosavi-Movahedi, A.A.; Ghourchian, H.; Sheibani, N. Direct Electrochemistry of Hemoglobin Immobilized on a Functionalized Multi-Walled Carbon Nanotubes and Gold Nanoparticles Nanocomplex-Modified Glassy Carbon Electrode. *Sensors* **2013**, *13*, 8595–8611. [[CrossRef](#)]
110. Nur-e-alam, M.; Basher, M.K.; Vasiliev, M.; Das, N. Physical Vapor-deposited Silver (Ag)-based Metal-dielectric Nanocomposites for Thin-film and Coating Applications. *Appl. Sci.* **2021**, *11*, 6746. [[CrossRef](#)]
111. Vignesh, R.; Sakthinathan, G.; Velusamy, R.; Ramakrishna, S. An In-Vitro Evaluation Study on the Effects of Surface Modification via Physical Vapor Deposition on the Degradation Rates of Magnesium-Based Biomaterials. *Surf. Coatings Technol.* **2021**, *411*, 126972. [[CrossRef](#)]
112. Arora, B.; Attri, P. Carbon Nanotubes (CNTs): A Potential Nanomaterial for Water Purification. *J. Compos. Sci.* **2020**, *4*, 135. [[CrossRef](#)]
113. Pinyou, P.; Blay, V.; Chansaenpak, K.; Lisnund, S. Paracetamol Sensing with a Pencil Lead Electrode Modified with Carbon Nanotubes and Polyvinylpyrrolidone. *Chemosensors* **2020**, *8*, 133. [[CrossRef](#)]
114. Long, D.; Wu, G.; Zhu, G. Noncovalently Modified Carbon Nanotubes with Carboxymethylated Chitosan: A Controllable Donor-Acceptor Nanohybrid. *Int. J. Mol. Sci.* **2008**, *9*, 120–130. [[CrossRef](#)]
115. Li, S.; Zhou, J.; Noroozifar, M.; Kerman, K. Gold-Platinum Core-Shell Nanoparticles with Thiolated Polyaniline and Multi-Walled Carbon Nanotubes for the Simultaneous Voltammetric Determination of Six Drug Molecules. *Chemosensors* **2021**, *9*, 24. [[CrossRef](#)]
116. Liu, Y.; Xia, C.; Zehri, A.; Ye, L.; Wang, N.; Zhmud, B.; Lu, H.; Liu, J. Surface Modification of Graphene for Use as a Structural Fortifier in Water-Borne Epoxy Coatings. *Coatings* **2019**, *9*, 754. [[CrossRef](#)]
117. Siddiki, M.K.; Venkatesan, S.; Qiao, Q. Nb 2O 5 as a New Electron Transport Layer for Double Junction Polymer Solar Cells. *Phys. Chem. Chem. Phys.* **2012**, *14*, 4682–4686. [[CrossRef](#)] [[PubMed](#)]
118. Shypylenko, A.; Pshyk, A.V.; Grześkowiak, B.; Medjanik, K.; Peplinska, B.; Oyoshi, K.; Pogrebniak, A.; Jurga, S.; Coy, E. Effect of Ion Implantation on the Physical and Mechanical Properties of Ti-Si-N Multifunctional Coatings for Biomedical Applications. *Mater. Des.* **2016**, *110*, 821–829. [[CrossRef](#)]
119. Pashkuleva, I.; Marques, A.P.; Vaz, F.; Reis, R.L. Surface Modification of Starch Based Biomaterials by Oxygen Plasma or UV-Irradiation. *J. Mater. Sci. Mater. Med.* **2010**, *21*, 21–32. [[CrossRef](#)]
120. Amiri, H.; Mohammadi, I.; Afshar, A. Electrophoretic Deposition of Nano-Zirconia Coating on AZ91D Magnesium Alloy for Bio-Corrosion Control Purposes. *Surf. Coatings Technol.* **2017**, *311*, 182–190. [[CrossRef](#)]

121. Pishbin, F.; Cordero-Arias, L.; Cabanas-Polo, S.; Boccaccini, A.R. *Bioactive Polymer-Calcium Phosphate Composite Coatings by Electrophoretic Deposition*; Elsevier Ltd.: Amsterdam, The Netherlands, 2015; ISBN 9781782423164.
122. Meng, X.; Kwon, T.Y.; Yang, Y.; Ong, J.L.; Kim, K.H. Effects of Applied Voltages on Hydroxyapatite Coating of Titanium by Electrophoretic Deposition. *J. Biomed. Mater. Res. Part B Appl. Biomater.* **2006**, *78*, 373–377. [[CrossRef](#)] [[PubMed](#)]
123. Kaya, C.; Singh, I.; Boccaccini, A.R. Multi-Walled Carbon Nanotube-Reinforced Hydroxyapatite Layers on Ti6Al4V Medical Implants by Electrophoretic Deposition (EPD). *Adv. Eng. Mater.* **2008**, *10*, 131–138. [[CrossRef](#)]
124. Drevet, R.; Ben Jaber, N.; Fauré, J.; Tara, A.; Ben Cheikh Larbi, A.; Benhayoune, H. Electrophoretic Deposition (EPD) of Nano-Hydroxyapatite Coatings with Improved Mechanical Properties on Prosthetic Ti6Al4V Substrates. *Surf. Coat. Technol.* **2016**, *301*, 94–99. [[CrossRef](#)]
125. Šugár, P.; Ludrovcová, B.; Kalbáčová, M.H.; Šugárová, J.; Sahul, M.; Kováčik, J. Laser Surface Modification of Powder Metallurgy-Processed Ti-Graphite Composite Which Can Enhance Cells' Osteo-Differentiation. *Materials* **2021**, *14*, 6067. [[CrossRef](#)] [[PubMed](#)]
126. Dong, H.; Liu, H.; Zhou, N.; Li, Q.; Yang, G.; Chen, L.; Mou, Y. Surface Modified Techniques and Emerging Functional Coating of Dental Implants. *Coatings* **2020**, *10*, 1012. [[CrossRef](#)]
127. Raghavan, R.; Ravindran, P. A.; Purushothaman, P. Surface Treatments of Implant: A Review. *Int. J. Sci. Healthc. Res.* **2020**, *5*, 128.
128. Kooaie, M.; Bordbar-Khiabani, A.; Kolahdooz, S.; Darbandsari, A.K.; Mozafari, M. Advanced Surface Treatment Techniques Counteract Biofilm-Associated Infections on Dental Implants. *Mater. Res. Express* **2020**, *7*, 015417. [[CrossRef](#)]
129. Vilardell, A.M.; Cinca, N.; Garcia-Giralt, N.; Dosta, S.; Cano, I.G.; Nogués, X.; Guilemany, J.M. In-Vitro Comparison of Hydroxyapatite Coatings Obtained by Cold Spray and Conventional Thermal Spray Technologies. *Mater. Sci. Eng. C* **2020**, *107*, 110306. [[CrossRef](#)]
130. Pantaroto, H.N.; Cordeiro, J.M.; Pereira, L.T.; de Almeida, A.B.; Nociti Junior, F.H.; Rangel, E.C.; Azevedo Neto, N.F.; da Silva, J.H.D.; Barão, V.A.R. Sputtered Crystalline TiO<sub>2</sub> Film Drives Improved Surface Properties of Titanium-Based Biomedical Implants. *Mater. Sci. Eng. C* **2021**, *119*, 111638. [[CrossRef](#)] [[PubMed](#)]
131. Polo, T.O.B.; da Silva, W.P.; Momesso, G.A.C.; Lima-Neto, T.J.; Barbosa, S.; Cordeiro, J.M.; Hassumi, J.S.; da Cruz, N.C.; Okamoto, R.; Barão, V.A.R.; et al. Plasma Electrolytic Oxidation as a Feasible Surface Treatment for Biomedical Applications: An in Vivo Study. *Sci. Rep.* **2020**, *10*, 10000. [[CrossRef](#)] [[PubMed](#)]
132. Verissimo, N.C.; Chung, S.; Webster, T.J. New Nanoscale Surface Modifications of Metallic Biomaterials. In *Surface Coating and Modification of Metallic Biomaterials*; Woodhead Publishing: Sawston, UK, 2015; pp. 249–273. [[CrossRef](#)]
133. Liu, J.X.; Yang, D.Z.; Shi, F.; Cai, Y.J. Sol-Gel Deposited TiO<sub>2</sub> Film on NiTi Surgical Alloy for Biocompatibility Improvement. *Thin Solid Films* **2003**, *429*, 225–230. [[CrossRef](#)]
134. Boccaccini, A.R.; Cho, J.; Subhani, T.; Kaya, C.; Kaya, F. Electrophoretic Deposition of Carbon Nanotube-Ceramic Nanocomposites. *J. Eur. Ceram. Soc.* **2010**, *30*, 1115–1129. [[CrossRef](#)]
135. Pishbin, F.; Simchi, A.; Ryan, M.P.; Boccaccini, A.R. A Study of the Electrophoretic Deposition of Bioglass® Suspensions Using the Taguchi Experimental Design Approach. *J. Eur. Ceram. Soc.* **2010**, *30*, 2963–2970. [[CrossRef](#)]
136. Esteban, J.; Vallet-Regí, M.; Aguilera-Correa, J.J. Antibiotics-and Heavy Metals-Based Titanium Alloy Surface Modifications for Local Prosthetic Joint Infections. *Antibiotics* **2021**, *10*, 1270. [[CrossRef](#)]
137. Lee, M.K.; Lee, H.; Kim, H.E.; Lee, E.J.; Jang, T.S.; Jung, H. Do Nano-topographical Control of Ti-nb-zr Alloy Surfaces for Enhanced Osteoblastic Response. *Nanomaterials* **2021**, *11*, 1507. [[CrossRef](#)] [[PubMed](#)]
138. Chico, B.; Pérez-Maceda, B.T.; José, S.S.; Escudero, M.L.; García-Alonso, M.C.; Lozano, R.M. Corrosion Behaviour and J774a.1 Macrophage Response to Hyaluronic Acid Functionalization of Electrochemically Reduced Graphene Oxide on Biomedical Grade CoCr. *Metals* **2021**, *11*, 1078. [[CrossRef](#)]
139. Rojas, O.; Prudent, M.; López, M.E.; Vargas, F.; Ageorges, H. Influence of Atmospheric Plasma Spraying Parameters on Porosity Formation in Coatings Manufactured from 45S5 Bioglass® Powder. *J. Therm. Spray Technol.* **2020**, *29*, 185–198. [[CrossRef](#)]
140. Zhang, M.; Pu, X.; Chen, X.; Yin, G. In-Vivo Performance of Plasma-Sprayed CaO–MgO–SiO<sub>2</sub>-Based Bioactive Glass-Ceramic Coating on Ti–6Al–4V Alloy for Bone Regeneration. *Heliyon* **2019**, *5*, e02824. [[CrossRef](#)]
141. Dudek, K.; Dulski, M.; Losiewicz, B. Functionalization of the NiTi Shape Memory Alloy Surface by HAp/SiO<sub>2</sub>/Ag Hybrid Coatings Formed on SiO<sub>2</sub>-TiO<sub>2</sub> Glass Interlayer. *Materials* **2020**, *13*, 1648. [[CrossRef](#)] [[PubMed](#)]
142. Cheang, P.; Khor, K.A. Addressing Processing Problems Associated with Plasma Spraying of Hydroxyapatite Coatings. *Biomaterials* **1996**, *17*, 537–544. [[CrossRef](#)]
143. Mavis, B.; Taş, A.C. Dip Coating of Calcium Hydroxyapatite on Ti-6Al-4V Substrates. *J. Am. Ceram. Soc.* **2000**, *83*, 989–991. [[CrossRef](#)]
144. Al-Amin, M.; Abdul-Rani, A.M.; Danish, M.; Rubaiee, S.; Bin Mahfouz, A.; Thompson, H.M.; Ali, S.; Unune, D.R.; Sulaiman, M.H. Investigation of Coatings, Corrosion and Wear Characteristics of Machined Biomaterials through Hydroxyapatite Mixed-Edm Process: A Review. *Materials* **2021**, *14*, 3597. [[CrossRef](#)] [[PubMed](#)]
145. Maleki-Ghaleh, H.; Khalil-Allafi, J. Characterization, Mechanical and in Vitro Biological Behavior of Hydroxyapatite-titanium-carbon Nanotube Composite Coatings Deposited on NiTi Alloy by Electrophoretic Deposition. *Surf. Coatings Technol.* **2019**, *363*, 179–190. [[CrossRef](#)]
146. Maleki-Ghaleh, H.; Khalil-Allafi, J.; Horandghadim, N.; Keikhosravani, P.; Hosseini, M.G. Structural Characterization, Mechanical, and Electrochemical Studies of Hydroxyapatite-Titanium Composite Coating Fabricated Using Electrophoretic Deposition and Reaction Bonding Process. *J. Biomed. Mater. Res. Part B Appl. Biomater.* **2020**, *108*, 2119–2130. [[CrossRef](#)] [[PubMed](#)]

- 
147. Khalili, V.; Khalil-Allafi, J.; Maleki-Ghaleh, H.; Paulsen, A.; Frenzel, J.; Eggeler, G. The Influence of Si as Reactive Bonding Agent in the Electrophoretic Coatings of HA-Si-MWCNTs on NiTi Alloys. *J. Mater. Eng. Perform.* **2016**, *25*, 390–400. [[CrossRef](#)]
  148. Maleki-Ghaleh, H.; Khalil-Allafi, J. Effect of Hydroxyapatite-Titanium-MWCNTs Composite Coating Fabricated by Electrophoretic Deposition on Corrosion and Cellular Behavior of NiTi Alloy. *Mater. Corros.* **2019**, *70*, 2128–2138. [[CrossRef](#)]